Mode of Emplacement and Petrogenesis of Volcanic Rocks of the Shirahama Group, Izu Peninsula, Japan

論文題目　伊豆半島白浜層群の火山岩類の定置様式と岩石学的成因

Yoshihiko TAMURA

December, 1990

①

Mode of Emplacement and Petrogenesis of Volcanic Rocks of the Shirahama Group, Izu Peninsula, Japan

Yoshihiko TAMURA

December, 1990

Abstract

The Neogene Shirahama Group in the Izu Peninsula has been studied from geological and petrological points of view. The Shirahama Group is mainly composed of products of submarine volcanism, which are subaqueous autobrecciated lava, volcanic breccia, and well-sorted (fines-are-depleted) tuff or tuff breccia. Cross beddings are often developing in pumice tuff. It is a dissected volcano group in the island-arc setting which was active from 7 to 8 Ma. The mode of emplacement of submarine pyroclastic deposits is presented in Part I, and the petrogenesis of volcanic rocks of the Shirahama Group is presented in Part II as a representative island-arc volcano.

The cooling history and mode of emplacement of coarse andesite blocks deposited in the shallow marine environment was investigated by paleomagnetic studies, geological observation and calculations on conduction of heat. Six to 13 samples were cored and measured from 6 large essential blocks of andesite, 1-5 m in diameter from a volcanic breccia in the Dogashima area. Thermal demagnetization techniqres were used to detect the directional change of remanence through demagnetization steps each of which represents different blocking temperatures (Tb). Each sample has three components of remanent magnetization with different Tb (C_1, C_2 and C_3). C_1 is characterized by Tb of 250° C and an

orientation coincident with the present geomagnetic field. C_2 has a Tb of 250-500° C and shows a consistent direction with reversed polarity. C_3 has a Tb of 500-600° C, and its orientation is nearly consistent only among samples collected from nearby parts of the same clast and are random among the different clasts. On the basis of the remanence direction of each component, Tb and the petrography of the samples, C_1 is interpreted as secondary viscous remanence, whereas C_2 and C_3 are the partial TRM's obtained during and immediately after emplacement. This suggests that C_3 was acquired while the blocks were rolling downslope, and that C_2 was acquired during continued cooling of the blocks just after they came to rest. Thermal history obtained by calculations based on conduction of heat revealed that these blocks were emplaced less than an hour after the eruption, and the slow velocity of transportation (less than 20 km/h) is suggested by the estimation of the distance from the eruption center.

It is revealed that hot pyroclastic deposit can exist in the shallow marine environment, and the thermal history and mode of transportation are illustrated. So far as is known, the work reported here is the first specifically designated to elucidate the dynamic submarine volcanism out of the static geological record.

Volcanic rocks of the Shirahama Group ranges from basalt to dacite, and rarely to rhyolite.

On the FeO^*/MgO vs. SiO_2 diagram, rocks in the Shirahama Group have continuous distribution ranging from tholeiitic to calcalkaline fields defined by Miyashiro (1974). These rocks are divided into tholeiitic, calcalkaline and mixed hybrid magmas.

The dualism of volcanic rocks in the island-arcs, which has been roughly represented by tholeiites and calcalkaline rocks, can be clearly recognized in the chemical composition of phenocrystic minerals in the Shirahama group. The FeO content in plagioclase on the FeO vs. An content diagram, and MgO plus TiO_2 contents in magnetite on the TiO2 vs. MgO diagram are higher in tholeiites than in calcalkaline rocks at a given bulk rock FeO^*/MgO. The two-pyroxene thermometer (Lindsley, 1983) showed that tholeiitic magma has much higher temperatures (1000-1100° C) than calcalkaline magma (800-900° C).

Magma mixing between tholeiitic and calcalkaline magmas is demonstrated by the existence of basic inclusions in dacite host, and by the conspicuous reverse zoning of hypersthene phenocrysts in andesite. Those mixed hybrids have compositions close to the boundary between calcalkaline and tholeiitic fields defined by Miyashiro (1974), and obscure the above mentioned dualism in arc volcanism.

Crystal fractionation in tholeiites and calcalkaline rocks are modelled on the basis of major-element least squares calculations and trace-element Rayleigh-type fractionation. It is concluded that the variation of chemical

composition in tholeiites can be explained by crystal fractionation of plagioclase + olivine or orthopyroxene + augite + magnetite. On the contrary, calcalkaline rocks or calcalkaline trend cannot be derived from tholeiites. Calcalkaline rocks can be derived from mantle-derived high-Mg andesite (boninites) magmas by crystal fractionation of plagioclase + olivine + orthopyroxene + augite. In the case of the Shirahama Group, low-Ca type 3 boninites (Mariana-Trench 50-23) is most appropriate as the primary magma. The origin of the dualism of the volcanism in the island-arcs could be originated from the formation of two different parental melts in the upper mantle.

From the review of eight boninites suites, a new fact has been revealed. In spite of pronounced variations within boninites suites, boninites have a general geochemical feature when their geochemical characteristics are compared to those of the coexisting tholeiites. This general geochemical feature against coexisting tholeiites also exists in calcalkaline rocks.

It is concluded from crystal fractionation modellig and the geochemical characteristics of calcalkaline rocks in the Shirahama Group that calcalkaline rocks are derived from mantle-derived high-Mg andesite magmas, which are named "boninites" by Crawford et al. (1989). The variation in island arc magmas is governed by mantle-derived bimodal magmatism which is symbolized by concomitant formation of boninites and tholeiites in the upper mantle as two con-

trasting primary melts in the subduction zones.

CONTENTS

Introduction

This thesis is composed of two parts. Part I is on the geology and part II is on the petrology of the Shirahama Group.

Part I deals with mode of emplacement of volcanic rocks of the Shirahama Group. The late Miocene and early Pliocene Shirahama Group is exposed in Izu Peninsula, Japan. It is mainly composed of products of submarine volcanism. Recently from a view of submarine volcanism, the geology of the Shirahama Group is reexamined (Kano, 1983; Ito et al., 1984; Matsumoto et al., 1985). However the mode of emplacement of the submarine pyroclastic deposits which are most spectacular in the Shirahama Group has not been dealt with yet. Subaqueous pyroclastic flow deposits have become increasingly recognized in the geologic record following the pioneering studies of Fiske (1963) and Fiske and Matsuda (1964). Fisher and Schmincke (1984) presented a good review on several examples of subaqeous pyroclastic flow deposits which have been reported from marine to lacustrine rock sequences from the Archean of Canada (Dimroth and Demarcke, 1978) to the Recent in the Lesser Antilles (Carey and Sigurdsson, 1980). It seems that the four main problem areas which are summarized by Fisher and Schmincke (1984) have not been clarified yet. Those are:

(1) Whether a subaqueous pyroclastic flow was indeed deposited under water or on land?

(2) Whether a mass flow originated from a subaqueous or subaerial eruption?

(3) How reliable are the criteria that distinguish between flows that are underwater continuation of a subaerial pyroclastic flow or the direct result of an subaqueous eruption and flows that are generated by slumping and resedimentation of unstable volcanic debris that had accumulated on the subaerial or submarine slope of a volcano?

(4) Whether a primaly flow was hot during underwater emplacement some times causing welding or textural suggesting welding are actually due to diagenetic compaction.

The above problems are tackled in part I of this thesis which presents the cooling history of large andesite blocks deposited proximally in the shallow marine environment. By using paleomagnetic technique, it was revealed that the studied blocks were hot (450 ˚C -500˚C) when deposited, and therefore that the pyroclastic debris flow in which they are contained was the direct product of a contemporaneous eruption. Time and velocity of transportation of these blocks are deduced from a combination of geology, paleomagnetic study and theoretical calculations on conduction of heat in the andesite blocks.

Part II deals with the petrogenesis of volcanic rocks of the Shirahama Group. The studied area of the Shirahama Group, western and southern Izu Peninsula, is a dissected volcano group from 7 to 8 Ma ago.

For the last three decades, in spite of innumerable research papers, the petrogenesis of island-arc magmas has not been clearly understood. Two different processes remain as the dominant mechanism for the origin of island-arc magmas, especially of calcalkaline andesites. One of them is POAM-fractionation (Gill,1981). It is concluded that crystal fractionation of phenocrysts phases from basalt, i.e., usually of plagioclase + orthopyroxene/olivine + augite + magnetite (POAM), is the most common and dominant process, supplemented to an unknown extent by magma mixing, selective interaction with crust, and vapor fractionation. The other is lower crust melting. Takahashi (1986) presented a petrological model of the lower crust and upper mantle beneath the Ichinomegata volcano and proposed that calcalkaline andesite of the volcano was produced by partial melting of hornblende- rich rocks at the crust-mantle boundary beneath the volcano upon transit of hot basaltic magma body.

The author cannot agree with both hypotheses on the origin of calcalkaline andesite. Andesite genesis by POAM-fractionation is denied in the Shirahama Group on the basis of least squares calculations, in which there are discrepancies between crystal fractionation deduced from major element content and calculated Rayleigh type trace element concentrations, but it is thought not to be fair to apply lower crust melting to andesite genesis as an alternative to basalt fractionation beyond its ambiguity.

A new hypothesis on the petrogenesis of island-arc

magmas will be presented in Part II. The clue to the new idea came first from the observation that calcalkaline rocks tend to occur in association with tholeiites in orogenic zones. Masuda and Aoki (1979), Aoki and Fujimaki (1982) and Fujinawa (1988) concluded from the study of volcanic rocks in the northeast Japan that the tholeiitic magma and the calcalkaline magma are not derived from a common parental magma. The former two suggested that both basalt and andesite magmas generated independently in the upper mantle.

To promote the idea of mantle-derived bimodal magmatism, the removal of the effect of magma mixing and the establishment of crystal fractionation model based on it are essential. And if calcalkaline rocks are derivatives of mantle-derived primary andesite, the geochemical characteristics inherited from the primary andesite should be clarified.

Part II takes the following logical steps to reveal the origin of island-arc magmas.

Firstly, the recognition of the bimodal volcanism of calcalkaline and tholeiitic series in the Shirahama Group is demonstrated by comparing the chemical compositions of phenocryst phases, plagioclase, augite, orthpyroxene and magnetite, and magmatic temperatures measured by two pyroxene thermometer (Lindsley, 1983).

Secondly, it is demonstrated that magma mixing occured between the calcalkaline and tholeiitic magmas of the Shira-

hama Group and the evidence of magma mixing is clearly recognized only for the samples having intermediate petrochemical features between tholeiitic and calcalkaline magmas defined by Miyashiro (1974).

Thirdly, the role of crystal fractionation in the petrogenesis of the Shirahama Group is evaluated on the basis of major-element least squares calculations and trace-element Rayleigh type fractionation. New attempt was made to explain both of major- and trace element abundances in the calcalkaline series on the assumption that "boninite" (high-Mg andesite) is a primary magma of calcalkaline rocks.

Fourthly, it is examined whether boninites can be primary magma of calcalkaline rocks. Eight boninites suites, New Caledonia, Mariana forearc, Goshikidai, Shodo-shima, DSDP 458, Guam, Victoria and North Tonga Trench, where both tholeiites and boninites occur, are reviewed and the geochemical characteristics are compared.

Fifthly, a new hypothesis on the petrogenesis of island-arc magmas will be presented, that is, boninites are ubiquitous in island-arcs, and calcalkaline rocks are the differentiation products of boninites. Mantle-derived bimodal magmatism of boninite and tholeiite is thought to be the essential mechanism in island-arcs.

Acknowledgements

The author wishes to express his thanks to Professor Ikuo Kushiro of the University of Tokyo and Dr. Richard S. Fiske of the Smithsonian Institution for constant guidance in the course of the work. Thanks are also due to Professor Shigeo Aramaki of Earthquake Reseach Institute, University of Tokyo for some valuable suggestions and XRF analysis. He also indebted to Dr. Kazuhito Ozawa of the University of Tokyo for his critical reading of this manuscript. During the course of this study, he has benifitted from discussions with Profs. Mitsuhiro Toriumi, Toshizugu Fujii, Yasuo Nakamura, Dr. Hiroko Nagahara of the University of Tokyo and Dr. Masato Koyama of the Shizuoka University. He also thanks to all these persons. He also express his thanks to Mr. Katsuya Kaneko, Ms. Akiko Nomizo and Ms. Teruyo Kawazu for invaluable help with the preparation of the manuscript.

PART I

Mode of emplacement of volcanic rocks of the Shirahama Group

INTRODUCTION

Numerous workers have used paleomagnetic techniques to estimate emplacement temperatures of pyroclastic deposits. Aramaki and Akimoto (1957) measured the orientations of natural remanent magnetizations (NRM's) of fragments contained in subaerial pyroclastic deposits in Japan and estimated whether emplacement temperatures of the deposits were higher than the Curie temperature of the constituent ferromagnetic mineral. Similar studies had been carried out on the subaqueous Donzurubo formation in Japan (Yamazaki et al., 1973) and on the subaerial products of the 1470 B.C. eruption of Santorini (Wright, 1978).

More detailed estimates of emplacement temperatures have been made by using the technique of progressive thermal demagnetization in the absence of a magnetic field (Hoblitt and Kellogg, 1979; Kent et al., 1981; Brown, 1981; and McClelland and Druitt, 1989). These studies depend on the theory of thermoremanent magnetization (TRM). If TRM in each fragment has two components, the emplacement temperature can be determined as the upper limit of the lower temperature component of TRM, provided that these are uniform in all fragments. However, uncertainties can be introduced in the measurements, by mineralogical transformations after emplacement (or during the process of thermal demagnetization), or by the effects of viscous remanent magnetization in the present geomagnetic field.

In this study, we reduced these uncertainties by

comparing the differences in thermal history of cores obtained from different parts of the same fragment. This approach has enabled us to determine emplacement temperatures in a deposit that was deposited hot, but at temperatures lower than the Curie temperature of the constituent ferromagnetic minerals.

GEOLOGICAL SETTING

The late Miocene-Pliocene Shirahama Group underlies the southern part of the Izu Peninsula, Japan (Fig.1), and consists chiefly of basaltic to dacitic pyroclastic rocks erupted and deposited in the shallow marine environment (Koyama, 1988). Available data suggest that the Shirahama volcanism took place from numerous scattered vents, producing a submerged volcanic field consisting of small overlapping pyroclastic cones and associated lave flows; large volcanic edifices have not been recognized. The Shirahama rocks, uplifted from the sea in the early Pleistocene, are little deformed and virtually unaltered; volcanic glass is abundant in all of the deposits studied.

Fig.2 is a geological map of the western Izu area. The Miocene Nishina Group and the Yugashima group are unconformably overlain by, or are in fault contact with the Shirahama Group. The quaternary Jaishi volcano unconformably overlies the Shirahama Group. The Shirahama Group in this area is divided into four units: the Iwachi Tuff, Ishibu Intrusives, Matsuzaki Volcanics and Dogashima Dacites in ascending order. The Iwachi Tuff is composed of volcanic breccia and tuff breccia, which is intruded by andesitic and dacitic dikes of the Ishibu Intrusives and conformably overlain by andesitic subaqueous autobrecciated lava and tuffaceous sandstone of the Matsuzaki Volcanics. The Dogashima Dacites are composed of volcanic breccia, tuff, tuffaceous sandstone, subaqueous autobrecciated lava and dikes of andesitic

Fig. 1. Map showing location of Izu Peninsula, Japan. Outcrop area of the Shirahama Group shown by ruled pattern (Tsuchi et al. 1986). Selected Quaternary volcanoes shown by solid triangles. The area studied is located near the town of Dogashima of the west coast of the Izu Peninsula.

Fig. 2. Geological map of the western Izu area.

to dacitic compositions. No time gap can be seen between the Matsuzaki Volcanics and the Dogashima Dacites. Layers of andesitic breccia of the Matsuzaki Volcanics can be seen to pinch out in the Dogashima Dacites. So the eruption of the Dogashima Dacites followed just after, or slightly overlapped the eruption of the Matsuzaki Volcanics.

In Dogashima area, a sequence of pumice tuff and volcanic breccia is well exposed. Fig. 3 shows the block diagrams of volcanic sections in the Dogashima area and the distribution of the andesitic volcanic breccia I in which our palaeomagnetic study was carried out. (1) These rocks show a well-sorted texture, that is, most lithic fragments range from lapilli to coarse-sand size; finer particles are depleted. (2) They often show conspicuous vertical grading of pumice and lithic fragments. (3) Cross-bedding develops in the pumice tuff. (4) In volcanic breccia, lithic fragments of boulder size often have thick chilled or fractured rims. (5) Dacitic intrusives are exposed in the adjacent area, which have autobrecciated texture at the margin and change into subaqueous autobrecciated lava. These features, especially (1) and (2), are thought to be characteristic to the products of submarine volcanism.

In Fig. 3 andesitic brecciated lava of the Matsuzaki Volcanics and the andesitic volcanic breccia I of the Dogashima Dacites become thinner toward the north. The Dogashima Dacites contain blocks of andesitic lava of the Matsuzaki Volcanics at site 6 which can be seen to have rolled down the slope of the ancient volcano from south to north. These

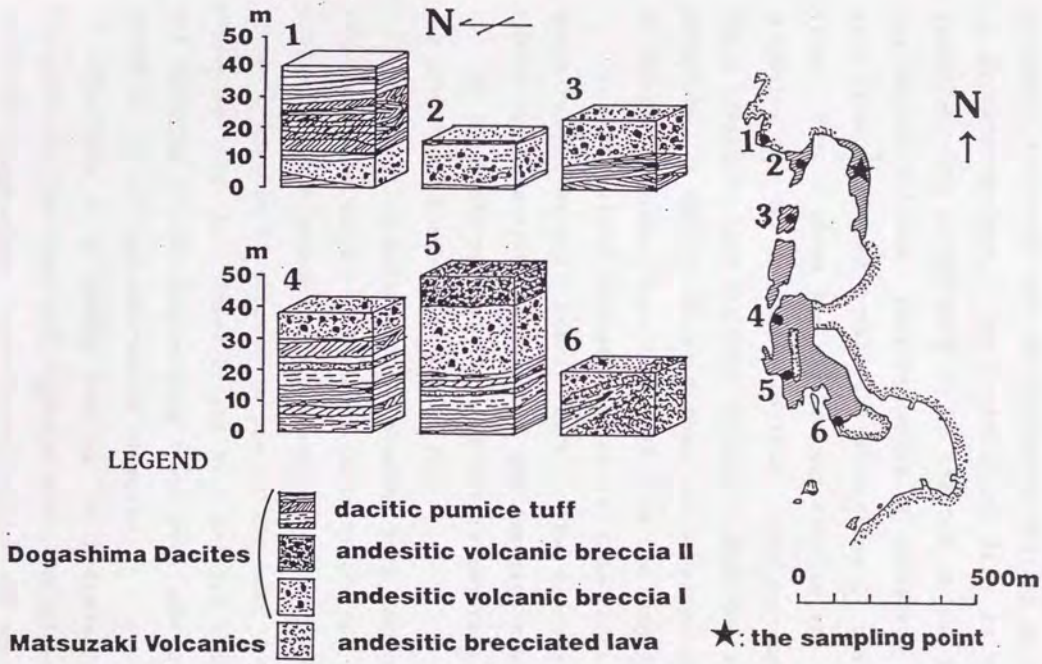

Fig. 3. Block diagrams of volcanic sections in the Dogashima area. The distribution of andesitic volcanic breccia I, in which our paleomagnetic study was done, is shown by the shaded area.

features suggest the locality of eruption center to be in somewhere south of this area. The eruption center of the Matsuzaki Volcanics and the Dogashima Dacites is estimated by palaeogeography. The strikes and dips in these two formations are interpreted to be related to the slopes of the ancient volcano. Because layers of lavas and pyroclastics often pinch out toward the directions of the inclinations. Fig. 4 shows the strikes and dips in the Matsuzaki Volcanics and the Dogashima Dacites. The contours are at equal distances from the area studied. From the geological structure, it can be inferred that the eruption center was in Matsuzaki harbor, 2 or 3 km away from the Dogashima area.

The andesitic volcanic breccia I is interlaid in cross-bedded dacitic pumice tuff. The deposit locally scours the underlying pumice tuff and contains fragments of it. So the basal part of this deposit is interpreted to be the product of a submarine debris flow.

Our detailed paleomagnetic studies were carried out on large andesite blocks (< 5m dia.) contained in the lower 5-8 m of a 10-20 m submarine pyroclastic sequence "andesitic volcanic breccia I" exposed in sea cliffs near the town of Dogashima (Fig. 5). These blocks have chilled glassy rinds and cooling cracks suggesting that they are essential products of a contemporaneous eruption.

The rock is a quartz bearing two pyroxene andesite (SiO_2=62 wt%, FeO^*/MgO=2.5, K_2O=1.0 wt%), containing phenocrysts of plagioclase, hypersthene, augite and titanomagnetite and rarely quartz and ilmenite. It shows porphyritic

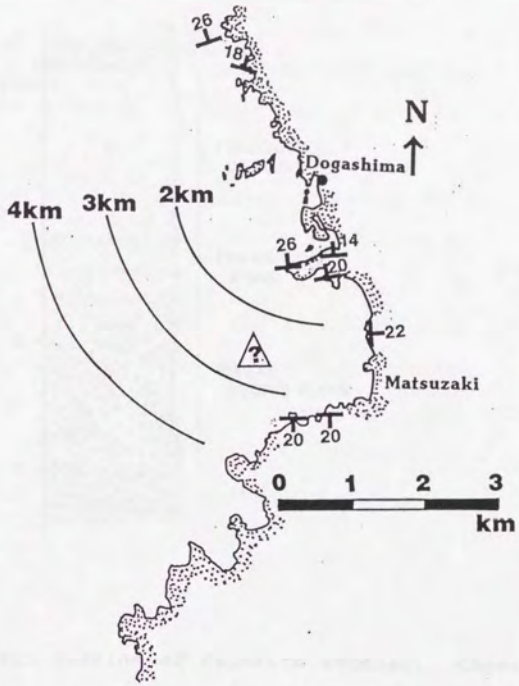

Fig. 4. Geological structure of the Shirahama Group in the Dogashima area. The contours are equal distances from the sampling point. Triangle is the infered eruption center of Matsuzaki Volcanics and Dogashima Dacites.

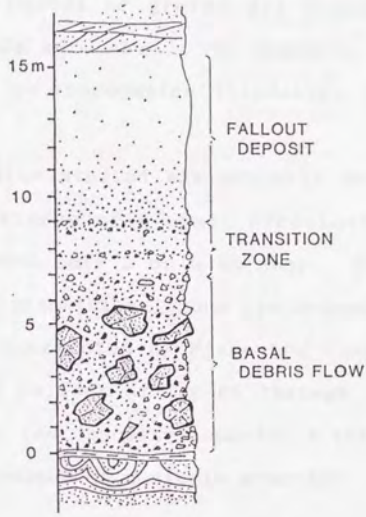

Fig. 5. Schematic section of deposits studied. Cores for paleomagnatic studies were obtained from large andesite blocks in the basal debris-flow deposit. The overlying transition zone, fallout deposit, as well as the basal debris-flow deposit, have been interpreted to be the product of a single eruption from a nearby submarine volcano (Fiske and Cashman, 1989).

texture and fresh brown glass occurs in interstices between grains of clustered phenocrysts. Phenocrysts of titano-magnetite are euhedral to subhedral and smaller than 0.2 mm in length. The inside of grains are homogeneous and no alteration minerals were seen. The magmatic temperature by the two pyroxene geothermometer (Lindsley, 1983) is about 850 °C.

The debris flow studied was probably deposited on the upper, proximal slopes of a small pyroclastic cone whose summit may have been only 2 or 3 km away. The debris flow and the overlying transitional zone are capped by a 5m layer of lapillistone interpreted by Fiske and Cashman (1989) to be the product of fallout of tephra through the water column. All three of the deposits comprising this sequence are interpreted the product of a single eruption.

Procedure

6-13 oriented cores were obtained from each of 6 large blocks, each at least 80 cm in maximum dimention (Fig. 6). The deposit is so fresh that erosional surfaces do not cut through the middle of any of these clasts; cores could therefore taken only from the outermost 10 cm of the blocks. A total of 55 cores was obtained.

All cores were subjected to progressive thermal demagnetization at 50°C intervals from 100° - 600°C using a Schonstedt thermal demagnetizer (model TSD-1). A magnetic field intensity of about 10 nT was maintained in the cooling chamber. The remanent magnetizations of the cores were measured with a ring-core-type fluxgale spinner magnetometer at the Earthquake Research Institute, University of Tokyo.

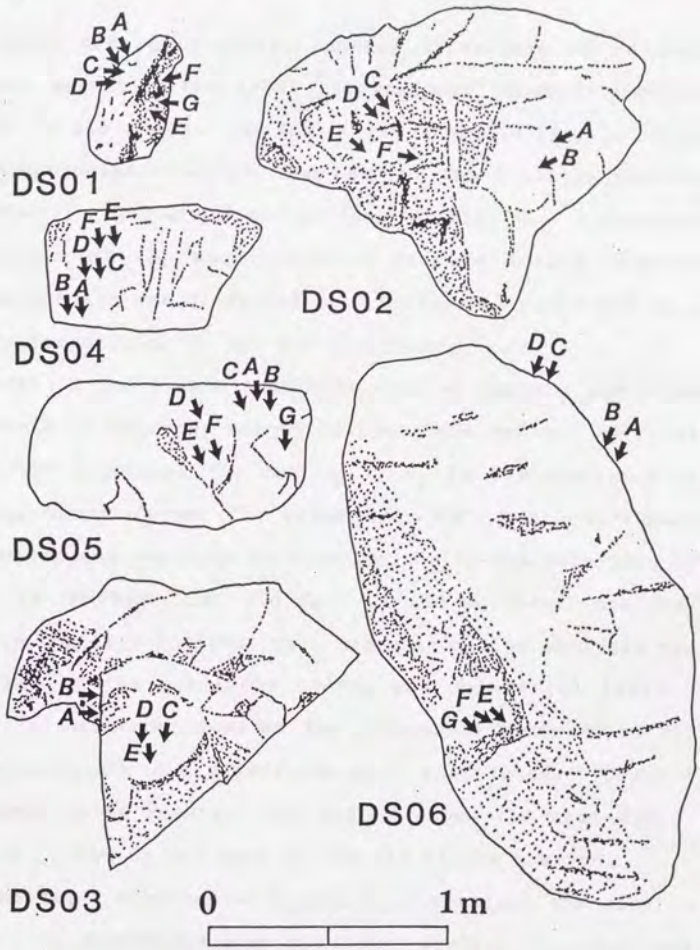

Fig. 6. Six blocks in the volcanic breccia of the Dogashima Dacites in which paleomagnetic samples are taken. Arrows point to the locations of sampled cores.

Results

Equal area projections showing directions of natural remanent magnetization (NRM) and residual remanent vectors at 200° or 250°, 450°, and 500° C are shown in Fig. 7. Data from representative cores from each of the 6 blocks studied are shown in orthogonal projections in Fig. 8. Successive end points of the magnetization vectors during thermal demagnetization are projected on a horizontal plane and on a plane perpendicular to the E-W direction.

Figs. 7 and 8 show that most samples contain two major components of remanent magnetization, here defined as first and second component (C_1 and C_2). C_1 is characterized by blocking temperatures (Tb) below 200°-250° C and northward declination and positive inclination; C_2 is characterized by higher Tb (between 250° and 500° C) and southwest declination and negative inclination. Regression line analysis was performed on the sublinear vector end points (at least 3 points) of each component on the orthogonal plots (Fig. 8), and least-square fit directions were calculated. Table 1 summarizes these results, and Fig. 9 shows the mean directions of C_1 and C_2 for each of the six blocks sampled.

The tight clusters of C_1 and C_2 directions are seen in Fig. 9. C_1 directions show the least scatter (A_{95}=2.5) and align closely with the axial geocentric dipole field at the present latitude. In contrast, C_2 directions have reversed polarity and declinations that are deflected clockwise from the present geographical north. The deflection angle is

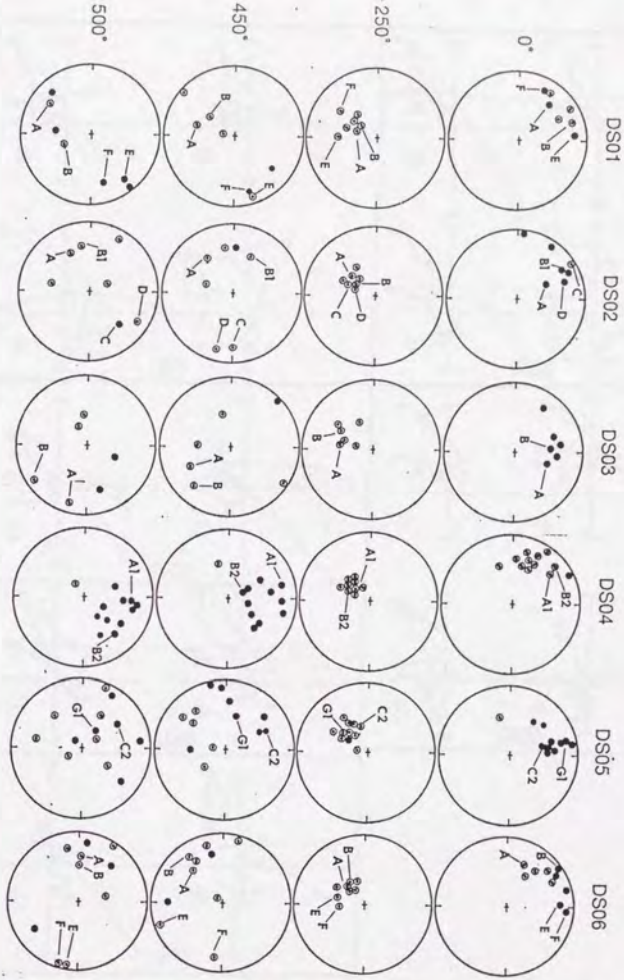

Fig. 7. Equal-area projections showing directons of NRM and residual remanent vectors at 500°, 450°, and 250° C; solid and open symbols represent projections on lower and upper hemispheres, respectively. Letters show results from representative cores obtained from different parts of the 6 andesite blocks studied.

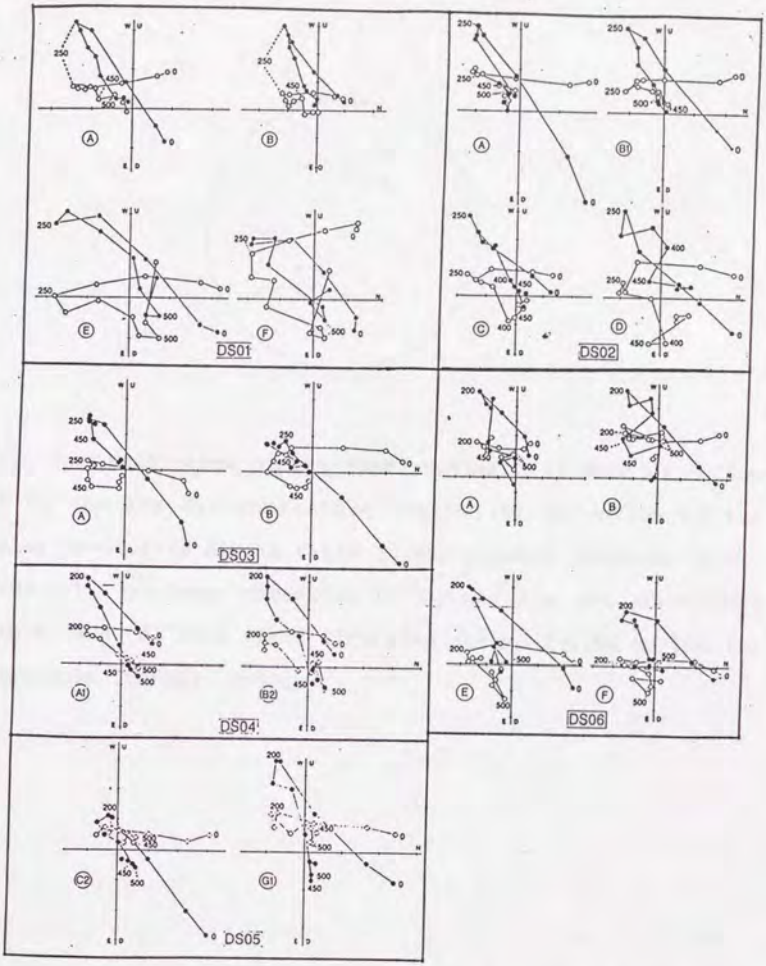

Fig. 8. Orthogonal projections of successive end points of magnetization vectors obtained during progressive thermal demagnetization of representative samples. Open circles are projections to a horizontal plane; solid circles are projections to a north-south vertical plane. Unit of the scale is 1×10^{-4} kA/m.

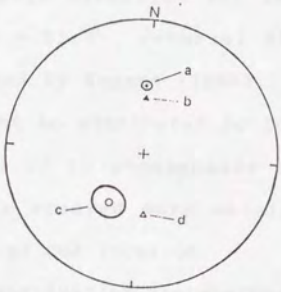

Fig. 9. Equal-area projections showing: (a) mean direction of C_1 and its 95% confidence limit, (b) direction of the axial geocentric dipole field at the present latitude (D=0°, I=54.5°), (c) mean direction of C_2 and its 95% confidence limit, and (d) mean field direction during 2-5 Ma on the Izu Peninsula (Koyama, 1983).

about 30°, seems to be discordant significantly with the Pliocene paleomagnetic direction for the upper Shirahama Group (D = 354°, I = 52.7°, reversal directions shown in Fig. 9) as determined by Koyama (1983). The deflection of the declination might be attributed to local tectonic rotation (Koyama, 1983) or to geomagnetic secular variation, because all samples studied were obtained from a single pyroclastic deposit at one location.

At higher demagnetization temperature, there is greater variability in orientations of remanent vectors, but patterns of coherence can still be recognized. For example, cores from DS04 at above 450° C yield vectors that are clustered (A_{95}= 19.8; Fig. 8, Table 1). Non-random, but less-well developed clustering of vectors can be seen in the other blocks as well. Interestingly, cores obtained from nearby parts of the same block yield similar remanent vectors, and this is shown clearly in Fig. 8. In DS01, cores A and B, separated by only 11 cm, show similar patterns of remanent vectors; the same is true for cores E and F, which are only 26 cm apart. At 450° C, vectors from cores A and B are oriented upward toward SW, whereas at 500° C, vectors from cores E and F, collected from the opposite site of the same block, are oriented downward toward the NE. In block DS02, at 450° C, vectors from cores A and B1, collected from one side of the block, turn upward to the west, whereas cores C and D, from the other side of the block, turn upward to the east. Similarly, cores A and B from block DS06 are oriented toward the west at 500° C, whereas cores E and F,

Block	Jn	Comp.	N	Tb	D	I	k	α_{95}	VGP Lat.	VGP Long.
DS01	1.92×10^{-4}	1	7	RT-250	355.1	+48.5	88.7	6.5	83.1N	2.7W
		2	7	250-500	211.8	-58.7	37.5	10.0	64.5S	29.6E
DS02	2.49×10^{-4}	1	7	RT-250	354.6	+47.3	34.8	10.4	82.0N	4.1W
		2	7	250-500	221.5	-43.7	15.7	15.7	53.2S	52.3E
DS03	3.50×10^{-4}	1	6	RT-200	0.1	+45.3	144	5.6	81.8N	41.3W
		2	4	250-450	193.9	-44.9	40.8	14.6	75.3S	80.8E
DS04	2.59×10^{-4}	1	12	RT-200	358.9	+47.5	100	4.4	83.6N	32.1W
		2	12	250-500	211.8	-54.6	134	3.8	64.1S	39.3E
		3	11	500-600	46.9	+50.0	6.3	19.8	50.7N	138.5W
DS05	2.90×10^{-4}	1	13	RT-200	4.6	+49.2	296	2.4	83.7N	80.0W
		2	13	250-500	196.7	-54.6	23.2	8.8	76.3S	43.8E
DS06	3.14×10^{-4}	1	10	RT-200	1.3	+45.5	171	3.7	81.9N	49.3W
		2	10	200-500	225.0	-65.4	52.2	6.7	54.5S	14.3E
total	2.77×10^{-4}	1	6		359.1	+47.3	729	2.5	83.4N	34.1W
		2	6		209.3	-54.2	53.0	9.3	66.1S	41.1E

Table 1. Summary of paleomagnetic result from each of the six blocks studied (DS01-DS06). Jn, intensity of natural remanent magnetization; Comp., remanent magnetization components obtained by line fitting on each Zijderveld diagram; N, number of specimens; Tb, range of blocking temperature for each component (RT = room temperature); D, I; declination and inclination of each component; k, precision parameter; A_{95}, 95% circle of confidence; VGP Lat., Long.; latitude and longitude of virtual geomagnetic pole.

from the opposite side of the block, are oriented toward the east. Such relationships are summarized in Figs. 10 and 11. Fig. 10 shows the relationship between the distance and the angular difference of the remanent vectors at 450° C and 500° C among all pairs of the samples in each block. Distance between each pair of the samples were measured along the surface of each block. The distance between two samples collected from a single drilled core were measured along the core. Specimens including weathered surface were omitted. Fig. 11 shows the histogram of intensity of remanent magnetization of the samples at the demagnetization temperature of 450° C and 500° C in each block. Blocks can be divided into two categories according to the characteristics of the remanent vectors at higher demagnetization temperature. Blocks DS01, DS02, DS04 and DS06 are included in Category I. In these blocks, closer samples generally have smaller angular differences. Blocks in Category II show no apparent correlation between distance and angular difference and even closer samples have random magnetizations at higher temperatures. DS03 and DS05 are included in this category.

In general, samples collected from the blocks in Category I have higher remanence intensities than those in Category II (Fig. 11).

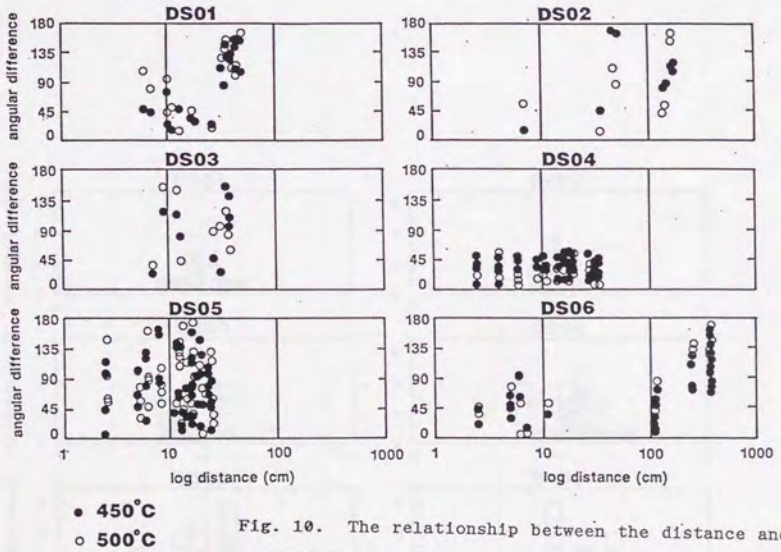

Fig. 10. The relationship between the distance and angular difference of remanent vectors at 450 °C and 500 °C. All pairs of sampled cores are plotted. DS03 and DS05 have no correlation between distances among samples and magnetization at 450 °C and 500 °C. In DS01, DS02, DS04 and DS06, cores obtained from nearby parts of the same block yield similar remanent vectors.

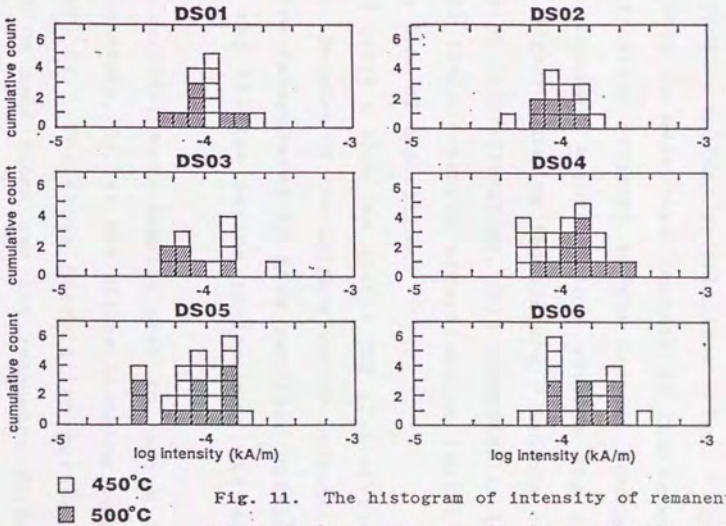

Fig. 11. The histogram of intensity of remanent magnetization of the samples at the demagnetization temperature of 450 °C and 500 °C. At 500 °C, cores of DS03 and DS05 have smaller intensities than other blocks.

DISCUSSION

Vectors removed after thermal demagnetization up to 200-250° C (C_1) are parallel to the present geomagnetic field. After removal of these vectors, a second component emerges (C_2), showing uniform orientations (Figs. 7 and 8). We interpret this to mean that removal of the secondary unstable magnetization parallel to the present geomagnetic field (viscous remanent magnetization) reveals the stable component of a higher blocking temperature. Because of the virtual absence of rock alteration, this component is likely to be the total thermoremanent magnetization (total TRM) acquired at the time of deposition.

Fig. 9 and Table 1 show the stable TRM (C_2) of the six blocks studied. Because of the uniform vector orientations, these blocks are interpreted to have retained sufficient heat, even in the shallow marine environment, to aquire stable TRM's.

As stated earlier, many samples seem to have a third component of remanence, C_3, at the higher blocking temperatures (500°-600° C). The close correlation between the sample location on each block and the remanence direction indicates that C_3 cannot be attributed to noise overprinted during the measurements. Moreover, if C_3 was somehow caused by chemical remanence at a high blocking temperature (despite the freshness of the studied deposit), the large directional scattering of C_3 cannot be explained. Thus, C_3 is most reasonably interpreted as a partial TRM, acquired by

the blocks as they travel downslope.

Ideally, violent rolling down of blocks at higher temperatures may have the effect of "demagnetization". The distinction of Category I and II seems to correlate average remanence intensities of samples at higher temperature. Thus the difference in remanence vectors can be interpreted to mean that blocks in Category II moved more violently than those in Category I at higher temperature before the emplacement.

Thermal history of blocks in submarine pyroclastic deposit

First, andesite block of isotropic sphere which has radius **b** is supposed. The equation of conduction of heat in spherical coordinates is;

$$\frac{\partial u}{\partial t} = k\left(\frac{\partial^2 u}{\partial r^2} + \frac{2}{r}\frac{\partial u}{\partial r}\right)$$

u=u(r,t)=temperature, **r**=distance from the center $0 \leq r \leq b$, k=diffusivity of heat, 6.3×10^{-7} m^2/s for andesite (Kobranova,1989)

The boundary conditions are:

(1) **u(r,0)=800°C**; The andesite sphere was 800°C at t=0.

(2) **u(b,t)=0°C (t>0)**; The surface of sphere is kept 0°C at t>0.

Suppose **u(r,t)=R(r)T(t)** to separate variables,

$$RT'=kT(R''+2R'/r)$$

that is, $T'/kT=(R''+2R'/r)/R=-\lambda^2$ (λ =constant, $\lambda>0$).

Therefor, $T'=-k\lambda^2 T$ (a)

$$R''+2R'/r+\lambda^2 R=0 \quad \text{(b)}$$

The particular solution of (a) is,

$$T=e^{-k\lambda^2 t}$$

In the equation (b), change variables,

$$\lambda r=x,\ R(x)=v(x)x^{-1/2}$$

Then the equation (b) becomes,

$$d^2v/dx^2+1/x\cdot dv/dx+(1-(1/2)^2/x^2)v=0$$

This is the Bessel function of 1/2 order. So,

$$v(x)=J_{1/2}(x)=(2/\pi x)^{1/2}\sin x$$

The particular solution of R(r) is,

$$R(r)=(\lambda r)^{1/2}J_{1/2}(\lambda r)=(2/\pi)^{1/2}\sin\lambda r/\lambda r$$

At the surface of sphere, $u(b,t)=0$, $R(b)=0$. So,

$$\lambda = m\pi/b \quad (m=1,2,3,4,\cdots)$$

General solution of $u(r,t)$ is expressed by,

$$u(r,t)=\sum_{m=1}^{\infty} A_m \frac{\sin\frac{m\pi}{b}r}{\frac{m\pi}{b}r}\cdot e^{-k\left(\frac{m}{b}\pi\right)^2 t}$$

Then from the boundary condition $u(r,0)=800$,

$$u(r,0)=800=\sum_{m=1}^{\infty} A_m \frac{\sin\frac{m\pi}{b}r}{\frac{m\pi}{b}r}$$

if $2r/b=x$, $0\leq x\leq 2$ and

$$800=\sum_{m=1}^{\infty} A_m \frac{\sin\frac{m\pi}{2}x}{\frac{m\pi}{2}x}$$

$$x=\sum_{m=1}^{\infty} \frac{A_m}{400m\pi}\sin\frac{m\pi}{2}x \qquad (c)$$

In the other hand, $f(x)=x$ $(0<x<2)$ can be expressed by Fourier series,

$$x=\sum_{m=1}^{\infty} b_m \sin\frac{m\pi}{2}x, \qquad b_m=(-1)^{m-1}\frac{4}{m\pi} \qquad (d)$$

By comparing coefficients of (c) with (d),

$$A_m=1600(-1)^{m-1}$$

The solution is,

$$u(r,t)=\sum_{m=1}^{\infty} 1600(-1)^{m-1}\frac{\sin\frac{m\pi}{b}r}{\frac{m\pi}{b}r}\cdot e^{-k\left(\frac{m\pi}{b}\right)^2 t}$$

Fig. 12 and 13 are thermal history of cooling andesitic spheres calculated by this equation. Fig. 12 shows temperatures from core to rim of the sections of spheres which have different radii. As a whole, the thermal history of a cooling sphere is size-dependent; smaller spheres cools more rapidly than bigger ones. The center of the sphere of radius 0.25 m becomes almost ambient temperature (0 ˚C) in one day (1440 minutes), whereas the center of a large sphere of radius 1 m is 761 ˚C.

On the other hand, Fig. 13 shows thermal history of outermost 10 cm of each sphere. The outermost part of a

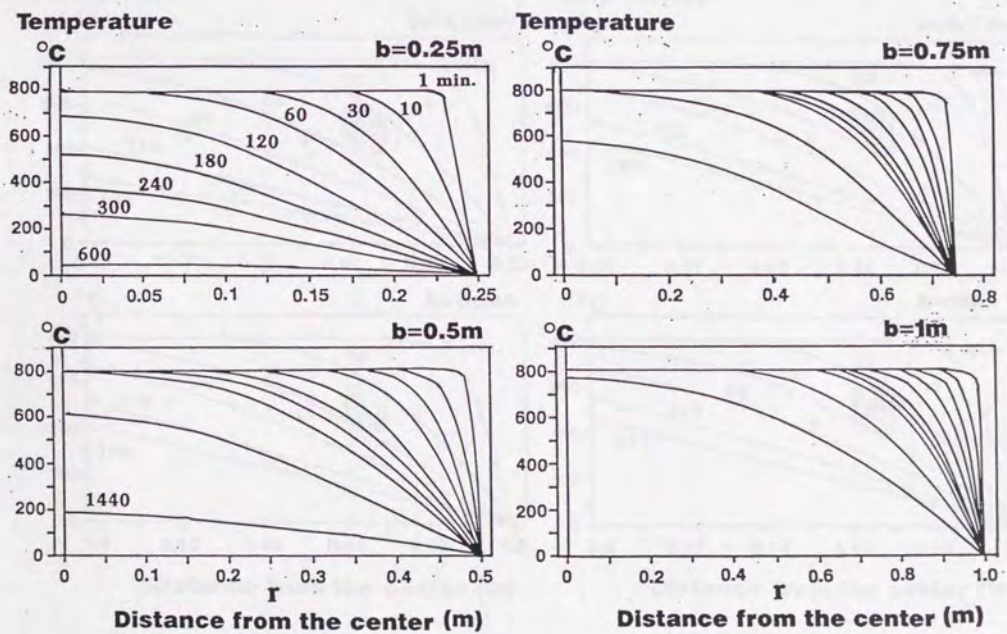

Fig. 12. Thermal history of andesitic spheres of four different radii of 0.25m, 0.5m, 0.75m and 1m at the time from 1 minute to 1 day after quenching.

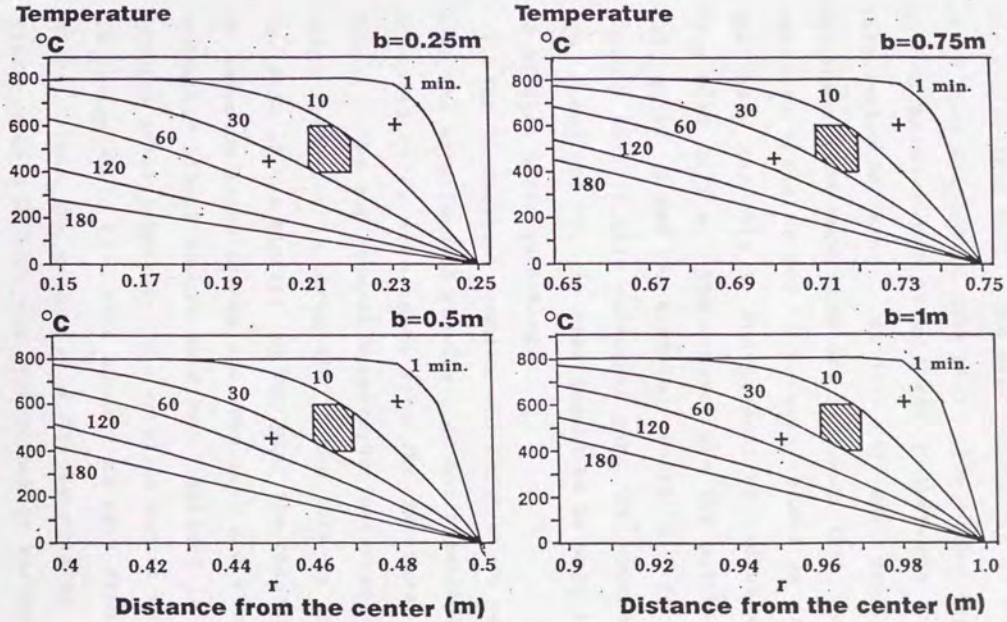

Fig. 13. Thermal history of outermost 10 cm of andesitic spheres of four different radii from 1 minutes to 3 hours. See text for explanations.

sphere has thermal characteristics that are different from the whole inner part. The size-dependency of thermal history is much diluted in this part. The shaded area is inside of b-0.04(m)<r<b-0.03(m), 400 (°C)<T<600 (°C), and 10 (min.)<time<30 (min.). At this outermost part, temperature decreases from more than 600 °C (more than Curie temperature) to close to 400 °C between 10 and 30 minutes after quenching and this is independent of radius size ranging from 0.25 to 1 m. The crosses are the points of r=b-0.05 (m), u=450 °C and r=b-0.02 (m), u=600 °C. We can estimate roughly that if this outermost part has temperature between 450 °C and 600 °C, the time should be between 1 minutes and 60 minutes after quenching.

The theoretical results are instructive and consistent with the experimental results. In our palaeomagnetic study, oriented cores were taken from the outermost 5 cm of the blocks. The emplacement temperature measured by palaeomagnetic technique is about 450 °C and this is independent of the size of the blocks. By applying the theoretical results by assuming these blocks are spherical and isotropic, these andesitic blocks should have been emplaced in less than 60 minutes after eruption. The eruption center of this deposit is estimated to have been about 3 km away from the sampling point. Then the velocity of blocks rolling downslope is faster than 3 km/hour and slower than 20 km/hour. This slow mode of transportation would have made it possible to acquire the third component of TRM in these blocks. And a little anisotoropy in cooling history would be sufficient to

produce the characteristics stated before.

CONCLUSION

We conclude that the studied blocks were hot (450°-500° C) when deposited, and therefore the pyroclastic debris flow in which they are contained was the direct procuct of a contemporaneous eruption. Our findings demonstrate that freshly erupted volcanic material can retain significant heat while being transported in the marine environment, especially if the essential clasts are large, relatively impermeable, and are deposited close to the eruptive vent. The thickening and coarsening of the pyroclastic debris flow towards the southwest and other geological informations suggest that the eruptive vent may have been only 2 or 3 km away.

In other studies, two components of TRM have been attributed to reheating of fragments incorporated in a pyroclastic flow or fall (e.g. McClelland and Druitt, 1989). In our study, the comparison of TRM's of multiple samples collected from differnt parts of the same blocks indicates a single cooling history from magmatic to ambient temperature-- complicated by differing cooling rates and continuing downslope motion of the essential blocks as their TRM's were acquired.

PART II

Petrogenesis of volcanic rocks of the Shirahama Group

CHAPTER 0

Mixed and Unmixed: A Tacit Agreement?

The aim of this paper is to reveal the genesis of volcanic rocks of the Shirahama Group. To accomplish this the following steps are taken, each of which except 1 corresponds a chapter.

1. Division of volcanic rocks into mixed and unmixed.
2. Illustration of the dualism of the Shirahama Group by focusing on unmixed rocks.
3. Presentation of mixing processes which are a natural consequence of the dualism of unmixed volcanic rocks.
4. Major-element least squares modellig and trace-element Rayleigh fractionation modelling of crystal fractionation for two distinct magma series.

In the first step, strict division of the volcanic rocks into mixed and unmixed is thought to be impossible only from the petrographical information, and probably meaningless.

The grouping is based on the occurrence of conspicuous reverse zonings of orthopyroxene phenocrysts, which presents the clear evidence that the host rocks are mixed hybrids. The nonoccurrence of them, however, does not always deny the mixing events, which may be obscured by diffusion, or after which orthpyroxene may be crystallized.

Fig. 46 illustrates two magma series which are deduced from crystal fractionation models which assumed two kinds of primary magmas, basalt and high-Mg andesite (Chapter 3).

The dualism discussed in Chapter 1 is presented by

using these possibly unmixed rocks, which have no evidence of magma mixing and can be deduced from crystal fractionation models.

It should be emphasized that Chapter 1 and 2 are composed of observations. The observations themselves have the independent information beyond the biased choice of samples.

Analytical Method

Whole rock major element (10 oxides) and some trace element analysis were carried out by the X-ray flourescence method with Rigaku 3080E3 spectrometer at the Earthquake Research Institute of the University of Tokyo. Details of the analytical method have been reported by Kaneko (1990). Mineral compositions and some glass compositions were determined by electron probe microanalysis, using the JCMA-733mkII at the Geological Institute, University of Tokyo. The analytical procedure is similar to that given by Nakamura and Kushiro (1970), and the corellation factor of Bence and Albee (1968) was applied.

CHAPTER 1

Calcalkaline versus tholeiitic rocks: Petrogenesis of bimodal volcanism in the Shirahama Group.

1.1 GEOLOGICAL SETTING

Izu Peninsula is located on the northern tip of the Philippine Sea plate, which is subducted by the Pacific plate along the Izu-Bonin trench. The late Miocene-Pliocene Shirahama Group is distributed in the southern part of the Izu Peninsula, Japan, and consists chiefly of basaltic to dacitic pyroclastic rocks erupted and deposited in the shallow marine environment (Koyama, 1986; Kano, 1983; Matsumoto et al., 1985; Ito et al., 1984). Fig. 14 presents the simplified geological map and the sampling points in the studied area, southeastern area of the Izu Peninsula. The outline of geology of this area is described in the previous chapter and Kano (1983). The K-Ar ages obtained from the southern end of the Shirahama Group range from 7 to 8 Ma (Kaneoka et al., 1982). Formations in the Shirahama Group of this area are essentially conformable with each other and have nearly horizontal structure as a whole (Kano,1983; Koyama, 1986). As the result of this, Shirahama Group in this area are thought to belong to formations deposited with a limited period of time, which means that they were consisted of a volcano group. There exists little spacial variation of wholerock chemistry which would be recognized on Harker variation diagram, such as spatial difference of

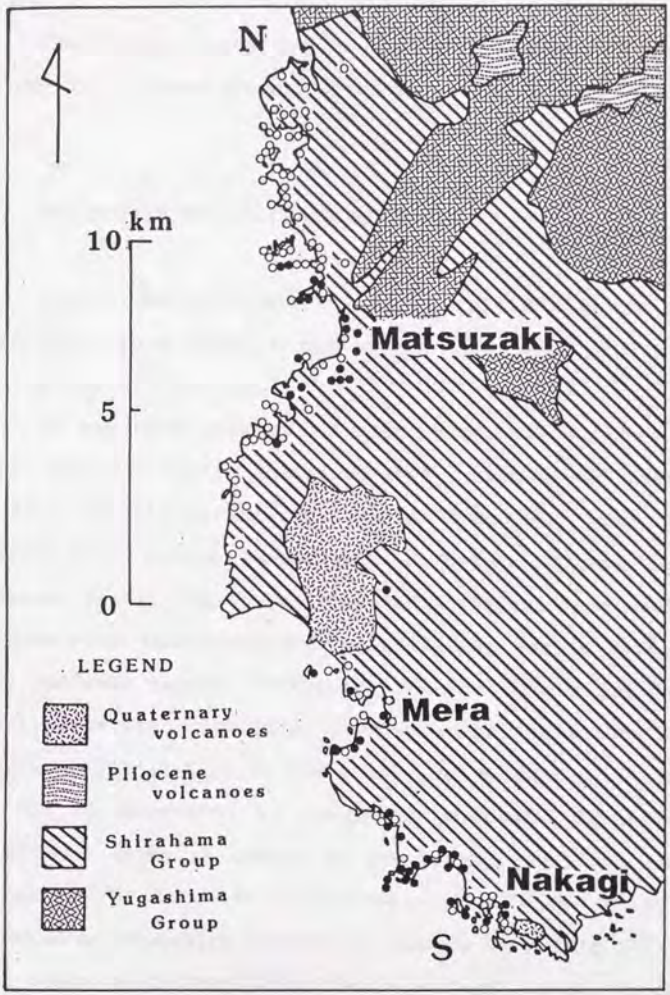

Figure 14. The simplified geological map of the studied area. Black and white points indicate sampled localities. Blacks are tholeiitic and whites are calcalkaline rocks following Miyashiro (1974).

K_2O content at a given SiO_2 content, or of phenocryst assemblage.

The studied area is thought to represent a dsisected island-arc volcano group, which were active from 7 to 8 Ma ago.

1.2 THOLEIITES VS. CALCALKALINE ROCKS

Bulk chemical compositions of volcanic rocks of the Shirahama Group cover a wide range from basalt to dacite, and rarely to rhyolite.

It has been rocognized since Kuno (1950) that there exist two rock series in island-arcs. Kuno (1950) designated them as "pigeonitic rock series (P-series)" and "hypersthenic rock series (H-series)" in Hakone volcano and its adjacent areas. These P-series and H-series are almost synonymous with tholeiitic and calcaklaline series difined in SiO_2-FeO^*/MgO diagram (Miyashiro, 1974). Irvine and Baragar (1971) separated tholeiitic from calcalkaline suites on AFM diagram (A, Na_2O+K_2O; F, $FeO+0.9xFe_2O_3$; M, MgO).

It is essential to recognize that the diversity of island-arc magma is caused by coexisting two magma series. Definition of tholeiitic (TH) vs. calcalkaline (CA) rocks proposed by Miyashiro (1974) is adopted here (Fig.15). The real issue of concern with the island-arc volcanism is the petrogenetic bimodal volcanism. It is arbitrary to divide rocks into TH and CA by the boundary line ($FeO^{\#}$/MgO= $0.1562xSiO_2-6.685$), and it is often meaningless to classify

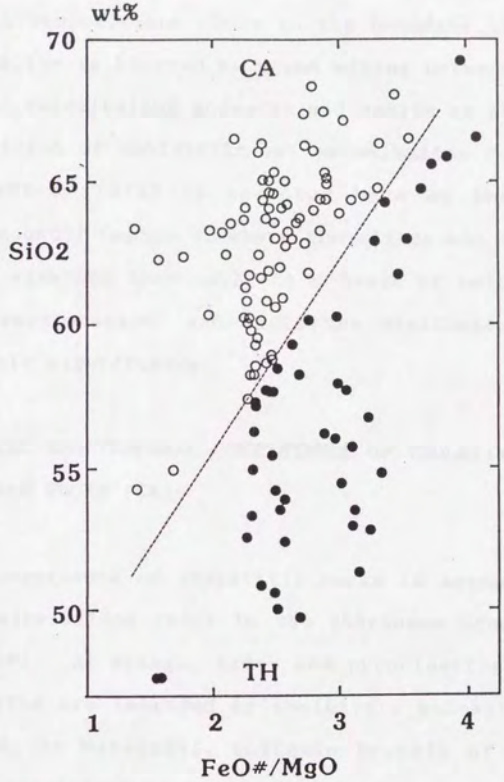

Figure 15. SiO_2 contests vs. $FeO^{\#}/MgO$ ratios in volcanic rocks of the Shirahama Group. The tholeiitic/ calcalkaline division follows Miyashiro (1974).

rocks with compositions close to the boundary. In addition, the bimodality is blurred by magma mixing between tholeiitic basalt and calcalkaline andesite and dacite as stated later. The definition of tholeiitic vs. calcalkaline rocks following Miyashiro (1974) is accepted here as the available compromise until Capter 3, where tholeiites and calcalkaline rocks are examined thoroughly on a basis of calculations of crystal fractionation, and until the distinction has the petrogenetic significance.

1.3 SPACIAL AND TEMPORAL COEXISTENCE OF THOLEIITES (TH) AND CALCALKALINE ROCKS (CA)

The occurrence of tholeiitic rocks is accompanied with that of calcalkaline rocks in the Shirahama Group (Fig. 14 and Fig. 16). At Nakagi, lavas and pyroclastics of calcalkaline dacite are intruded by tholeiitic andesite. On the other hand, at Matsuzaki, volcanic breccia of tholeiitic basalt is overlain by lavas and volcanic breccia of calcalkaline andesite and dacite. Futher more, pumice tuff of calcalkaline dacite is interstratified with scoria tuff of tholeiitic andesite. Basic inclusions of tholeiitic andesite are included in the intrusive rock of calcalkaline dacite. These facts suggest that tholeiitic and calcalkaline magmas were active at the same time, and that they closely coexisted at least in a magma chamber or in a vent.

On the other hand, both Fig. 14 and Fig. 16 suggest that there are two zones, north of Matsuzaki and between

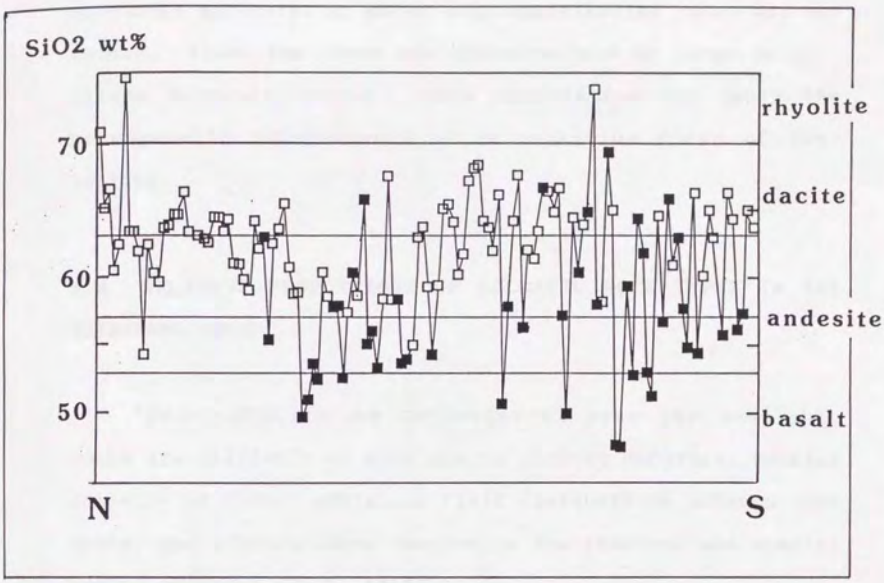

Figure 16 . SiO_2 contents of samples are arranged in order from north to south. Blacks are tholeiitic and whites are calcalkaline rocks. The close association between calcalkalines and tholeiites can be shown spacially.

Matsuzaki and Mera, in which only calcalkaline rocks are obtained. These two zones are characterized by large calcalkaline intrusive rocks. This observation may imply the petrogenetic independence of calcalkaline rocks of tholeiites.

1.4 RELATIVE PROPORTIONS OF VOLCANIC ROCK TYPES IN THE SHIRAHAMA GROUP

"Meaningful volume estimates of even the available rocks are difficult to make due to limited exposure, complex geometry of flows, ambiguous field distinctions between rock types, and arbitrariness concerning the temporal and spacial scales employed (Gill, 1981)."

Rock samples are collected along the coastline so that continuous outcrops may be traced. Large intrusive bodies more than hundred meters in length along the coastline are always composed of calcalkaline rocks, and small dikes less than several meters in length are often composed of tholeiites. Relative volume of tholeiites to calcalkaline rocks never exceeds relative numbers of samples of tholeiites to those of calcalkaline rocks, because tholeiites are less voluminous but more conspicuous than calcalkaline rocks in the field.

Fig. 17 presents relative proportion of volcanic rock types of the Shirahama Group. The length of the rectangle is divided into five, which are basalt, basic andesite, acid

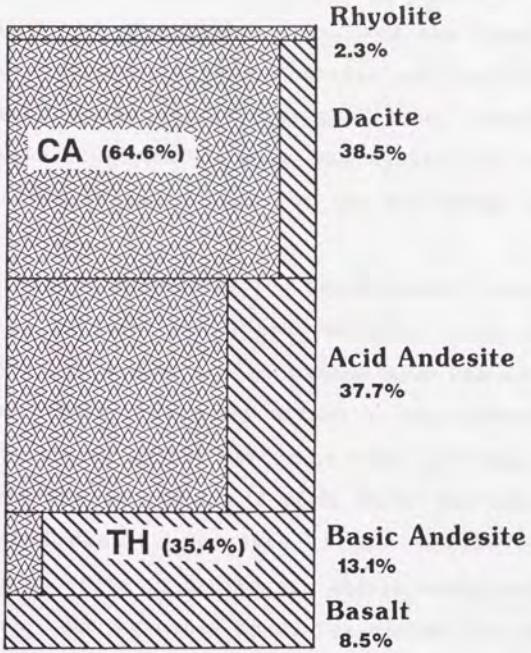

Figure 17. Relative proportions of volcanic rock types of the Shirahama Group based on 127 chemical analyses. The size of each division corresponds to the estimated volume. The domain with oblique lines is tholeiitic and the other is calcalkaline.

andesite, dacite and rhyolite, and the length of each division correspond to the percentage ratio of each rock types. The width of the rectangle is divided into two, which are calcalkaline and tholeiitic rocks, and the length of each division corresponds to the percentage ratio of calcalkaline to tholeiitic rocks in the five rock type. Classification according to SiO_2 content plus the distinction between TH and CA divide volcanic rocks of the Shirahama Group into eight divisions.

Each figure represents the percentage of rock types of 127 samples in total which are collected along the coastline. No great weight can be placed upon the each figure, but the percentage ratio may afford a rough measure of the relative frequency of the different types of rocks.

Apparently the dominant rock types are calcalkaline andesite and dacite. Decrease in the volume ratio from tholeiitic andesite to dacite are mostly explained by crystallization. On the other hand, the explanation of calcalkaline andesite or dacite genesis by fractional crystallization of more mafic parental magmas is obstructed by the fact that acid rocks are much more voluminous than basic ones in the Shirahama Group. This tendency is not unique in the Shirahama Group but general at convergent plate boundaries, suggesting that andesite genesis cannot be explained by differentiation of basalt.

1.5 MINERAL ASSEMBLAGE IN THOLEIITES AND CALCALKACLINE ROCKS

Types of mineral assemblage which occur in 7 divisions of rock types are shown in Fig. 18. The marks representiing mineral assemblages, mainly follow Kuno (1950) and it is mentioned as "+qtz" in Fig. 18 when quartz occurs as rounded or embayed phenocrysts. Specimens without information of groundmass pyroxene phases have glassy groundmass. Absence of hornblende and, or quartz phenocrysts in tholeiites should be recognized as the dualism between tholeiites and calcalkaline rocks.

1.6 THE DUALISM SHOWN IN CHEMICAL COMPOSITION OF MINERALS

As stated before, calcalkaline rocks are distinct from tholeiites both in bulk rock chemistry and mineral assemblage. In this section, chemical composition of phenocrystic minerals common to both tholeiites and calcalkaline rocks is investigated to make the dualism more clear. These minerals are plagioclase, titanomagnetite, augite and hypersthene. Chemical compositions of both core and rim of each mineral are measured by EPMA and plotted in respective figures. FeO^*/MgO ratio (FeO^*: total iron as FeO) is often used as an indicator of differentiation of both tholeiites and boninites (Umino, 1986). From this point of view, it is significant to compare minerals in tholeiitic and calcalkaline rocks which have similar Fe^*O/MgO ratio. Six pairs are picked out to compare tholeiites with calcalkaline rocks on plagioclase, titanomagnetite and augite and two pairs on

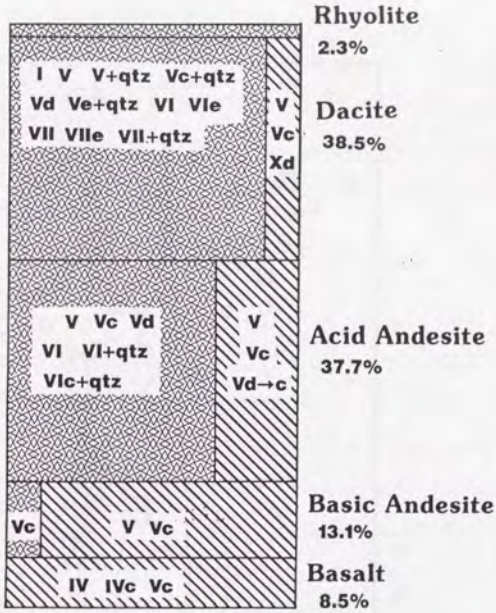

phenocrysts

- **I** Opx
- **IV** Olivine Cpx
- **V** ±Olivine Cpx Opx
- **VI** ±Olivine Cpx Opx Hornblende
- **VII** ±Olivine Opx Hornblende
- **X** Cpx

groundmass

- **c** Cpx
- **d** Cpx Opx
- **e** Opx

Figure 18. Types of mineral assemblage which occur in 7 divisions of rock types. The marks which indicate types of assemblage follow Kuno (1950).

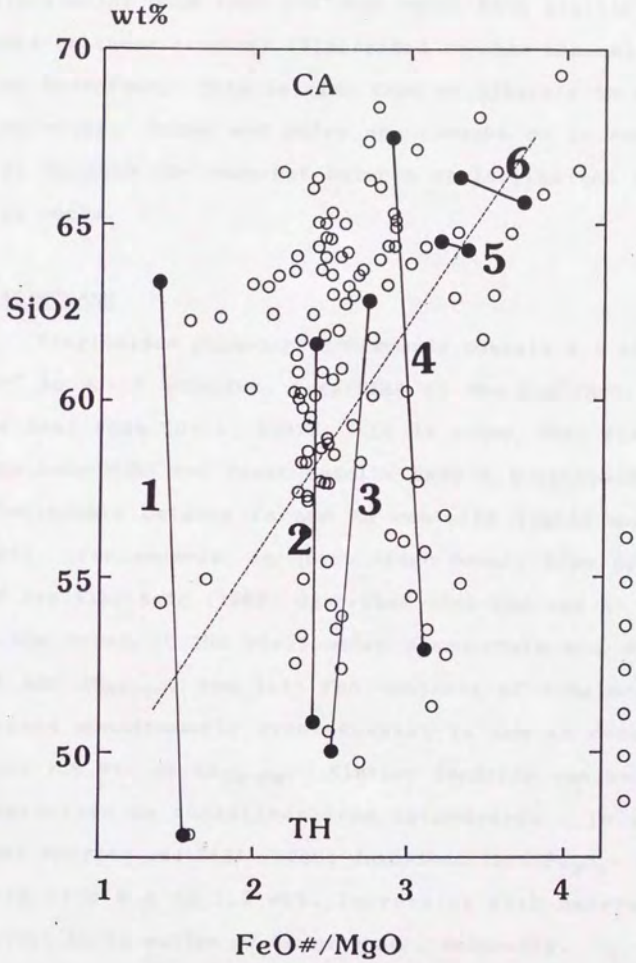

Figure 19. Six pairs picked out to compare TH with CA in terms of chemical composition of phenocrysts of plagioclase, titanomagnetite and augite.

hypersthene (Figures 19 and 23). Minerals in tholeiites with similar bulk rock FeO^*/MgO ratio have similar compositions on these diagrams illustrated to show mineral composition hereafter. This is also true of minerals in calcalkaline rocks. These six pairs are thought to be representative to show the contrast between tholeiites and calcalkaline rocks.

PLAGIOCLASE

Plagioclase phenocrysts commonly contain 0.5 to 1.0 wt% FeO^* in solid solution, regardles of the FeO^*/MgO ratio of the host rock (Gill, 1981). It is known that plagioclase from many MORB and lunar basalts have a continuous inverse relationship between Fe and An contents (Smith and Brown, 1988). For example, in ocean ridge basalt from Hole 504B, ODP leg 111, Sato (1989) described that FeO and An contents of the cores of the plagiocalse phenocrysts are about 0.4 wt% and An_{80-88}, and that FeO contents of plagioclase increases monotonously with decrease in the An contents to about 1.0 wt% at An_{50-60}. Similar tendency can be seen on plagioclase in tholeiites from island-arcs. In a recent paper Morrice and Gill (1986) described that Fe_2O_3- contents range from 0.4 to 1.3 wt%, increasing with decreasing An content in TH suites of Sangihe arc, Indonesia.

Longhi et al. (1976) experimentally determined distribution coefficients for Fe and Mg between plagioclase and basaltic liquid for lunar, terrestrial and synthetic systems. One of their results is that with increase of oxygen

fugacity, ferric iron becomes important and Fe^{3+} is preferentially incorporated into plagioclase with respect to Mg.

Little work, however, has been done on dependence of FeO^*-contents of plagioclase on magmatic composition and temperature in combination with oxygen fugacity.

Figure 20 illustrates FeO content of plagioclase from 12 volcanic rocks plotted against major element content. These 6 pairs are thought to be representative to bring out the contrast between TH and CA. Host magma are differentiated with regard to FeO^*/MgO ratio from 1 to 6. It is apparent that plagioclase phenocrysts in tholeiites have higher FeO content than those in calcalkaline rocks. Concerning tholeiitic basalt and andesite, plagioclase has a inverse relationship between Fe and An content (black points in 1,2,3 and 4 in Fig. 20), and this is the same tendency with plagioclase in MORB and other tholeiitic rocks. Plagioclase from calcalkaline rocks shows the opposite relationship to tholeiitic rocks. They have a positive correlation between Fe and An contents. Differentiated tholeiites (5 and 6) bear plagioclase phenocrysts having lower FeO content than relatively primitive tholeiitic basalt and andesite but still have more FeO-rich plagioclase than calcalkaline dacite.

Although it is ambiguous what causes the difference of FeO content to plagioclase in volcanic rocks which have wide compositional range, systematic difference between tholeiites and calcalkaline rocks indicates that it would be resulted from a combination of oxygen fugacity, magmatic

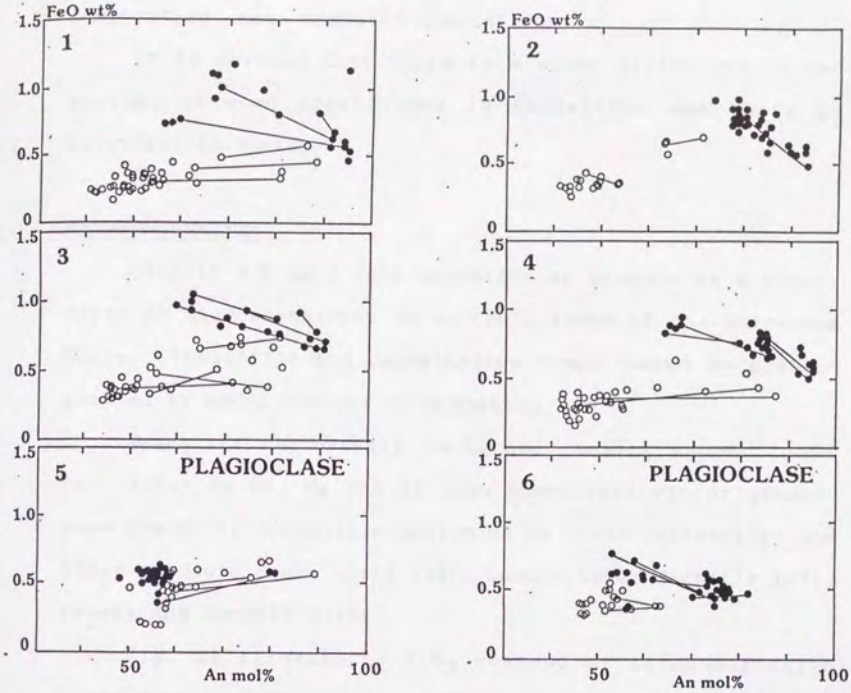

Figure 20. FeO content of plagioclase from 12 volcanic rocks plotted against An content. Blacks and whites indicate compositions of plagioclase from tholeiitic and calcalkaline rocks. Some normally zoned cores are connected with rims by solid lines. Six pairs correspond to those in Fig. 19.

temperature and magmatic composition.

It is obvious that there is a clear difference in FeO content between plagioclase in tholeiites and those in calcalkaline rocks.

TITANOMAGNETITE

Usually 0.5 to 1 vol% magnetite is present as a phenocryst or microphenocryst in volcanic rocks of the Shirahama Group. Tholeiitic and calcalkaline rocks cannot be distinguished by modal content of magnetite.

Magnetite phenocrysts cores are usually poorer in Ti but richer in Fe, Mg and Al than phenocryst rim or groundmass grains in orogenic andesite as in other terrestrial and lunar volcanic rocks (Gill 1981; Lowder 1970; Nicholls 1971; Prevot and Mergoil 1973).

Fig. 21 illustrates TiO_2 content of titanomagnetite plotted against MgO content. Pairs are the same as those in Fig. 20 and shown in Fig. 19. Titanomagnetite from tholeiites have an inverse relationship between TiO_2 and MgO contents. On the other hand, those from calcalkaline rocks tend to cluster in Fig. 21 and have lower MgO or lower TiO_2 contents than those from tholeiites. Chemical zoning of magnetite from tholeiites is more conspicuous than that from calcalkaline rocks.

AUGITE

Augite is ubiquitous as a phenocryst in basalt, andesite and dacite both in tholeiitic and calcalkaline groups. Fig. 22 illustrates Wo content of augite plotted against Mg

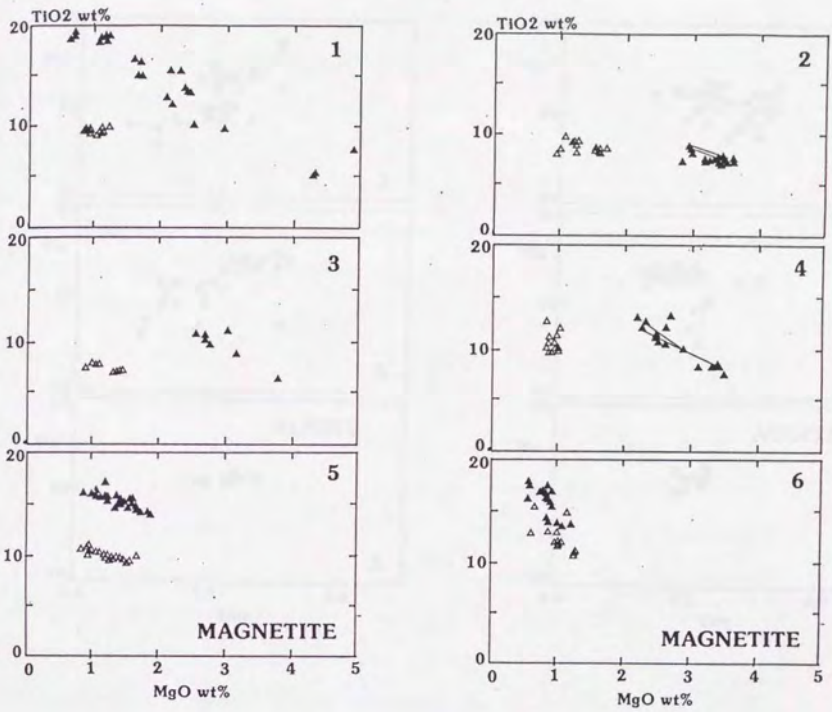

Figure 21. TiO_2 content of titanomagnetite plotted against MgO content. Blacks and whites indicate compositions of titanomagnetite from tholeiitic and calcalkaline rocks. Some normally zoned cores are connected with rims by solid lines. Six pairs correspond to those in Fig. 19.

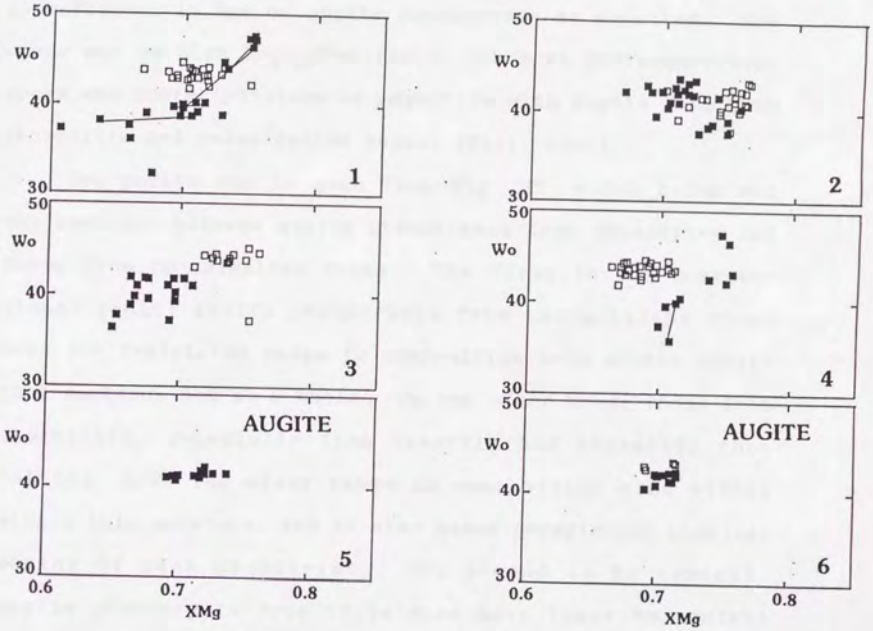

Figure 22. Wo content of augite plotted against Mg value (Mg/(Mg+Fe) mol ratio). Blacks and whites indicate compositions of augite from tholeiitic and calcalkaline rocks. Some normally zoned cores are connected with rims by solid lines. Six pairs correspond to those in Fig. 19.

value. Variations in FeO^*/MgO ratios of whole rocks are not so reflected in Mg# of augite phenocrysts as expected. The cause may be high Fe_2O_3/FeO ratios for more differenrtiated rocks and coprecipitation of magnetite with augite from both tholeiitic and calcalkaline magmas (Gill, 1981).

Two points can be seen from Fig. 22, which bring out the contrast between augite phenocrysts from tholeiites and those from calcalkaline rocks. The first is the compositional range: augite phenocrysts from calcalkaline rocks have the restricted range in composition both within single thin sections and as a whole. On the other hand, those from tholeiites, especially from basaltic and andesitic tholeiites, have the wider range in composition even within single thin sections, and it also means conspicuous chemical zoning of each phenocryst. The second is Wo content. Augite phenocrysts from tholeiites have lower Wo content than those from calcalkaline rocks. This is much clear in rocks with two-pyroxene phenocrysts as illustrated in Fig. 24 and is roughly applied for those augite phenocrysts which do not coexist with orthpyroxene.

ORTHOPYROXENE

Orthopyroxene is always present as phenocrysts in andesite and dacite with rare exceptions but rather rare in basalt and basic andesite. Fig. 23 illustrates 2 pairs of volcanic rocks representative to compare chemistries of hypersthene phenocrysts from tholeiites with those from calcalkaline rocks. It is apparent that Wo contents are

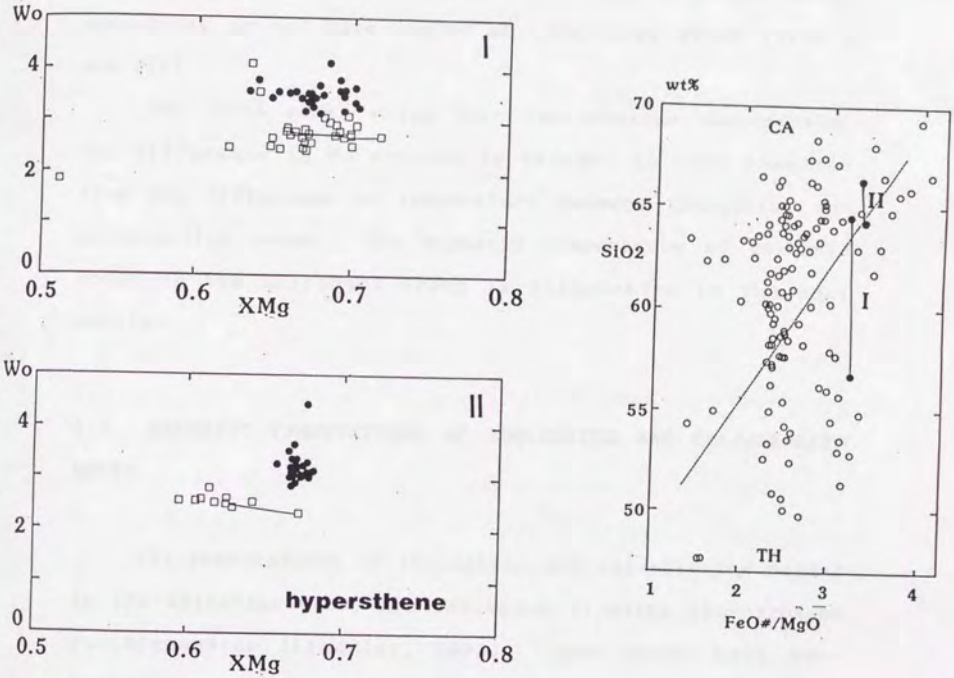

Figure 23. The right illustrates 2 pairs of volcanic rocks to compare hypersthene phenocrysts between tholeiiites and calcalkaline rocks. The left illustrate Wo content of hypersthene plotted against Mg value. Blacks and whites indicate compositions of hypersthene from tholeiitic and calcalkaline rocks.

higher in tholeiites than calcalkaline rocks. As be shown in Fig. 6, some calcalkaline dacite having orthpyroxene phenocryst do not have augite as coexisting phase (Type I and VII).

For those rocks which bear two-pyroxene phenocrysts, the difference in Wo content is thought to have resulted from the difference of temperature between tholeiites and calcalkaline rocks. The magmatic temperature of volcanic rocks in the Shirahama Group is illustrated in the next section.

1.7 MAGMATIC TEMPETATURES OF THOLEIITES AND CALCALKALINE ROCKS

The temperatures of tholeiitic and calcalkaline magmas in the Shirahama Group are estimated by using two-pyroxene geothermometer (Lindsley, 1983). Some rocks have two-pyroxene phenocrysts which have diverse composition and conspicuous reverse zoning owing to magma mixing (Chapter 2). It is often difficult to pick out orthopyroxene and augite phenocrysts which are thought to be in equilibrium each other under microscope. Phenocrysts in rocks which do not have the evidence of magma mixing (e.g. conspicuous reverse zoning in hypersthene phenocrysts) have fairly uniform composition and zoning of them are not conspicuous. Accordingly, the average compositions of coexisting orthopyroxene and augite are used respectively as representatives

of these chemistries. The calculated temperature is the magmatic temperature which is represented by average composition of two-pyroxene phenocrysts.

The results are given in Figure 24. As may readily be seen, tholeiites hold much higher temperatures (950-1100 ˚C) than those of calcalkaline rocks (800-900 ˚C). Even the tholeiitic dacite possesses the high temperature about 1000 ˚C. This result reveals that it is not probable to produce calcalkaline andesite by magma mixing between tholeiitic basalt and its derivatives.

Systematic temperature decrease can be seen in tholeiites accompanying the increase of FeO^*/MgO and SiO_2 content from basalt to dacite. It can be explained that this temperature decrease had resulted from differentiation of tholeiitic magma by crystal fractionation (Chapter 3). On the other hand, no systematic temperature decrease can be seen in calcalkaline rocks, which is related with FeO^*/MgO or SiO_2 content. It would be owing to the mode of differentiation of calcalkaline rocks.

Most of calcalkaline rocks except mixed hybrid can be produced by crystal fractionation from parental high-Mg andesite (Chapter 3), but the differentiation paths are diverse from a common parental magma due to the variation in the fraction of minerals to be subtracted. Rocks in calcalkaline field are not always connected each other by crystal fractionation. Compared to the calcalkaline rocks, the differentiation path of tholeiites is narrow, and rocks are often connected each other with crystal fractionation.

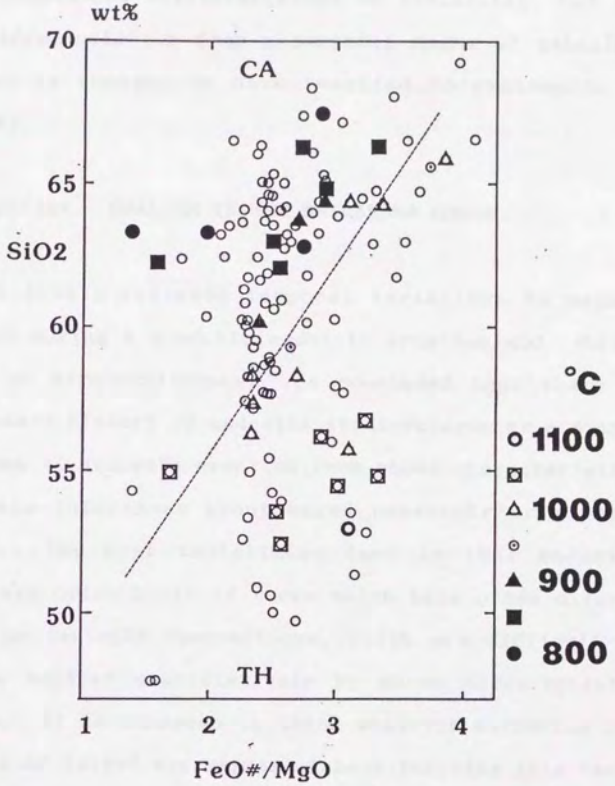

Figure 24. The estimated temperatures of tholeiitic and calcalkaline magmas based on two-pyroxene geothermometer (Lindsley, 1983).

Systematic temperature decrease would have resulted from the monotonous differentiation of tholeiites, but the diverse differentiation from a parental magma of calcalkaline rocks is thought to have resulted no systematic in temperature.

1.8 DISCUSSION. DUALISM IN THE SHIRAHAMA GROUP.

Gill (1981) reviewed temporal variations in magma composition during a historic andesite eruption and during evolution of stratovolcanoes. He concluded that there is not a standard history of andesite stratovolcano or a standard sequence of andesite eruption from whose characteristics one can make inferences about magma reservoir or genetic processes. The most tantalizing fact is that andesite volcanoes are often built of rocks which have often diverse elemental or isotopic compositions, which are difficult to relate one another quantitatively by known differentiaton mechanisms. It is nonsense to think whatever mechanism for the genesis of island arc magmas without pursuing this fact.

For example, if crystal fractionation of basaltic magma were the main process for andesite genesis, temporal variations in magma composition would be expected to start from parental basalt and to end in differentiated products. Accordingly, the history of andesite volcano should reflect the temporal variation in magma composition, with which the formation of stratified magma reservoir is included.

If partial melting of lower crust upon transit of hot

basaltic magma body (tholeiites) were the main process for the generation of calcalkaline magma (Takahashi, 1986), the sequence of magma composition would be expected to be from tholeiitic to calcalkaline if tholeiites is too impatient to wait for calcalkaline magma produced by their own heat.

Temporal and spatial variation in magma composition of the Shirahama Group supports no such inferences stated above. It is emphasized that tholeiitic and calcalkaline magmas coexisted in a close relationship and that calcalkaline magma can occur independently of tholeiites. It is infered that magmas of the Shirahama Group are petrogenetically bimodal.

The dominant rock types are calcalkaline andesite and dacite in the Shirahama Group. This observation is also inconvenient for ideas that the genesis of calcalkaline magma depends on tholeiites, which need crystal fractionation or lower crust melting by voluminous basalt. Even though it is possible to think that large volume of basaltic magma cannot reach to the earth's surface owing to the density filtering of crust, no geophysical data support such phenomenon (existence of large volume of liquid) at the crust-mantle boundary in island-arcs.

The dualism in the volcanism of the Shirahama group is investigated in this chapter. The distinction between tholeiitic and calcalkaline rocks which coexist together in space and time were presented in terms of magmatic temperature, mineral assemblage and chemical composition of phenocrystic minerals. In summary, calcalkaline magma bears

hornblende and quartz phenocrysts and hold lower temperature than tholeiitic magma. The temperature difference between two magma series has been recognized since Kuno (1950), but it is indicated in the Shirahama Group that even tholeiitic dacite has higher temperature (1000 °C) than calcalkaline andesite (800-900 °C). From the thermal relations, it is not probable that calcalkaline andesite is produced by mixing between tholeiitic basalt and dacite. FeO contents in plagioclase from calcalkaline magma are lower than those from tholeiites. TiO_2 or MgO contents or both in magnetite from calcalkaline magma are lower than those from tholeiites. The chemical difference of plagioclase and titanomagnetite between tholeiites and calcalkaline rocks cannot be thought to be attributed to a unique cause. Temperature, oxygen fugacity, magmatic composition and, or combination of these will cause the distinct characteristics of phenocruysts both in tholeiitic and calcalkaline magmas.

Chapter 2

Mixing between calcalkaline and tholeiitic magmas

2.1 INTRODUCTION

The theme of this chapter is to locate magma mixing in the evolution of island-arc magmas. In other words, magma mixing occurs whether between parent and daughter magmas in a sequence of a differentiation of basalt, or between two petrogenetically different magmas.

Magma mixing is a widespread igneous phenomenon in island-arcs (e.g. Eichelberger, 1978; Sakuyama, 1981; Koyaguchi, 1984), which is thought to be closely related to the genesis of andesite. Sakuyama (1981) concluded that some rocks of the H-series (equivalent to the calcalkaline rock series) in Japan represent magmas formed by mixing. On the other hand, Morrice and Gill (1986) indicated in the study of the Sangihe arc, Indonesia that alternative explanations are necessary to explain CA characteristics because of the lack of widespread evidence for mixing. It is consequently important to distinguish the effect of magma mixing from other facters such as source material, melting extent and conditions, and fractional crystallization.

In chapter 1, it is presented that two compositionally distinct magmas, calcalkaline and tholeiitic magmas, existed in the same region at the same time. As the result of the

coexistence, hybrid magmas are produced. Anderson (1976) defined magma mixing in the strict sense, as the processes whereby two or more compositionally distinct magmas are mixed together giving rise to a compositionally uniform single magma (uniform melt plus crystals plus gas). Thompson and Dungan (1985) distinguished mingled hybrids from mixed hybrids by degree of homogenization of hybrid magmas. As representative mingled hybrid, they studied inclusions of quenched basalt in rhyodacite at Handkerchief Mesa where both components retain their primary chemical and textual homogeneity outside of the immediate contact zone.

Here magma mixing is used in the broad sense as the process to produce hybrid magma. Hybrid magmas are roughly divided into mingled hybrids and mixed hybrids as indicated by Thompson and Dungan (1985).

In this chapter, examples of mingled hybrids and mixed hybrids in the Shirahama Group are shown. First, it is shown that mixing between calcalkaline and tholeiitic magmas occurs on a scale of outcrop to produce mingled hybrid. An intrusive body of calcalkaline dacite has many dispersed inclusions of basic andesite of tholeiites. Secondly, rocks which have compositions close to the boundary between TH and CA in the Shirahama Group are shown to be mixed hybrids which are characterised by reversly zoned hypersthene phenocrysts. Other phenocrysts from the rocks such as plagioclase, magnetite and augite have intermediate compostions between representative TH and CA, which are presented in

chapter 1.

These observations suggest the role of magma mixing in the Shirahama volcanism. The end members of magma mixing are petrogenetically distinct two magmas, which are tholeiitic and calcalkaline magmas. On the one hand, magma mixing suggest the coexistence of two distinct magma series in a magmatic system, but on the other hand, it obscures the dualism of the island-arc magmas.

2.2 BASIC INCLUSIONS IN DACITE: Mingled hybrid magma in the Shirahama Group.

Basic inclusion and banded pumice are the typical macroscopic disequillibrium features which are recognized as evidence for magma mixing (e.g. Eicherberger 1975, Sakuyama 1984).

A group of dikes and intrusive rocks occur in southern part of the Matsuzaki area, from Ishibu to Hagachizaki. It covers about 8.3 km^2 and most part of it is composed of calcalkaline dacite and andesite of which SiO_2 content ranges from 61 to 68 wt% (Ishibu Intrusives). At the northern tip of the Ishibu Intrusives, along the western coast of Ishibu for 500 m, the dikes of basic andesite and dacite occur with close relationship, both rocks intrude into the same tuff breccia (Iwachi Tuff) in an adjacent distance. Accordingly, in this place, the rocks of the Ishibu Intrusives exceptionally show a wide rang of chemical composition, from tholeiitic basic andesite to calcalkaline dacite,

which have SiO_2 content of 53-65 wt%. In addition to the coexistence with basic intrusives, the dacite intrusive at the west coast of Ishibu is characterized by scattered basic inclusions (Fig. 25). The dacite host is a hornblende-bearing two-pyroxene calcalkaline dacite which has phenocrysts of hornblende, hypersthene, augite, plagioclase and quartz. Quartz phenocrysts are partly corroded. Phenocrysts are embedded in a groundmass of plagioclase microlites with interstitial glass and specks of augite and iron ore. The inclusions are tholeiitic basic andesite and have phenocrysts and microphenocrysts of augite, plagioclase and silica mineral. Microphenocrysts of plagioclase have skeltal texture, which have elongate shapes with hollow inside. Alkali feldspar is found in groundmass though minor in abundance. About 30 vol% of glass is contained in basic inclusions. These textures which have skeletal crystals in a glassy matrix are rare in effusive rocks in the Shirahama Group, which have similar compositions of tholeiitic basic andesite, and are thought to have resulted from rapic cooling (e.g. Lofgren, 1980). These inclusions are 5-40 cm in diameter and have irregular shapes (Fig. 26, 27). Every basic inclusion has a rind of 0.5 to 1 cm thick.

Koyaguchi (1984) concluded that basic inclusions in dacite at the Abu volcano group crystallized after the incorporation of basalt into the host dacite magma in a liquid state because they have finer- grained quenched rim which has the same mineral assemblage and chemical composi-

Figure 25. Basic inclusions in the dacite body of the Ishibu Intrusives. The distribution of basic inclusoins in the intrusive rock is not homogeneous. Inclusions are concentrated in the left side of the intrusive rock. The stem of the hammer in the middle of the figure is 1m long.

Figure 26. Basic inclusions in the dacite body. The width of the figure is 1 m. Every inclusion has a rind of 0.5-1 cm thick which has the mixed composition of basic andesite and surrounding dacite.

Figure 27. Basic inclusion in the dacite body. Some inclusions have irregular concave shapes which indicate that the basic inclusion mingled with dacite magma in a liquid or a semisolic state.

Figure 28. Cross section of hand specimen containing basic inclusion (right) and host dacite (left). The rind of the basic inclusion is apparently shown both on the fresh surface (upper) and on the weathered surface (lower). .

tion as those of the core of inclusions.

These basic inclusions in the Shirahama Group have a different characteristics with those in the Abu volcano group. Under the microscope, the rind is identical with the inner part of the basic inclusion in terms of mineral assemblage and size of phenocrysts or microphenocrysts. It is considered that basic inclusions of 5-40 cm in diameter have experienced a rapid cooling as a whole, but quench rinds have not been formed around them.

A basic inclusion and the host dacite are divided into 10 pieces along the cross section and checked up the chemical compositions (Fig. 28, 29 and 30). Fig. 29 shows the profile of the SiO_2 content. Chemical composition of these 10 pieces are plotted on the Harker diagram in Fig. 30. It is clearly shown that the rind is richer in SiO_2 than the inner part of the basic inclusion. The rind has the composition on the mixing lines between the inner part of basic inclusion and the host dacite in Na_2O, MgO and P_2O_5 in the Harker diagram, but the FeO, K_2O, Al_2O_3, CaO, TiO_2 and MnO contents are substantially deviated from the mixing trend. Heiken and Eichelberger (1980) studied basic inclusion of Chaos Crags and showed that the rind is not a simple linear combination of core and dacite host composition. They concluded that formation of rinds must involve diffusion between host and globule rather than mechanical mixing alone. The same interpretation seems to be applicable to the basic inclusions in the Shirahama Group.

In either case, mechanical mixing or diffusion, it

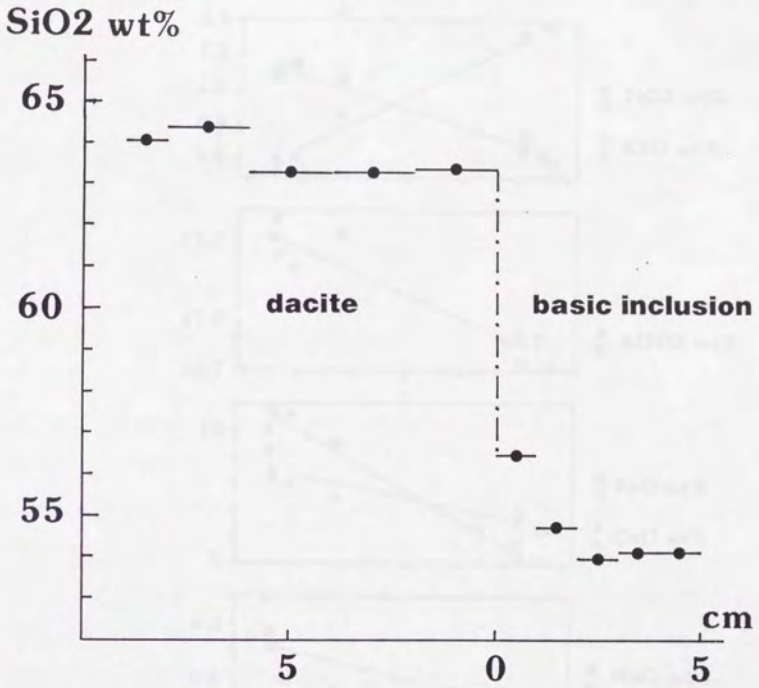

Figure 29. SiO2 content of basic inclusion and host dacite measured along the cross section of Fig. 28. 0 cm of the abscissa is the boundary between the basic inclusion and the host dacite. The just boundary is carefully removed for the measurement to prevent contamination.

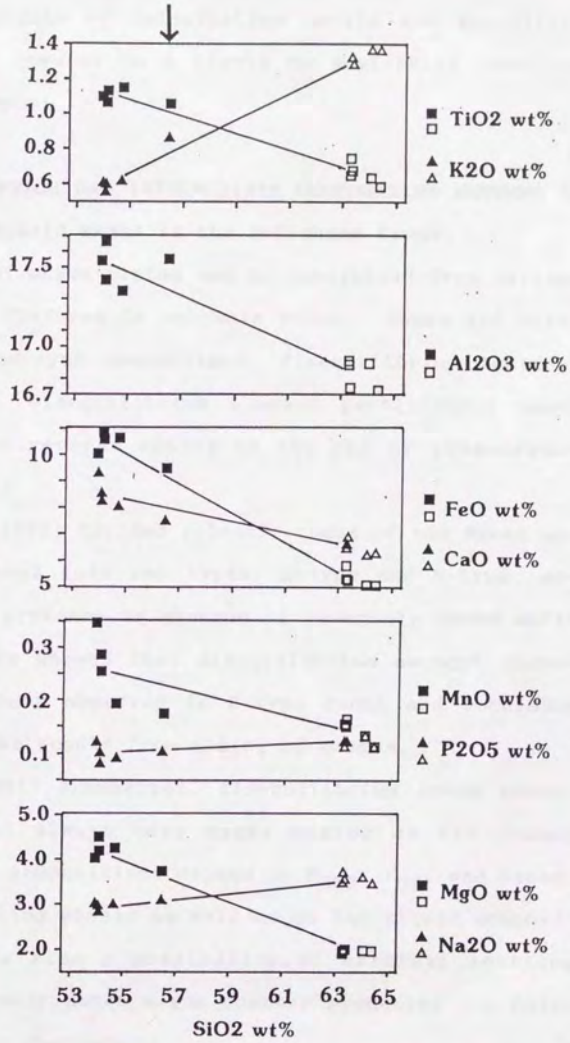

Figure 30. Harker variation diagram of basic inclusion and host dacite. The arrow indicates the chemical composition of the rind of the basic inclusion. Mixing lines are fitted by eye.

requires two magmas of calcalkaline dacite and tholeiitic basic andesite coexist in a liquid or semi-solid state in the magma system.

2.3 ANDESITE WHICH HAS INTERMEDIATE COMPOSITION BETWEEN TH AND CA: Mixed hybrid magma in the Shirahama Group.

Evidence of magma mixing can be recognized from various disequilibrium features in volcanic rocks. Those are disequilibrium phenocryst assemblages, disequilibrium textures in phenocrysts, disequilibrium element partitioning among phenocrysts and reverse zoning on the rim of phenocrysts (Sakuyama, 1984).

Sakuyama (1981) divided volcanic rocks of the Myoko and Kurohime volcanoes into two types, R-type and N-type, according to the presence or absence of reversely zoned mafic phenocrysts. He showed that disequilibrium amongst phenocrysts is commonly observed in R-type rocks and concluded that R-type rocks result from mixing of magmas.

As Gill(1981) summarized, disequilibrium among phenocrysts does not always have magma mixing as its common cause. Mineral compositions depend on P_{H2O}, f_{O2}, and assemblage of coexisting phases as well as on the liquid composition. There is also a possibility of crystasl settling within a chemically zoned magma chamber producing the disequilibrium among phenocrysts.

Even though slight reverse zoning of mafic phenocrysts may be a result from some cause other than magma mixing, the

abrupt and conspicuous reverse zoning strongly indicates mixing of mafic and silicic magmas. As illustrated in Fig. 31, it is rather rare for volcanic rocks in the Shirahama Group not to bear more or less reversely zoned orthopyroxene phenocrysts. Most rocks can be classified into R-type by the presence of reversely zoned mafic phenocrysts, which means that the division into N-type and R-type is not successful in the Shirahama Group. It can be seen clearly, however, that some rocks have orthopyroxenes with conspicuous reverse zonings. These conspicuous reverse zonings are distinct from others, and the presence of these can be an indicator for magma mixing. In this section, conspicuous reverse zoning of orthopyroxene phenocryst (some are more than 10 mol.% En) is adopted as a evidence of magma mixing. Non-occurrence of orthopyroxene phenocrysts with conspicuous reverse zoning does not always deny the mixing event as stated in Chapter 0. Possible unmixed rocks in the Shirahama Group are deduced from the observations (the absence of orthopyroxene phenocrysts with conspicuous reverse zonings) and the crystal fractionation models.

(1) OPX PHENOCRYSTS IN VOLCANIC ROCKS FROM THE SHIRAHAMA GROUP

Chemical compositions of phenocryst and bulk of the host rocks are intimately related in the Shirahama Group. The principal relationships are stated in Chapter 1 as one of the evidence for the dualism of CA and TH in the Shiraha-

ma Group. In this section, reverse zoning of orthopyroxene phenocryst is used as an indicator of magma mixing and then the role of the magma mixing in the evolution of the Shirahama volcanism is infered.

Fig. 31 illustrates compositions of orthopyroxene in tholeiitic and calcalkaline rocks from the Shirahama Group. Orthopyroxene phenocrysts which have conspicuous reverse zonings (some are up to 10 mol.% En) are observed in rocks close to the boundary between TH and CA (e.g., 851208-1, 205 and 51). Fig. 32 shows back scattered electron image of orthopyroxene phenocryst in 205 as an representative example of reverse zoning. In these rocks, orthopyroxene phenocrysts which have core of En_{60} surrounded by 10-40 um rind of En_{70} are often observed. Minor reverse zonings with core-rind difference less than 4 mol.% in En are observed in 311-2 tholeiite. They are not conspicuous as compared with those observed in clearly mixed magmas plotted close to the TH-CA boundary. These rocks are not mentioned in the following discussion in order to make it clear.

Orthopyroxene phenocrysts both in possibly unmixed tholeiites (285-2, 285-1, 312-1 and 311-3) and in possibly unmixed calcalkaline dacite (230, 242, 325 and 330) have narrow compositional range in each rock. Tholeiites, even tholeiitic dacite showing no clear evidence for magma mixing, bear orthopyroxene phenocrysts which have relatively higher and consistent En content (higher than 65 mol.% En) than those in calcalkaline dacite (55-65 mol.% En). From the compositions of orthopyroxene phenocrysts, it is inter-

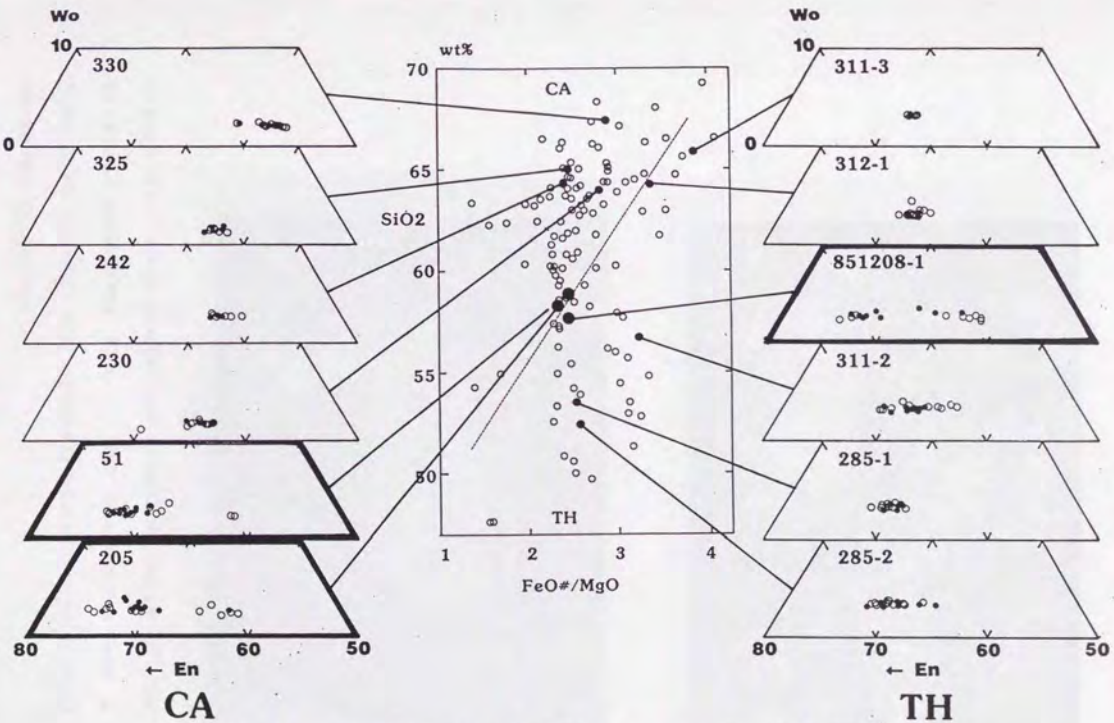

Figure 31. Composition of orthpyroxenes in tholeiitic and calcalkaline rocks from the Shirahama Group. Open and solid circles represent the core and rim of phenocryst. Andesite of 851208-1, 205 and 51 bear Opx phenocrysts which have conspicuous reverse zoning.

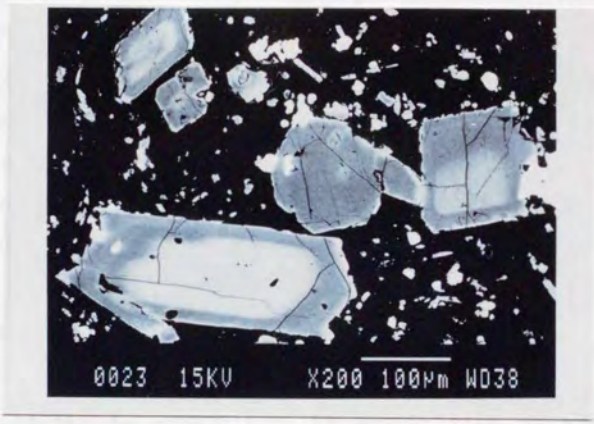

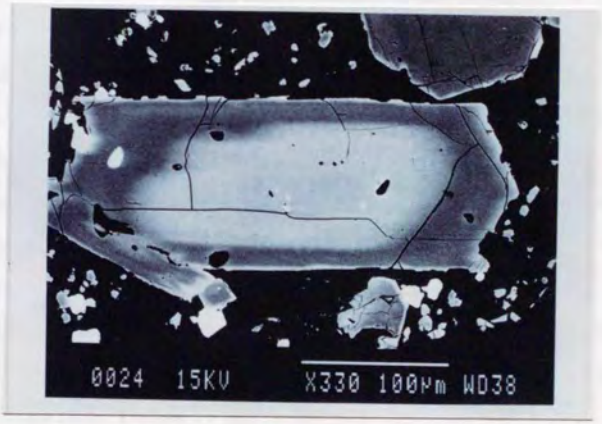

Figure 32. Back scattered electron image of Opx phenocryst in mixed andesitte 205. Opx phenocryst has a chemically flat core (En=62) and reversly zoned Mg-rich rind (En=70) of 10-40 um thickness.

preted that rocks (851208-1, 205 and 51) bearing orthopyroxene phenocrysts with conspicuous reverse zoning are mixed hybrids which have resulted from mixing of mafic and silicic magmas, in this case, tholeiitic basalt or basic andesite and calcalkaline dacite. Cores of the orthopyroxene phenocrysts are thought to be derived from calcalkaline dacite. Mg-rich rinds are formed on them after mixing of calcalkaline dacite and basic tholeiites.

(2) COMPOSITION OF PHENOCRYSTS IN MIXED HYBRIDS AND POSSIBLY UNMIXED ROCKS.

In chapter 1, composition of phenocrysts in possibly unmixed tholeiitic and calcalkaline rocks are discussed and the dualism between CA and TH are presented. This section deals compositions of phenocrysts in mixed hybrids.

Following the same method as Chapter 1, four triplets are picked out to compare minerals in mixed hybrids with those in unmixed TH and CA (Fig. 33). Compositions of plagioclase, titanomagnetite and augite phenocrysts are presented in Fig. 34, 35 and 36.

Plagioclase phenocrysts in mixed hybrids have an intermediate FeO content between those in unmixed tholeiitic and calcalkaline rocks (Fig. 34).

Phenocrysts of titanomagnetite in mixed hybrids also have intermediate compositions between those in unmixed tholeiites and calcalkaline rocks, in terms of TiO_2 and MgO content.

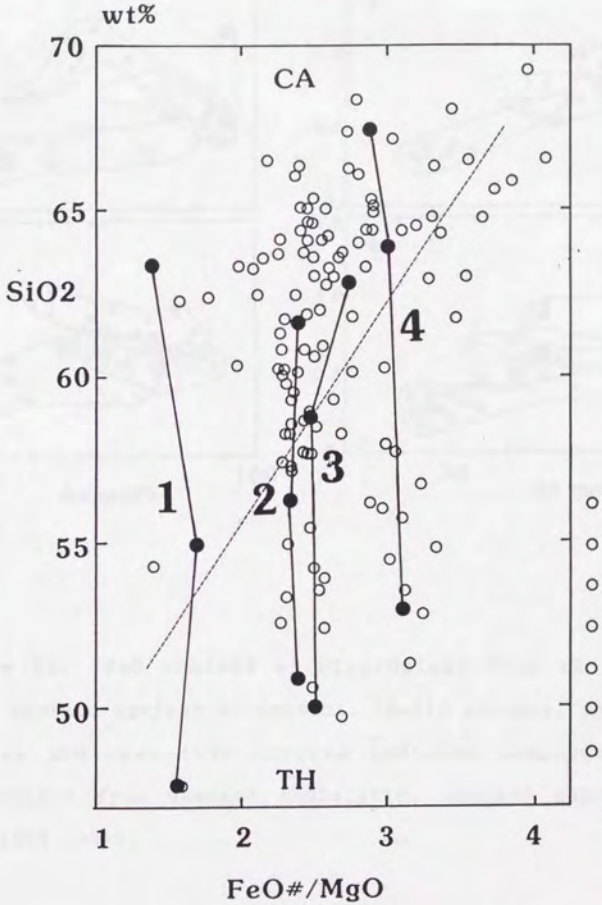

Figure 33. Four pairs picked out to compare mixed rocks with unmixed TH and CA in terms of chemical composition of phenocrysts of plagioclase, titanomagnetite and augite.

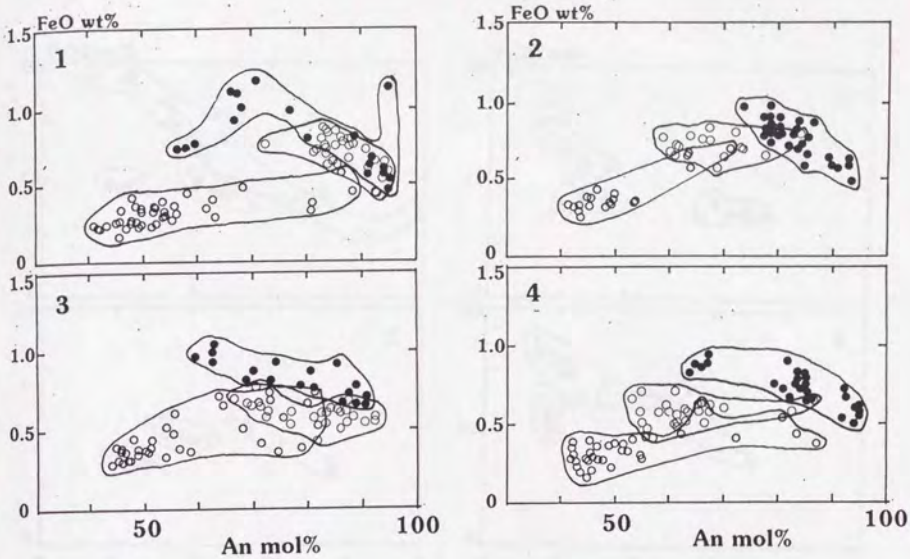

Figure 34. FeO content of plagioclase from 12 volcanic rocks plotted against An content. Solid circles, open thick circles and open thin circles indicate compositions of plagioclase from unmixed tholeiitic, unmixed calcalkaline and mixed rocks.

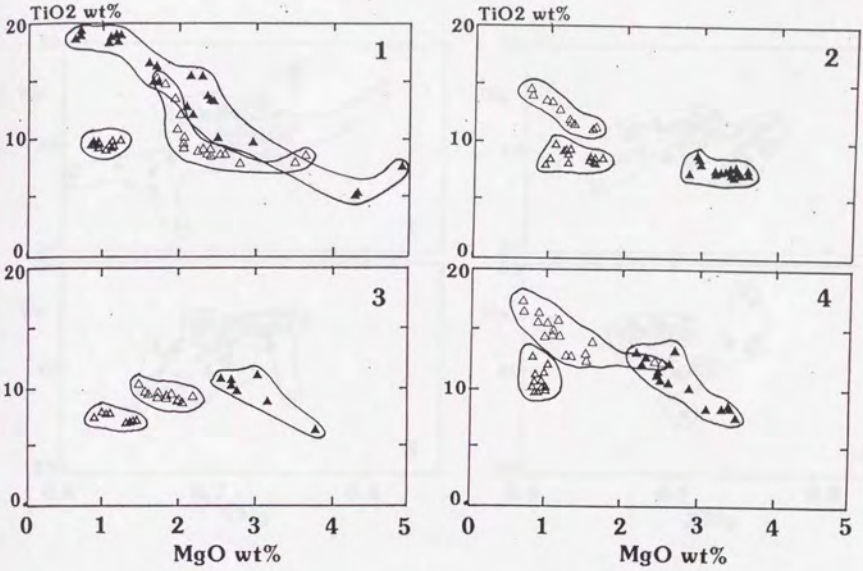

Figure 35. TiO_2 content of titanomagnetite plotted against MgO content. Pairs and distinctions between unmixed TH, CA and mixed rocks are the same as Fig. 34.

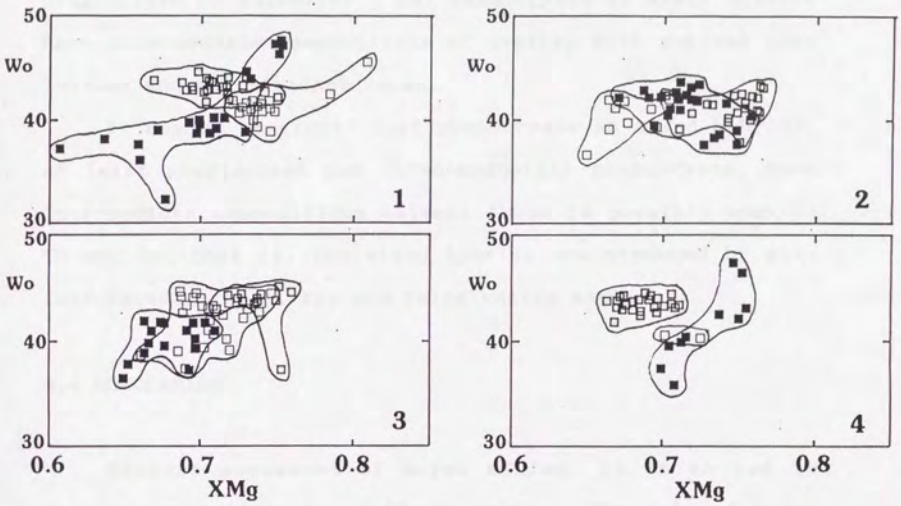

Figure 36. Wo content of augite plotted against Mg value (Mg/(Mg+Fe) mol. ratio). Pairs and distinctions are the same as Fig. 34.

Wo content of augite phenocrysts are not so distinct as plagioclase or magnetite. But phenocrysts in mixed hybrids have intermediate compositions or overlap with unmixed tholeiites and calcalkaline rocks.

It may be concluded that phenocrysts in mixed hybrids, at least plagioclase and titanomagnetite phenocrysts, have intermediate compositions between those in possibly unmixed TH and CA, that is, the mixed hybrids are produced by mixings between tholeiitic and calcalkaline magmas.

2.4 CONCLUSION

Without assesment of magma mixing, it is no use to discuss crystallization differentiation. The role of magma mixing in the evolution of island-arc magmas must be clarified first.

In the Shirahama Group, magma mixing is recognized in basic inclusions in dacite intrusive and in homogeneous two pyroxene andesites bearing conspicuously reversly zoned orthpyroxene phenocrysts. The former is the mingled hybrid and the latter is the mixed hybrid. It is concluded that both mingled and mixed hybrid magmas resulted from mixing between mafic tholeiitic and silicic calcalkaline magmas. In the evolution of island-arc magmas, here in the Shirahama Group, magma mixing occurred between petrogenetically different magmas, which are tholeiitic and calcalkaline. The "calcalkaline trend" in the Shirahama group, which increases SiO_2 content with constant FeO^*/MgO ratio (about 2.5), is

concluded to be a mixing trend between tholeiitic and calcalkaline magmas.

In chapter 1, a dual volcanism of the Shirahama Group is indicated, which is composed of possibly unmixed tholeiitic and possibly unmixed calcalkaline magmas. In this chapter, recognition and implication of magma mixing is presented. In summary, two things must be emphasized here. First, magma mixing indicates that two distinct magmas, one is tholeiitic and the other calcalkaline, exist in the same time at the same place. Magma mixing shows the petrogenetic bimodality of island-arc magmas. Magma mixing is the natural consequence of the dual volcanism of TH and CA magmas. Second, magma mixing itself, on the other hand, makes the dualism of island-arc magmas vague.

Capter 3

The Role of Crystal Fractionation in the Petrogenesis of the Shirahama Group

3.1 INTRODUCTION

In this chapter, the role of crystal fractionation is examined to account for variations in major and trace element contents within volcanic rocks of the Shirahama Group. There are three main problems to be solved.

1. Crystal fractionation in tholeiites.

As summarized in Gill (1981), compositional trends in tholeiitic rocks, from basalt through tholeiitic andesite to tholeiitic dacite, are often successfully modelled by fractional crystallization. Tholeiites in the Shirahama Group are examined to be modeled by simple fractional crystallization.

2. Do calcalkaline rocks or trends result from crystal fractionation of tholeiites?

Gill (1981) concluded that orogenic andesites and their plutonic equivalents result from crystal fractionation of basalt (POAM-fractionation), supplemented to unknown extent by magma mixing, selective interaction with crustal material and vapor fractonation. POAM-fractionation is reexamined

for the Shirahama group on both major and trace element behaviours, whether it can produce the calcalkaline rocks or trends from tholeiites.

3. Do calcalkaline rocks result from crystal fractionation of "boninite"?

Fujinawa (1988) showed that both major-elemental trends in the tholeiitic and calcalkaline series are modeled by fractional crystallization of plagioclase, hypersthene, augite, titanomagnetite and minor olivine. He concluded that tholeiitic magma and calcalkaline magma are not derived from a common parental (tholeiitic) magma and calcalkaline parental magma is richer in SiO_2 and incompatible elements (in particular Rb and Zr).

The rejection of the POAM-fractionations to produce calcalkaline rocks from tholeiites in the Shirahama Group also leads to the same conclusion that calcalkaline parental magma is different from tholeiites.

A primary magma of calcalkaline rocks in the Shirahama Group is examined, and the "boninite" magma is found to be the most likely candidate for the primary magma. The possible composition of the Shirahama "boninite", which can produce most of calcalkaline rocks by crystal fractionation, is estimated.

3.2 METHOD

Crystal fractionation models are based on least squares

solutions to linear mixing equations (Bryan, et al., 1969), wherein phenocryst minerals are subtracted from parental liquid in proportions which result in the closest approximation of derivative liquid compositions.

Results of least squares calculations on major elements are used to determine the fraction of liquid remaining and weight fraction of minerals to remove from starting compositions necessary to explain major element concentration in a evolved magma. Likely changes in trace element concentrations due to Rayleigh-type fractionation are calculated by using those values above, together with distribution coefficients of trace elements betweem phenocrysts and melt.

Table 2 shows crystal/liquid partition coefficients adopted in this calculations. Partition coefficients for K, Rb, Sr, Ba and V are values suggested by Gill(1981). Those for Ti, Zr, Y and Nb are values recommended by Pieace and Norry (1979). Bulk distribution coefficient D can be expressed as

$$D=\sum_{i=1}^{n} w_i K_{Di},$$

where K_{Di} is the partition coefficient and w_i is the weight fraction of mineral i. Total number of phenocrystic minerals involved is represented by n. The concentration of a trace element in the liquid which had undergone the Rayleigh fractionation (C_i) can be expressed as

$$C_i=C_o x F^{(D-1)},$$

where C_o is the concentration of a trace element in the "parent" magma and F is the fraction of melt remaining. The

Phenocryst/matrix partition coefficients

	Plag	Aug	Opx	Ol	Hb	Mt
K	0.11	0.02	0.01	0.01	0.33	0.01
Rb	0.07	0.02	0.02	0.01	0.05	0.01
Sr	1.8	0.08	0.03	0.01	0.23	0.01
Ba	0.16	0.02	0.02	0.01	0.09	0.01
V	0.01	1.1	1.1	0.08	32	30
Ti (basic)	0.04	0.3	0.1	0.02	1.5	7.5
(intermediate)	0.05	0.4	0.25	0.03	3.0	9.0
Zr (basic)	0.01	0.1	0.03	0.01	0.5	(0.1)
(intermediate)	0.03	0.25	0.08	0.01	1.4	0.2
Y (basic)	0.03	0.5	0.2	0.01	1.0	(0.2)
(intermediate)	0.06	1.5	0.45	0.01	2.5	0.5
Nb (basic)	0.01	0.1	0.15	0.01	0.8	(0.4)
(intermediate)	0.025	0.3	0.35	0.01	1.3	1.0

Table 2. Phenocrysts/ matrix partition coefficients adopted in calculations. Partition coefficients for K, Rb, Sr, Ba and V are values suggested by Gill (1981). Those for Ti, Zr, Y and Nb are values recommended by Pieace and Norry (1979).

ratio of a real to an calculated trace element concentration (C/C_i) is examined for K, Rb, Sr, Ba, Ti, Zr, Y, Nb and V. $C/C_i=1$ means that a trace element concentration is equal to the value expected from the Rayleigh crystal fractionation.

Validity of crystal fractionation models are judged from magnitude of sum of square residual in major element least-squares solutions and agreement or disagreement between expected and real trace element concentrations. The sums of square residual for several assumed "daughters" have been compared. Differentiation trend from a "parent" can be indicated as acceptable or invalid according to the relative magnitude of the sum of square residual. The data of trace element (the relative magnitude of C/C_i) are also used to evaluate assumed parent-daughter relationship. In most case, the sum of square residual lower than 0.15 was chosen as an upper limit of acceptability (Fujinawa, 1988). In some cases, most assumed parent-daughter relationship resulted in the sum of square residual more than 0.15, but even in such cases, if an upper limit of acceptability is 0.5, daughters can be clearly divided into two kind with the gap (for example, one is lower than 0.5 and the other is above 1). This means that relative magnitude of the sum of square residual is useful to estimate the differentiation trend from a parent, and no great weight should be placed on the arbitraty upper limit of a sum of square residual. This is the reason why the upper limit of acceptability is almost lower than 0.15, but sometimes it is 0.5.

3.3 CRYSTAL FRACTIONATION MODEL IN THE SHIRAHAMA GROUP

3.3.1 Where do crystal fractionation from tholeiites lead?

Chemical compositions of "parent" magmas, representative phenocrysts in the parents, and of assumed "daughter" magmas and the result of least squares calculations are presented from Tables 3 to 8. The ratio of the observed to the trace element concentrations calculated by using the results of least squares calculations (C/C_i) are also listed in the Tables. From Figs. 37 to 42, the results of crystal fractionation model from tholeiitic basalt (312-4,305 and 313) and tholeiitic andesite (326, 311-2 and 323) are illustrated.

(1) Fractionation starting from 312-4 (Fig. 37, Table 3)

In terms of major element content, the trend from tholeiitic basalt 312-4 to a group of least differentiated SiO_2-poor basalts, indicated as **C** in Fig. 37 may be accounted by crystal fractionation, but trend toward groups **A** or **B** which produce the calcalkaline trend, which have a variation in SiO_2 content with constant FeO^*/MgO ratio, have the sum of squares of the residuals > 0.5, much higher than that toward **C**, which are not acceptable to adopt crystal fractionation model. In terms of trace element, there are also inconsistencies, especially in Zr and V contents, in the trend toward **A** and **B**. The V content is two or three times higher than expected value in **A** and **B**. This is not owing to the adopted distribution coefficient of V shown in Table 2.

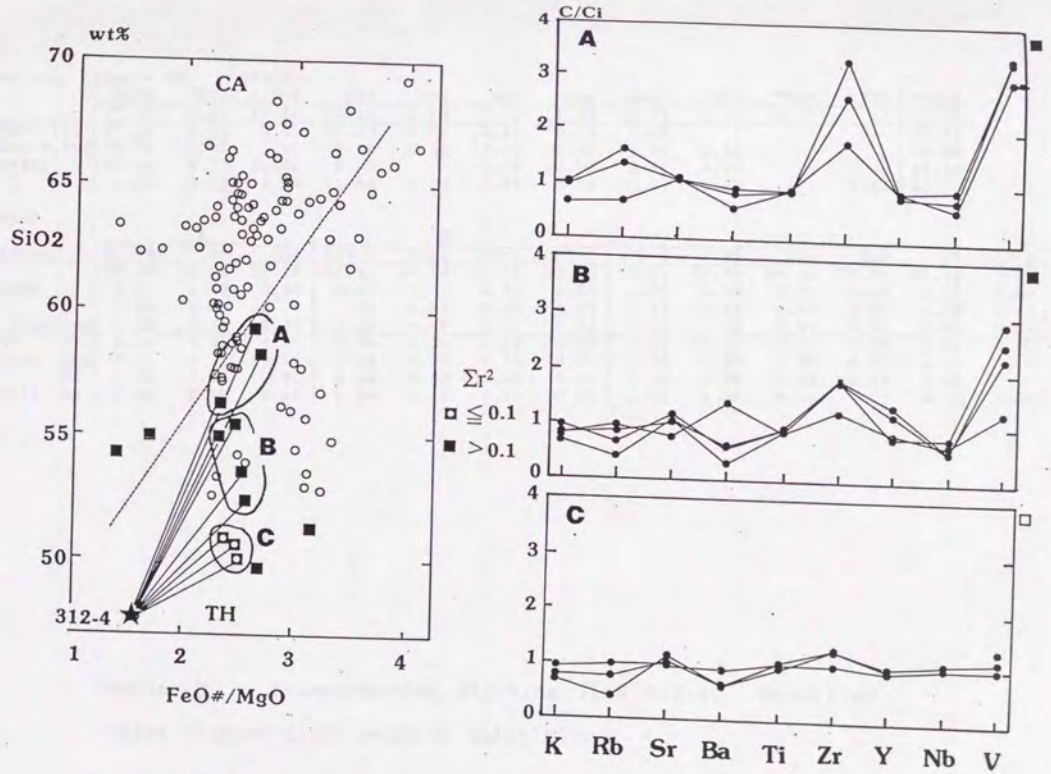

Figure 37. Fractionation starting from 312-4. Result of major element least squares calculations and ratios of real to calculated concentration of trace element through Rayleigh-type fractionation.

Parent	Sample No. 312-4											
	SiO2	TiO2	Al2O3	FeO	MnO	MgO	CaO	Na2O	K2O	P2O5	V2O3	Total
	47.63	0.97	17.39	12.11	0.19	7.72	11.32	2.17	0.39	0.10	-	100.00
Ol(XMg=0.71)	37.27	0.01	0.04	25.38	0.36	34.93	0.13	0.01	-	-	-	98.14
Cpx(XMg=0.75)	48.31	0.71	5.60	8.08	0.18	13.42	22.45	0.24	0.01	-	-	99.06
Pl(An=80)	47.14	0.03	31.46	0.80	-	0.09	16.37	2.17	0.06	-	-	98.16
Mt	0.19	12.73	3.94	71.84	0.38	2.09	0.04	0.04	0.03	-	1.40	92.72

Daughter		A			B				C				
Sample No.	312=4	206	304	284-1	200L	285-1	285-2	255-5	J-28	305	314	49	312-5
SiO2	59.26	58.20	56.19	55.41	54.94	53.55	52.38	50.91	50.64	50.04	51.31	49.75	47.69
FeO*/MgO	2.63	2.68	2.33	2.47	2.32	2.54	2.57	2.38	2.48	2.52	3.14	2.69	1.60
Σr^2	0.98	1.37	0.74	1.20	1.14	0.48	0.62	0.15	0.11	0.08	0.26	0.22	0.10
Melt Fraction	0.32	0.36	0.39	0.44	0.48	0.51	0.64	0.61	0.70	0.67	0.66	0.68	0.98
Weight fraction of minerals Ol	0.19	0.21	0.20	0.20	0.23	0.23	0.32	0.25	0.34	0.31	0.39	0.32	0.91
Cpx	0.21	0.21	0.20	0.28	0.23	0.32	0.30	0.23	0.32	0.22	0.21	0.25	-
Pl	0.51	0.49	0.51	0.43	0.45	0.35	0.27	0.45	0.26	0.43	0.34	0.40	-
Mt	0.09	0.09	0.08	0.09	0.10	0.10	0.11	0.06	0.08	0.04	0.07	0.03	0.09

Table 3 . Fractionation starting from 312-4. Result of major element least squares calculations.

C/C_i of V becomes lower as bulk partition coefficients, mainly affected by magnetite/ matrix partition coefficient, become lower. The range of reported values of magnetite/matrix partition coefficients are 24-60 (Gill, 1981). The adopted value is low enough in this range. The enrichment of V is hard to interpret by crystal fractionation model from basalt 312-4.

The trend toward **C** is acceptable as a fractionation trend from the basalt 312-4, explaining both major and trace element concentrations.

(2) Fractionation starting from 305 (Fig. 38, Table 4)

Major element least squares calculation exhibits that both tholeiitic and calcalkaline trends can be produced by fractionation of olivine, augite, plagioclase and magnetite from tholeiitic basalt 305. (As shown before, "tholeiitic and calcalkaline trends" are used on the basis of their ratio of change of FeO^*/MgO ratios versus SiO_2 contents. They are not the same as tholeiitic and calcalkaline fields defined by Miyashiro (1974).) As is shown in Table 4, weight fraction of fractionated olivine is a little higher and that of magnetite is a little lower in tholeiitic trend **B** than in calcalkaline trend **A**.

Calcalkaline trend **A** is rejected in terms of anomarously enriched V content just like the case with calcalkaline trend from basalt 312-4.

(3) Fractionation starting from 313 (Fig. 39, Table 5)

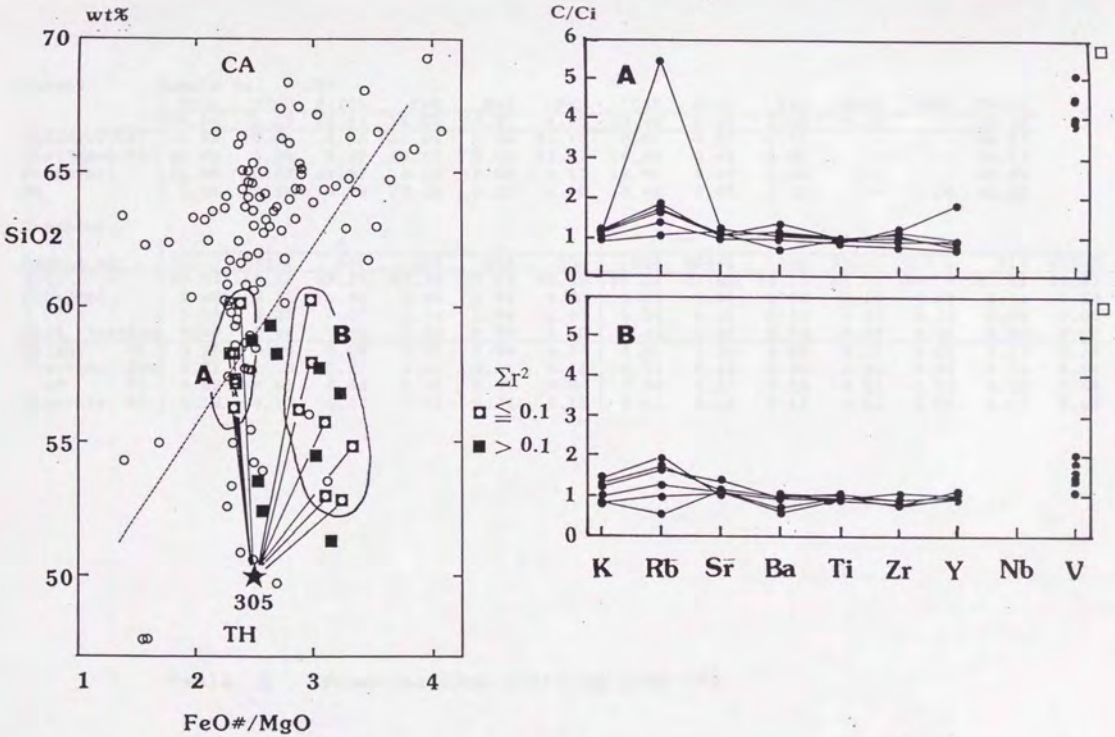

Figure 38 . Fractionation starting from 305.

Parent	Sample No. 305											
	SiO2	TiO2	Al2O3	FeO	MnO	MgO	CaO	Na2O	K2O	P2O5	V2O3	Total
	50.04	1.13	18.51	11.53	0.21	4.58	10.90	2.49	0.46	0.16	-	100.00
Ol(XMg=0.64)	36.55	0.04	0.03	31.06	0.58	31.19	0.30	0.17	0.01	-	-	99.93
Cpx(XMg=0.69)	50.66	0.58	3.45	10.81	0.31	13.77	19.86	0.44	0.01	-	-	99.89
Pl(An=81)	48.35	0.05	31.31	0.84	0.03	0.11	16.74	2.49	0.03	-	-	99.95
Mt	0.18	8.86	4.72	72.28	0.31	3.16	0.04	0.33	0.01	-	1.04	91.02

Daughter				A						B				
Sample No.		319-1	334-2	205	323	306	304	308	334-1	326	322-1	317-1	313	312-2
SiO2		60.07	58.18	58.17	57.29	57.15	56.19	60.20	57.89	56.15	55.71	54.77	52.96	52.82
FeO*/MgO		2.39	2.30	2.34	2.35	2.34	2.33	2.98	2.99	2.89	3.10	3.32	3.10	3.23
Σr^2		0.09	0.05	0.07	0.04	0.08	0.03	0.04	0.03	0.03	0.01	0.10	0.04	0.08
Melt Fraction		0.45	0.49	0.50	0.53	0.52	0.56	0.42	0.49	0.54	0.60	0.58	0.75	0.75
Weight	Ol	0.08	0.08	0.08	0.07	0.06	0.07	0.11	0.10	0.09	0.11	0.10	0.13	0.15
fraction	Cpx	0.21	0.19	0.21	0.21	0.20	0.18	0.22	0.19	0.21	0.25	0.22	0.35	0.34
of	Pl	0.59	0.61	0.58	0.60	0.61	0.63	0.58	0.61	0.60	0.51	0.59	0.38	0.38
minerals	Mt	0.13	0.12	0.13	0.12	0.12	0.12	0.11	0.10	0.10	0.12	0.09	0.13	0.13

Table 4. Fractionation starting from 305.

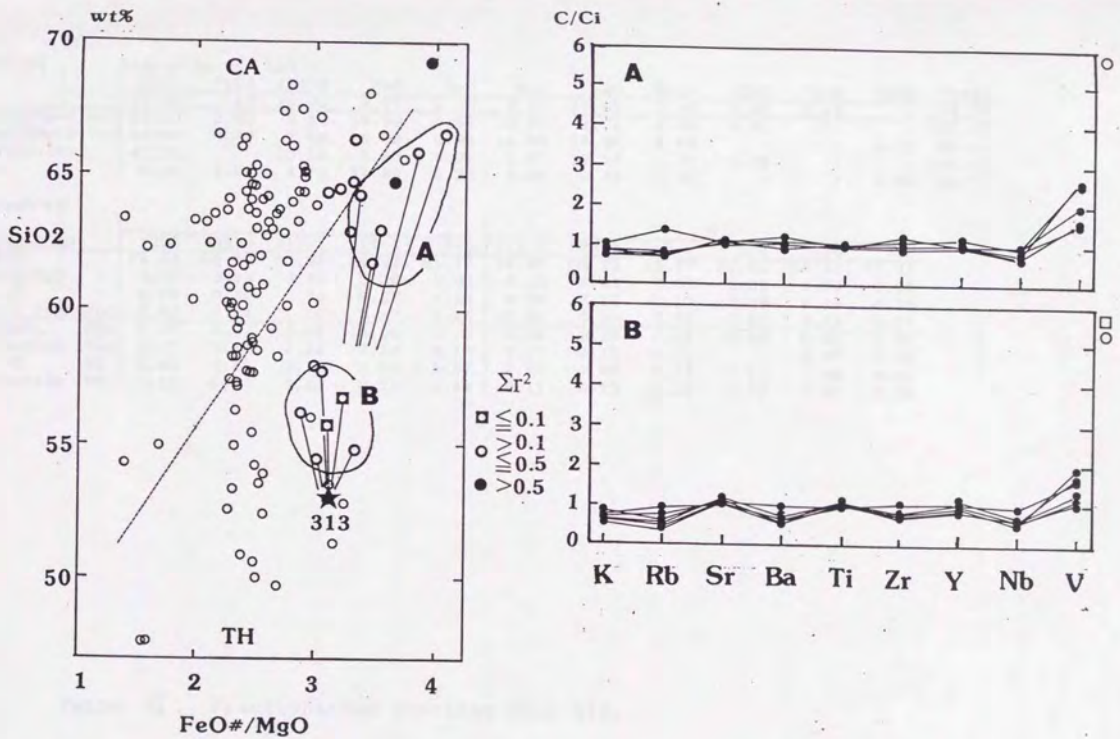

Figure 39. Fractionation starting from 313.

Parent	Sample No. 313											
	SiO2	TiO2	Al2O3	FeO	MnO	MgO	CaO	Na2O	K2O	P2O5	V2O3	Total
	52.96	0.92	20.04	9.07	0.19	2.93	10.03	2.89	0.80	0.19	-	100.00
Opx(XMg=0.69)	52.60	0.29	2.14	18.99	0.55	23.90	1.78	0.03	0.01	-	-	100.31
Cpx(XMg=0.71)	50.79	0.49	2.86	10.56	0.38	14.63	18.95	0.32	-	-	0.11	99.25
Pl(An=85)	47.38	-	33.18	0.83	0.01	0.07	17.25	1.70	0.05	-	-	100.47
Mt	0.08	9.92	4.73	74.88	0.33	2.88	0.02	0.05	-	-	0.83	93.73

Daughter

		A					B					
Sample No.		301	311-3	315-2	312-1	312-3	311-2	322-1	317-1	318	326	328
SiO2		66.52	65.80	62.91	64.27	61.76	56.67	56.15	54.77	54.41	56.15	57.71
FeO*/MgO		4.07	3.85	3.54	3.36	3.46	3.23	2.89	3.32	3.02	2.89	3.05
Σr^2		0.33	0.46	0.20	0.27	0.28	0.06	0.10	0.17	0.26	0.18	0.33
Melt Fraction		0.43	0.44	0.50	0.47	0.55	0.72	0.81	0.79	0.82	0.75	0.67
Weight	Opx	0.06	0.07	0.08	0.06	0.08	0.06	0.09	0.05	0.03	0.01	0.08
fraction	Cpx	0.17	0.14	0.12	0.14	0.14	0.17	0.10	0.05	-	0.07	0.02
of	Pl	0.66	0.68	0.71	0.68	0.67	0.66	0.69	0.88	0.94	0.86	0.82
minerals	Mt	0.11	0.11	0.10	0.11	0.12	0.11	0.12	0.02	0.03	0.07	0.08

Table 5. Fractionation starting from 313.

In marked contrast to calcalkaline trend A from basalt 305, trend A and B from basalt 313 which produce tholeiitic andesite and dacite does not have anomalous V enrichment in spite of the similarlity of weight fraction of magnetite (0.10-0.13).

(4) Fractionation starting from 326 (Fig. 40, Table 6)

Crystal fractionation from tholeiitic andesite 326 can produce only tholeiitic dacite on least squares calculations, and the derivation of calcalkaline andesite and dacite are rejected in comparison. A little disaccorded enrichment of Rb, Ba and V and depletion of Ti and Y are also indicated in calcalkaline trend.

Fraction of olivine in the minerals to be removed from parent 326 is about 10% to produce the calcalkaline trend and is almost nil in the tholeiitic trend. On the other hand, tholeiitic andesite 326 contains about 0.1 vol% olivine phenocryst, which is much smaller than augite phenocryst of 0.7 vol%. Olivine phenocryst should play an important role without orthopyroxene phenocrysts to produce the calcalkaline trend, but it is not realistic from the mode of phenocrysts of olivine, augite and orthopyroxene in 326 and more differentiated rocks. Olivine is rare in rocks which have SiO_2 content above 56 wt%, and instead of olivine, orthopyroxene becomes one of the dominant mafic minerals in the Shirahama Group.

A point which should be noted is that some "calcalkaline dacite", which are close to boundary, can be

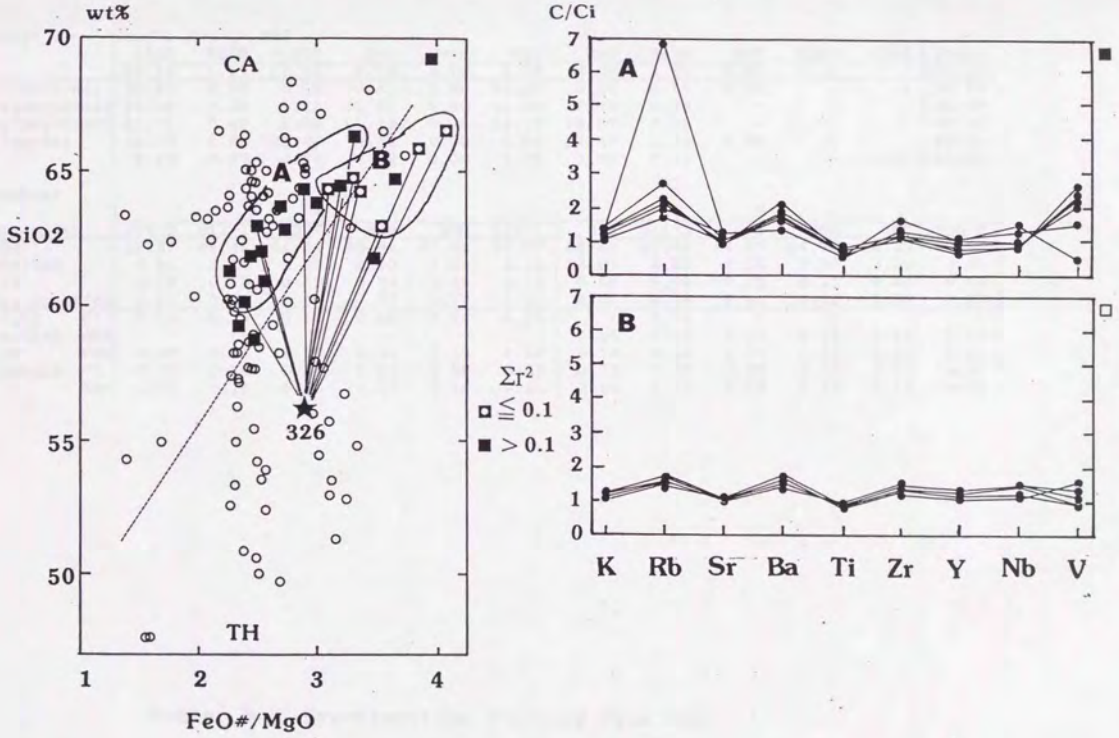

Figure 40. Fractionation starting from 326.

Parent	Sample No. 326											
	SiO2	TiO2	Al2O3	FeO	MnO	MgO	CaO	Na2O	K2O	P2O5	V2O3	Total
	56.15	1.11	17.20	9.79	0.19	3.39	8.06	3.21	0.70	0.19	-	100.00
Ol(XMg=0.64)	36.89	0.05	0.02	30.81	0.60	31.09	0.28	0.12	0.02	-	-	99.88
Opx(XMg=0.64)	51.98	0.33	1.12	21.51	0.80	21.05	1.77	0.03	-	-	-	98.59
Cpx(XMg=0.69)	51.71	0.45	1.70	11.16	0.45	14.12	19.37	0.20	-	-	-	99.16
Pl(An=86)	46.72	0.03	32.46	0.64	0.02	0.08	17.47	1.54	0.03	-	-	99.01
Mt	0.12	10.52	4.27	74.92	0.34	1.76	0.06	0.01	-	-	0.92	92.93

Daughter				A						B			
Sample No.		309-2	311-1	327	320	190	319-1	301	311-3	312-1	300	307	315-2
SiO2		66.27	64.48	64.32	62.98	61.95	60.07	66.52	65.80	64.27	64.72	64.30	62.91
FeO*/MgO		3.32	3.20	2.89	2.50	2.54	2.34	4.07	3.85	3.36	3.30	3.09	3.54
Σr^2		0.18	0.13	0.41	0.34	0.30	0.15	0.08	0.02	0.05	0.11	0.07	0.03
Melt Fraction		0.61	0.67	0.69	0.72	0.77	0.84	0.56	0.58	0.61	0.60	0.62	0.65
Weight	Ol	0.10	0.10	0.12	0.08	0.10	0.08	-	0.01	-	-	-	-
fraction	Opx	-	-	-	-	-	-	0.14	0.16	0.17	0.13	0.14	0.19
of	Cpx	0.20	0.24	0.16	0.20	0.15	0.18	0.19	0.16	0.15	0.22	0.22	0.12
minerals	Pl	0.55	0.50	0.56	0.55	0.56	0.50	0.53	0.55	0.55	0.53	0.50	0.57
	Mt	0.15	0.16	0.16	0.17	0.18	0.24	0.13	0.13	0.13	0.13	0.14	0.12

Table 6 . Fractionation starting from 326.

derived from tholeiite 326. Magmatic temperature of this "calcalkaline dacite" is higher than calcalkaline andesite as illustrated in Chapter 1. These "calcalkaline dacite" are derived from tholeiitic basalt and andesite. This fact reflect the arbitrariness of the boundary between TH and CA.

(5) Fractionation starting from 311-2 (Fig. 41, Table 7)

311-2 is a tholeiitic two pyroxene andesite. The results of least squares calculation indicate that tholeiitic dacite is more acceptable to be a derivative of tholeiitic andesite than calcalkaline dacite. As for trace element concentration, the enrichment of Rb and V and the depletion of Ti are shown in calcalkaline dacite. As Ti and V are removed from parent magma mostly by fractionation of magnetite, depletion of Ti and enrichment of V are incompatible.

Fig. 41 is identical with Fig. 40 and the same conclusion as 326 is reached in this case, that is, tholeiitic dacite can be derived from tholeiitic andesite but calcalkaline dacite cannot.

(6) Fractionation starting from 323 (Fig. 42, Table 8)

323 is a tholeiitic andesite which has composition close to the TH-CA boundary. Both calcalkaline and tholeiitic trends can be led by crystal fractionation on the basis of major element least squares method. The sum of squares of residuals less than 0.1 is achieved in the both trends.

The enrichment of Rb, Ba and V and the depletion of Ti,

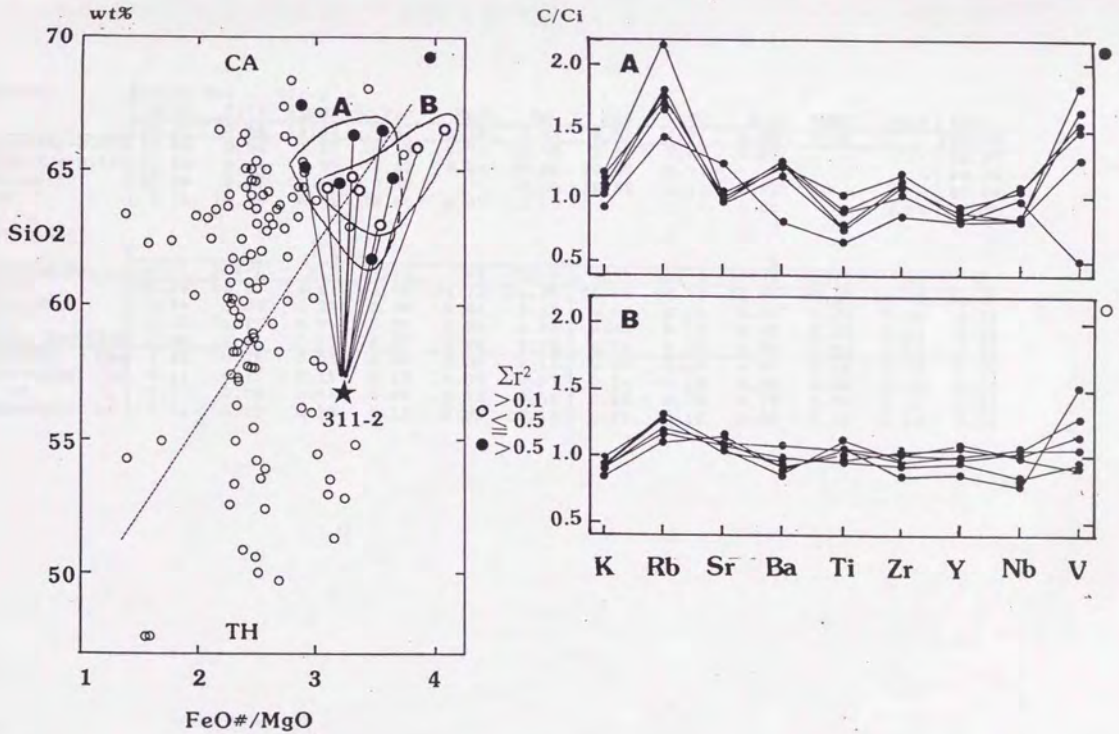

Figure 41. Fractionation starting from 311-2.

Parent	Sample No. 311-2											
	SiO2	TiO2	Al2O3	FeO	MnO	MgO	CaO	Na2O	K2O	P2O5	V2O3	Total
	56.67	0.85	18.84	7.87	0.19	2.44	8.23	3.71	0.93	0.26	-	100.00
Opx(XMg=0.67)	52.68	0.24	1.27	20.18	0.74	23.09	1.66	0.01	0.02	-	-	99.97
Cpx(XMg=0.68)	51.24	0.44	1.87	11.52	0.55	13.95	19.49	0.22	-	-	-	99.29
Pl(An=83)	47.79	0.02	32.44	0.80	-	0.06	16.82	1.91	0.05	-	-	99.89
Mt	0.11	11.49	3.61	76.08	0.49	2.53	-	-	0.01	-	0.69	95.03

Daughter

	A						B					
Sample No.	309-1	309-2	332	311-1	345	312-3	301	311-3	315-2	312-1	300	307
SiO2	66.48	66.27	64.97	64.48	64.72	61.76	66.52	65.80	62.91	64.27	64.72	64.30
FeO*/MgO	3.54	3.32	2.90	3.20	3.64	3.46	4.07	3.85	3.54	3.36	3.30	3.09
Σr^2	1.05	0.77	0.51	0.71	0.98	0.57	0.42	0.42	0.20	0.22	0.24	0.23
Melt Fraction	0.60	0.61	0.65	0.67	0.63	0.75	0.58	0.60	0.68	0.64	0.62	0.65
Weight fraction of minerals Opx	0.08	0.08	0.08	0.07	0.09	0.12	0.08	0.10	0.11	0.09	0.05	0.05
Cpx	0.11	0.11	0.11	0.13	0.07	0.07	0.14	0.10	0.04	0.09	0.16	0.16
Pl	0.70	0.70	0.68	0.68	0.74	0.68	0.67	0.70	0.77	0.72	0.69	0.67
Mt	0.11	0.12	0.13	0.12	0.09	0.12	0.11	0.10	0.08	0.10	0.10	0.12

Table 7. Fractionation starting from 311-2.

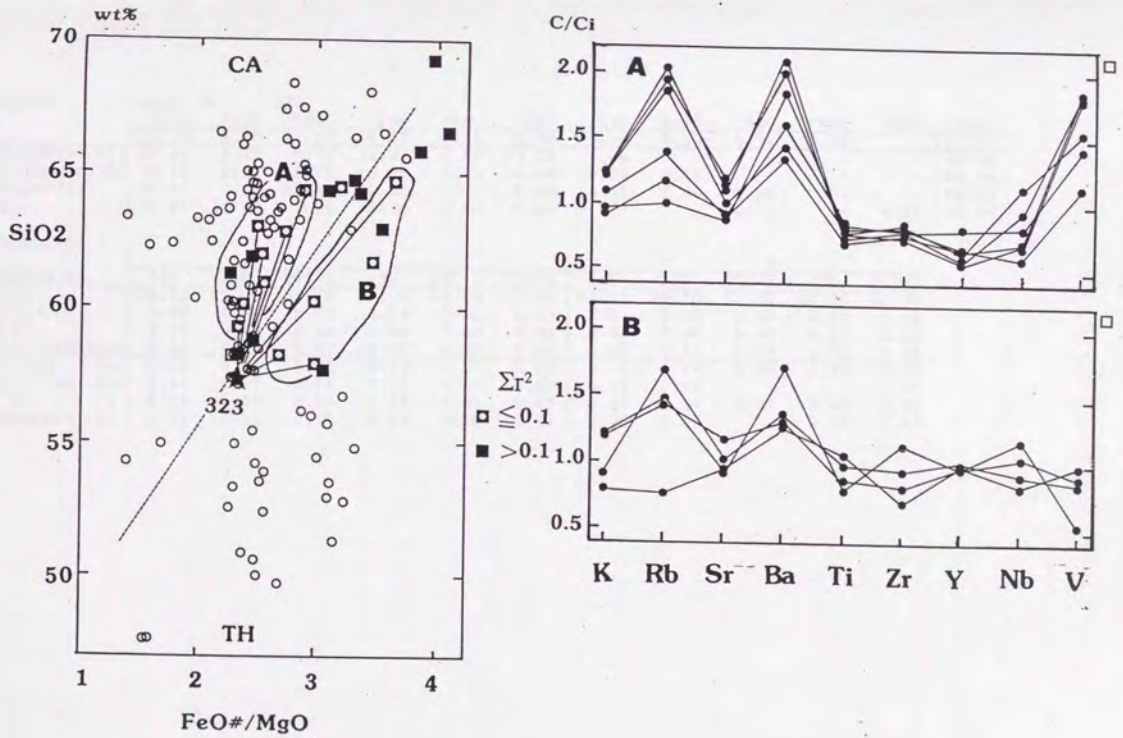

Figure 42. Fractionation starting from 323.

Parent	Sample No. 323											
	SiO2	TiO2	Al2O3	FeO	MnO	MgO	CaO	Na2O	K2O	P2O5	V2O3	Total
	57.29	0.90	17.18	8.68	0.18	3.70	7.96	3.13	0.78	0.19	-	100.00
Opx(XMg=0.69)	53.41	0.24	0.74	19.18	0.86	23.53	1.49	-	-	-	-	99.46
Cpx(XMg=0.72)	52.24	0.32	1.53	10.32	0.43	14.82	19.76	0.29	-	-	-	99.70
Pl(An=72)	50.58	0.02	30.46	0.73	-	0.06	14.56	3.06	0.04	-	-	99.51
Mt	0.09	10.95	3.16	75.90	0.40	1.66	-	-	0.01	-	0.61	92.83

Daughter

	A						B				
Sample No.	327	320	295-1	190	281-1	295-2	345	308	334-1	206	312-3
SiO2	64.32	62.98	62.79	61.95	60.89	63.55	64.72	60.20	57.89	58.20	61.76
FeO*/MgO	2.89	2.50	2.73	2.54	2.55	2.49	3.64	2.98	2.99	2.68	3.46
Σr^2	0.07	0.08	0.09	0.09	0.09	0.08	0.08	0.07	0.07	0.08	0.11
Melt Fraction	0.61	0.66	0.67	0.72	0.77	0.64	0.56	0.75	0.87	0.92	0.69
Weight fraction of minerals Opx	0.18	0.15	0.20	0.17	0.17	0.13	0.16	0.18	0.33	0.49	0.23
Cpx	0.13	0.17	0.12	0.13	0.13	0.20	0.15	0.19	-	-	0.17
Pl	0.59	0.58	0.58	0.59	0.60	0.57	0.63	0.54	0.67	0.43	0.51
Mt	0.10	0.11	0.10	0.10	0.10	0.11	0.08	0.08	-	0.08	0.10

Table 8. Fractionation starting from 323.

however, occur in the calcalkaline trend. As stated before, the enrichment of V and the depletion of Ti are incompatible.

Of course 323 andesite is not adequate to a parent magma, because it cannot be derived from tholeiitic basalt as stated before. In any case, it is concluded that tholeiitic trend is more acceptable than calcalkaline one even from the boundary between TH and CA.

In summary of 3.3.2, it is concluded that crystal fractionation leads production of tholeiites from tholeiites. Compositional trend in tholeiites is successfully modeled by crystal fractionation both on major element least squares solutions and on Rayleigh type fractionation of trace element. Tholeiitic andesites which have compositions close to the TH-CA boundary and on the "calcalkaline trend" from tholeiitic basalt cannot be derived by crystal fractionation, and those are thought to be mixed hybrids illustrated in Chapter 2. Neither can be accepted the production of calcalkaline rocks through POAM fractionation (Gill, 1981) in the Shirahama Group.

3.3.2 The origin of calcalkaline rocks (Crystal fractionation of boninites).

The crystal fractionation of tholeiitic magmas to produce calcalkaline rocks is rejected in the previous section.

High-alumina basalt (HAB) is often thought to be a parental magma of calcalkaline association (e.g. Jakes and White, 1972) and is sometimes called "calcalkaline basalt". To avoid confusion, the difference between Kuno's "tholeiite" and Miyashiro's "tholeiites" should be clarified first. Tholeiites defined by Miyashiro (1974) include basalt, andesite and dacite, and the definition has nothing to do with the alkali content in the rocks. On the other hand, tholeiite is used as one type of basalts of island-arcs in Kuno (1960), which has low Al_2O_3 and alkalis. Kuno (1960, 1966) divided basalt magma into three types, which are tholeiite, high-alumina basalt and alkali olivine basalt, and illustrated the lateral variation of magma types across continental margins and island-arcs, changing continuously from less alkalic and more siliceous type (tholeiite) to more alkalic and less siliceous type (alkali olivine basalt). High-alumina basalt with intermediate alkalis are geographycally distributed between the provinces of tholeiite and alkali olivine basalt in island-arcs.

Calcalkaline rocks are present in association with these three magma types (e.g. Fujinawa 1988, Koyaguchi 1986). If high-alumina basalt, which cannot be derived either from tholeiite or alkali olivine basalt, is a primary magma of calcalkaline rocks, it must always coexist both with tholeiite and alkali olivine basalt. The observation that the chemical composition of basalt magma changes laterally, however, conflicts with the above assumption.

Fig. 43 illustrates the compositions of basalts in the

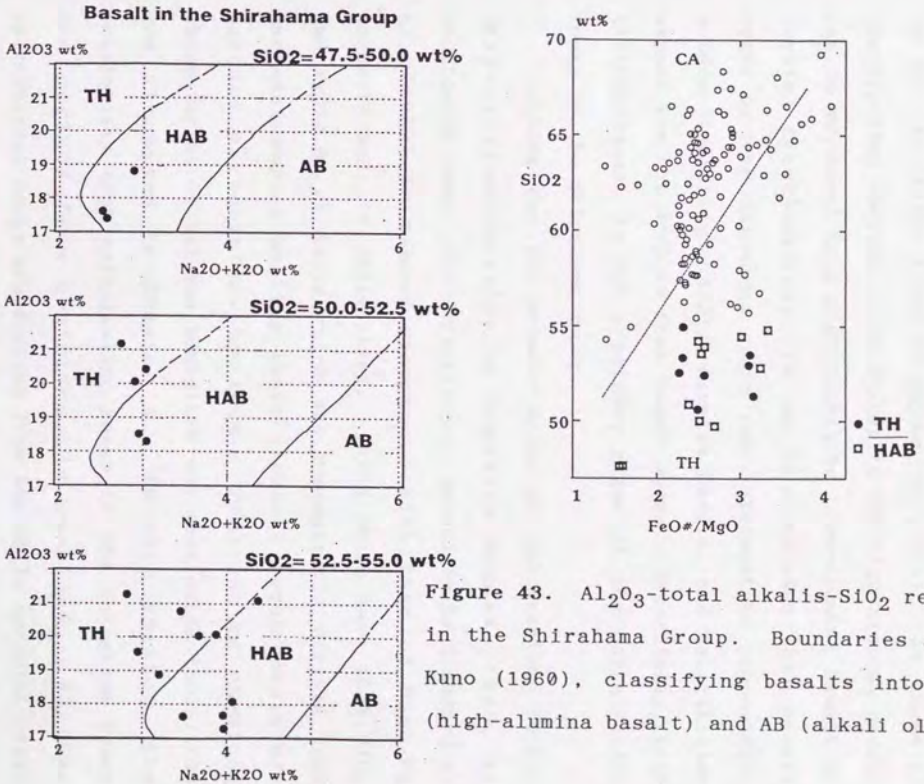

Figure 43. Al_2O_3-total alkalis-SiO_2 relation of the basalts in the Shirahama Group. Boundaries are those defined by Kuno (1960), classifying basalts into TH (tholeiite), HAB (high-alumina basalt) and AB (alkali olivine basalt).

Shirahama Group. There exist tholeiite and high-alumina basalt defined by Kuno (1960) in the Shirahama group, but this is not the coexistence of two types of basalt magma which are independent each other as indicated by Kuno (1960). Both tholeiite and high-alumina basalt are included in the tholeiitic field of Miyashiro (1974). As shown in the previous section, both tholeiite and high-alumina basalt can be produced from most primitive high-alumina basalt by crystal fractionation. It can be concluded that basalt magma in the Shirahama group has intermediate composition between tholeiite and high-alumina basalt, and calcalkaline magmas are not derived from basalt magma. Accordingly, high alumina basalt is not a primary magma of the calcalkaline rocks in the Shirahama group.

Looking for the primary magma of calclakaline rocks, crystal fractionation of boninite magmas, then, is considered here. The definition of boninites by Crawford et al. (1989) is almost synonymous with that of high-Mg andesite and its derivatives. Lavas which have >53% SiO_2 and Mg#>0.6, or lavas which are demonstrably derived from parental magmas meeting these chemical requirements are defined as boninites by them. Contrastive chemical characteristics between boninites and coexisting tholeiites are discussed in Chapter 4. In this chapter, the possibility that calcalkaline rocks in the Shirahama Group are derived from boninites, is examined. Whether calcalkaline rocks are derived from boninitic parental magma by crystal fractionation or not.

(1) First, what kind of boninites should be a parental magma in the Shirahama Group?

Crawford et al. (1989) divided boninites into two classes, low-Ca and high-Ca suites. High-Ca boninites, exemplified by the Upper Pillow Lavas of the Troodos Ophiolite in Cyprus, always have SiO_2<56% and CaO/Al_2O_3 >0.75. Low-Ca boninites are subdivided into three types by diagnostic plots: oxides, CaO/Al2O3 and Mg# versus total alkalis.

On these diagrams, low-Ca type 3 boninites have smooth trend toward calcalkaline rocks in the Shirahama Group. Low-Ca type 2 boninites are rejected as a parental magma of the Shirahama calcalkaline rocks by having higher total alkalis. Low-Ca type 1 boninites are also rejected by having lower CaO content, lower CaO/Al_2O_3 ratio and higher SiO_2 content. As candidate for primary magma of calcalkaline rocks in the Shirahama Group, low-Ca type 3 boninites are picked out. Mariana trench 50-23 (Bloomer, 1987) is chosen as a representative low-Ca type 3 boninites to be a parent for major element least squares calculation and trace element Rayleigh fractionation.

(2) What kind of minerals should be subtracted from boninites to produce calcalkaline rocks?

Bloomer and Hawkins (1987) presented a detailed description of boninites and genetically related andesitic and dacitic rocks (boninite series volcanic rocks) from the Mariana trench. They concluded that most of the major and trace element variations in the series from boninite to

boninitic dacite can be modelled by fractionation of olivine, orthpyroxene, clinopyroxene and plagioclase leaving 47% residual liquid.

In the Shirahama Group, olivine two-pyroxene hornblende gabbro xenoliths are found in the intrusive rock of calcalkaline andesite 320 at Nakagi area. They are concluded to be an early stage cumulate of calcalkaline magma from chemical composition of minerals (Tamura, 1989). Olivine is altered. Mg value of orthopyroxene and augite are 0.79-0.73 and 0.82-0.76. Magmatic temperature measured by two-pyroxene geothermometer (Lindsley, 1983) is about 900°C. An content in plagioclase is 94-82. Anhedral hornblende and magnetite exist interstitially. Both hornblends and magnetite are not cumulus phases. Olivine is thought to be fractionated first from the texture of gabbro; euhedral olivine is always surrounded by other minerals.

Fo contents of olivine in boninite from Bonin Islands range from Fo_{90} to Fo_{85} (Umino, 1986). Those in calcalkaline rocks from Abu volcano group range from Fo_{90} to Fo_{80} (Koyaguchui, 1984). An approximate value of Fo_{86} is adopted to be a value of an representative subtracted olivine.

The representative chemical compositions of orthpyroxene, augite and plagioclase from olivine two-pyroxene hornblende gabbro are used to be those of subtracted minerals. Mg value of olivine is highest but mafic phenocrysts should not be in equilibrium each other, that is, olivine which has higher Mg value than augite or orthopyroxene is

subtracted first as shown in the texture of gabbro.

The incorporation of magnetite or hornblend or both into least squares calculation results badly, calling for the addition of phases to the parent.

The phases to be subtracted from boninites are thought to be olivine, orthpyroxene, augite and plagioclase and chemical composition of those are presented in Table 3-7.

(3) Fractionation starting from boninites, Mariana trench 50-23 (Bloomer, 1987) and "Shirahama boninite". (Figs. 44, 45, Tables 9, 10)

Most calcalkaline andesite and dacite are acceptable to be derivatives from Mariana trench 50-23 after major element least squares calculation in agreement of the sum of square residual less than 0.5, as compared with calcalkaline andesite which has composition close to TH-CA boundary (Fig. 44). Rocks which are close to the boundary are mixed hybrid between calcalkaline and tholeiitic magmas (Chapter 2). This observation well accord with the result of least squares calculation which does not approve those rocks to be derivatives of boninites.

What is most interesting thing is fairly uniform trace element patterns in Fig. 44. As C/C_i (observed to calculated ratio) of each element is fairly uniform, trace element in the "Shirahama Boninite" can be deduced from these ratios. As $C_i=C_0xF^{(D-1)}$, if $C/C_i=3$, it means that C_0 in "Shirahama Boninite" is as three times as that in Mariana trench 50-23. The averages of C/C_i for K, Rb, Sr, Ba, Ti, Zr, Y

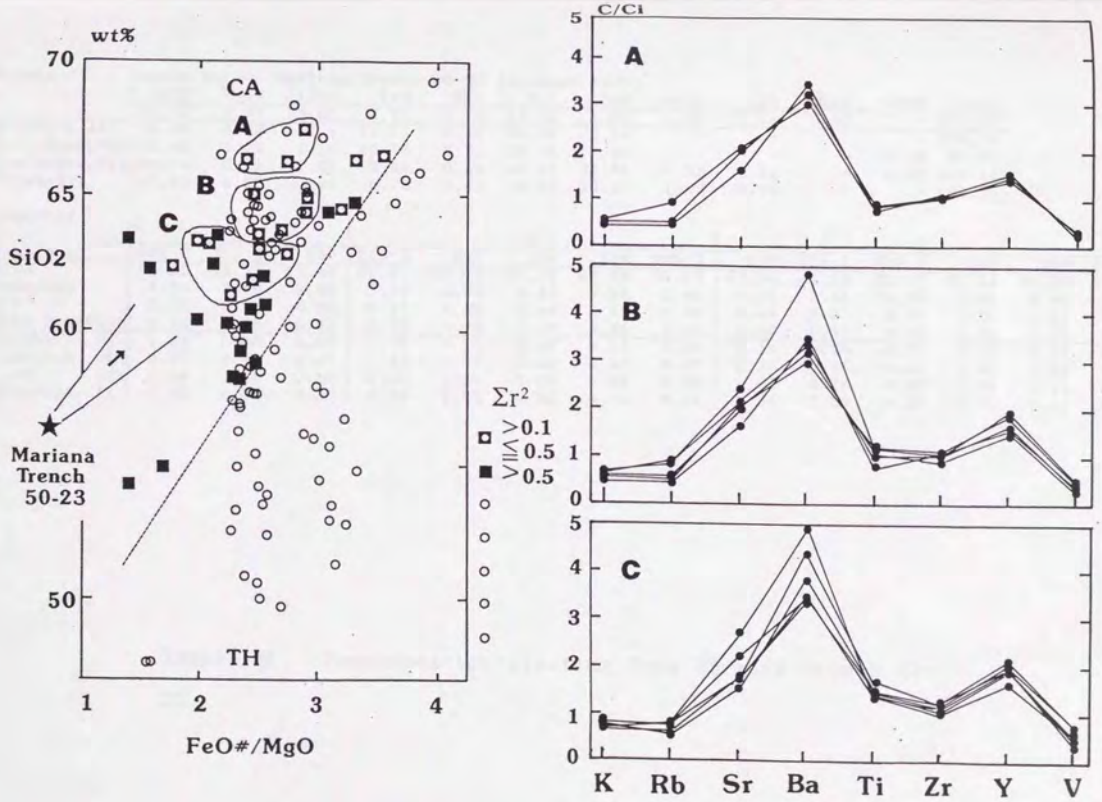

Figure 44 . Fractionation starting from Mariana Trench 50-23.

Parent	Sample No.		Mariana Trench 50-23 (Bloomer 1978)									
	SiO2	TiO2	Al2O3	FeO	MnO	MgO	CaO	Na2O	K2O	P2O5	V2O3	Total
	56.33	0.27	13.66	7.71	0.13	11.03	8.34	1.54	0.94	0.05	-	100.00
Ol(XMg=0.86)	39.98	0.03	-	14.01	0.22	45.51	0.25	-	-	-	-	100.00
Opx(XMg=0.75)	52.48	0.24	2.18	15.76	0.51	25.96	1.46	-	-	-	0.03	98.67
Cpx(XMg=0.77)	53.14	0.25	1.28	8.41	0.33	15.59	21.08	0.23	0.01	-	0.05	100.43
Pl(An=82)	47.65	0.03	32.84	0.73	0.01	0.05	16.43	1.93	0.03	-	-	99.70

Daughter

		A			B					C				
Sample No.		322-2	317-2	330	319-2	327	325	324	295-2	320	303-1	302-2	263	264	295-1
SiO2		66.22	66.28	67.40	60.07	64.32	64.98	63.69	63.55	62.98	61.88	61.27	63.24	63.21	62.79
FeO*/MgO		2.74	2.40	2.89	2.39	2.89	2.45	2.68	2.49	2.50	2.45	2.27	1.99	2.09	2.73
Σr^2		0.25	0.30	0.35	0.27	0.35	0.40	0.34	0.41	0.45	0.37	0.38	0.24	0.11	0.42
Melt Fraction		0.36	0.35	0.33	0.39	0.42	0.40	0.45	0.43	0.46	0.55	0.60	0.49	0.50	0.47
Weight	Ol	0.04	0.03	0.02	0.06	0.10	0.07	0.12	0.04	0.12	0.23	0.32	0.16	0.18	0.14
fraction	Opx	0.43	0.45	0.47	0.42	0.38	0.40	0.35	0.37	0.34	0.26	0.16	0.24	0.26	0.34
of	Cpx	0.19	0.18	0.17	0.20	0.20	0.19	0.22	0.23	0.23	0.24	0.26	0.28	0.25	0.22
minerals	Pl	0.33	0.34	0.35	0.32	0.32	0.33	0.31	0.31	0.30	0.26	0.26	0.31	0.31	0.30

Table 9. Fractionation starting from Mariana Trench 50-23.

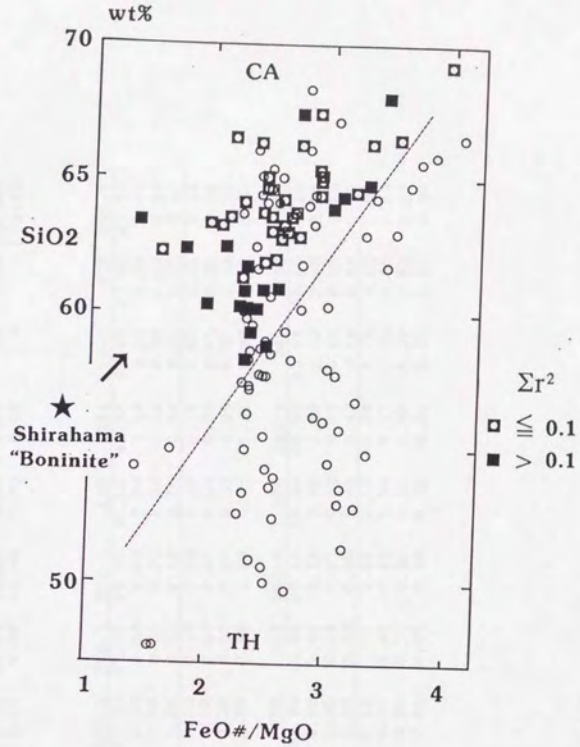

Figure 45. Fractionation starting from Shirahama "Boninite"

Parent	Sample No.		Shirahama "Boninite"									
	SiO2	TiO2	Al2O3	FeO	MnO	MgO	CaO	Na2O	K2O	P2O5	V2O3	Total
	56.09	0.36	13.61	7.78	0.22	10.98	8.34	1.94	0.59	0.07	-	100.00
Ol(XMg=0.86)	39.98	0.03	-	14.01	0.22	45.51	0.25	-	-	-	-	100.00
Opx(XMg=0.75)	52.48	0.24	2.18	15.76	0.51	25.96	1.46	-	-	-	0.03	98.67
Cpx(XMg=0.77)	53.14	0.25	1.28	8.41	0.33	15.59	21.08	0.23	0.01	-	0.05	100.43
Pl(An=82)	47.65	0.03	32.84	0.73	0.01	0.05	16.43	1.93	0.03	-	-	99.70

Daughter

Sample No.		319-1	285-3	260	315-1	303-2	265-1	303-1	190	261	280-1	273	295-1
SiO2		60.07	60.20	60.32	60.80	61.27	61.70	61.88	61.95	62.23	62.42	62.69	62.79
FeO*/MgO		2.40	2.24	1.97	2.43	2.27	2.30	2.45	2.54	1.58	2.12	2.58	2.73
Σr^2		0.35	0.41	0.30	0.49	0.09	0.31	0.02	0.08	0.04	0.29	0.04	0.03
Melt Fraction		0.65	0.66	0.60	0.58	0.60	0.51	0.55	0.56	0.54	0.41	0.51	0.47
Weight	Ol	0.42	0.43	0.30	0.30	0.32	0.19	0.23	0.26	0.19	0.05	0.21	0.14
fraction	Opx	0.05	0.02	0.09	0.14	0.16	0.20	0.27	0.19	0.20	0.41	0.25	0.34
of	Cpx	0.35	0.33	0.39	0.28	0.26	0.30	0.24	0.27	0.30	0.21	0.22	0.22
minerals	Pl	0.19	0.22	0.23	0.29	0.26	0.30	0.26	0.27	0.31	0.32	0.31	0.30

Sample No.		271	320	264	282	263	302	280-2	270	295-2	266	324	346
SiO2		62.92	62.98	63.21	63.22	63.24	63.32	63.48	63.49	63.55	63.69	63.69	63.82
FeO*/MgO		2.65	2.50	2.08	2.59	1.99	1.40	2.15	2.66	2.49	2.43	2.68	3.00
Σr^2		0.02	0.04	0.07	0.01	0.01	0.12	0.07	0.03	0.02	0.01	0.00	0.25
Melt Fraction		0.52	0.46	0.49	0.49	0.48	0.38	0.40	0.46	0.43	0.44	0.44	0.39
Weight	Ol	0.23	0.13	0.16	0.18	0.16	-	0.05	0.13	0.09	0.11	0.12	0.04
fraction	Opx	0.23	0.34	0.28	0.28	0.25	0.45	0.41	0.34	0.37	0.35	0.36	0.43
of	Cpx	0.23	0.23	0.25	0.23	0.28	0.20	0.21	0.21	0.23	0.22	0.22	0.22
minerals	Pl	0.31	0.30	0.31	0.31	0.31	0.35	0.33	0.32	0.31	0.32	0.31	0.30

Table 10. Fractionation starting from Shirahama "Boninite".

Sample No.		329	12	283	307	327	311-1	267	268	300	319-2	332	325
SiO2		64.00	64.03	64.13	64.30	64.32	64.48	64.51	64.56	64.72	64.91	64.97	64.98
FeO*/MgO		2.55	2.28	2.60	3.08	2.89	3.20	2.49	2.45	3.29	2.91	2.91	2.46
Σr^2		0.01	0.06	0.00	0.10	0.00	0.03	0.02	0.02	0.11	0.00	0.01	0.02
Melt Fraction		0.43	0.38	0.44	0.37	0.42	0.39	0.40	0.45	0.36	0.38	0.35	0.40
Weight	Ol	0.10	0.04	0.12	0.03	0.10	0.06	0.08	0.15	0.04	0.06	0.02	0.07
fraction	Opx	0.40	0.44	0.35	0.44	0.38	0.41	0.39	0.29	0.41	0.42	0.47	0.40
of	Cpx	0.18	0.19	0.21	0.22	0.21	0.22	0.20	0.21	0.22	0.20	0.19	0.19
minerals	Pl	0.32	0.34	0.32	0.32	0.32	0.31	0.33	0.35	0.33	0.32	0.32	0.33

Sample No.		294	322-2	309-2	317-2	279	309-1	MZ1-W	330	236-3	333
SiO2		65.27	66.22	66.27	66.28	66.47	66.48	67.32	67.40	67.98	69.23
FeO*/MgO		2.89	2.73	3.31	2.40	2.19	3.55	2.74	2.88	3.42	3.96
Σr^2		0.06	0.06	0.01	0.03	0.07	0.01	0.16	0.06	0.18	0.05
Melt Fraction		0.40	0.36	0.34	0.35	0.37	0.34	0.36	0.33	0.31	0.29
Weight	Ol	0.09	0.04	0.02	0.03	0.05	0.03	0.05	0.01	-	0.01
fraction	Opx	0.38	0.44	0.45	0.45	0.39	0.43	0.41	0.47	0.48	0.45
of	Cpx	0.20	0.19	0.19	0.18	0.20	0.20	0.19	0.17	0.18	0.18
minerals	Pl	0.33	0.34	0.34	0.34	0.35	0.34	0.35	0.35	0.34	0.36

and V are 0.66, 0.70, 2.02, 3.63, 1.22, 1.09, 1.77 and 0.47 respectively. C_0 of "Shirahama Boninite" for K, Rb, Sr, Ba, Ti, Zr, Y and V are respectively 6200, 9.8, 181.8, 72.6, 3300, 54.5, 17.7, and 77.1 (ppm). Boninites themselves have wide range of chemical compositions, and these values in the Shirahama boninite are well in the range of those in boninites except Y and V. Y is little higher and V is little lower than representative boninites in Crawford et al. (1989).

Major element content of "Shirahama boninite" can be deduced from the result of least squares calculation. Doing the reverse of which were done in tholeiites, phenocryst minerals stated before are added to daughter liquid (calcalkaline rocks in the Shirahama Group) in proportion which result in the closest approximation of parental liquid compositions of Mariana trench 50-23. The average of these calculated value represents major element composition of "Shirahama boninite" and it is presented in Table 10. Fig. 45 and Table 10 present the result of major element least squares calculation from "Shirahama boninite". It is remarkable that most calcalkaline andesite and dacite except mixed hybrid can result from crystal fractionation of "Shirahama boninte", which is the modified Mariana trench 50-23, in agreement of the sum of square residual less than 0.1.

It is concluded that calcalkaline rocks in the Shirahama Group are can be derived by crystal fractionation of olivine, orthopyroxene, augite and plagioclase from a parental

"Shirahama boninite". The chemical diversity of calcalkaline rocks can be explained by the difference of fraction of minerals to be subtracted.

3.4 CONCLUSION

The role of crystal fractionation in the Shirahama Group is clarified in this chapter by using the methods of major-element least squares calculation and trace element calculation which assumed Rayleigh crystal fractionation.

Compositional trends in tholeiites, from basalt through tholeiitic andesite to tholeiitic dacite are successfully modelled by crystal fractionation of plagioclase, olivine or orthopyroxene, augite and magnetite.

Calcalkaline rocks or calcalkaline trend which increases SiO_2 content with constant FeO*/MgO ratio are not acceptable to be derivatives of tholeiites. Some are rejected by disagreement of major element least squares calculation, others by discrepancy between observed and calculated concentration in trace element.

On the other hand, crystal fractionation of "boninites" can successfully produce most of calcalkaline rocks in the Shirahama group. Low-Ca type 3 boninite (Mariana trench 50-23) is picked out as a dummy parental magma of calcalkaline rocks in the Shirahama Group. By major element least squares method, crystal fractionation of olivine, orthopyroxene, augite and plagioclase can approximately produce calcalkaline rocks from Marians trench 50-23 except for

mixed hybrid magmas. Using the result of above calculation, major and trace element composition of the "Shirahama boninite" is estimated. The little modification of Mariana trench 50-23, low Ca type 3 boninite, had greatly improved the acceptability of boninite as a primary magma of calcalkaline rocks in the Shirahama Group. Most of calcalkaline rocks except mixed hybrid can result from the "Shirahama boninite" through crystal fractionation of olivine, orthopyroxene, augite and plagioclase in agreement of sum (r^2) < 0.1. Fig. 46 illustrates the summary of the crystal fractionation model in the Shirahama Group. Rocks in the Shirahama Group can be divided into unmixed tholeiites, unmixed calcalkaline rocks and mixed hybrids. Unmixed tholeiites which are indicated by solid squares in Fig. 46 are those which can be produced by crystal fractionation from the primitive high-alumina basalt, and unmixed calcalkaline rocks are those which can be produced by crystal fractionation from the Shirahama boninite. Rocks which extend from unmixed tholeiites to unmixed calcalkaline rocks forming calcalkaline trend are mixed hybrids illustrated in Chapter 2.

Crystal fractionation model revealed the origin of the dualism in the Shirahama Group. The dualism of tholeiites and calcalkaline rocks is derived from the coexistence of tholeiites and boninites.

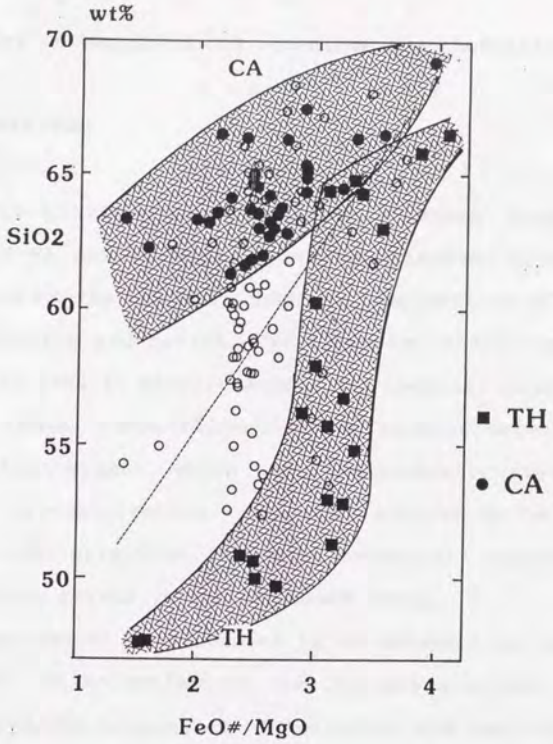

Figure 46. Summary of the crystal fractionation model in the Shirahama Group. Solid points (TH and CA) are those which can be produced by crystal fractionation from the primitive tholeiitic basalt or the "Shirahama boninite".

Capter 4

Geochemistry of boninites, CA andesites and tholeiites.

4.1 INTRODUCTION

In the previous chapters, the dualism, concurrent activity of CA and TH magmas, in the Shirahama Group, are demonstrated on the basis of chemical compositions of phenocrystic minerals and crystal fractionation modelling. The dualism also lead to petrographical and chemical diversities of the Shirahama rocks through mixing between calcalkaline and tholeiitic magmas, which were independently evolved by fractional crystallization. The next problem to be solved is what is the origin of (the most primitive) calcalkaline and tholeiitic magmas in the Shirahama Group.

The purpose of this chapter is to demonstrate that the dualism in the volcanism of the Shirahama Group is the result of bimodal generation of boninites and tholeiites in the upper mantle. This is inferred from comparison of geochemical patterns of boninitic and calcalkaline vs. tholeiitic rocks from various arc volcanic suits showing bimodal volcanism.

What are boninites?

Boninites, equivalent to high-Mg andesites and their derivatives, are thought to be mantle-derived magmas. Some boninites have characteristics of a primary magma, which is in equilibrium with mantle peridotite (high Mg# (>0.7), high

Ni content, and presence of magnesian, nickeliferous olivine ($Fo_{>88}$) (e.g. Umino and Kushiro, 1989)).

Crawford et al. (1989) defined boninites as those lavas either have SiO_2 >53wt% and Mg# >0.6, or are demonstrably derived from parental magmas meeting these compositional requirements. As indicated by them, whithin whole boninitic suits, there exist pronounced variations in wholerock compositions, modal phenocryst mineralogy and textures. Boninites have a diversity and cannot represented by a restricted range of chemical compositions, but this fact is the same with tholeiites and calcalkaline rocks, which are already known to have much variations.

In marked contrast to a diversity of chemical composition of boninites, there exists a rule of great generality for boninites; boninites and boninites series rocks coexist with tholeiites (e.g. Crawford et al., 1985), as calcalkaline rocks coexist with tholeiiites (e.g. Gill, 1981).

Although there exist pronounced temporal and spatial variations in wholerock compositions within boninites, within calcalkaline rocks and within tholeiites, boninites and tholeiites erupted with a close relation in time and space have chemical affinities. For example, low-Ca type 2 boninites, which are characterized by higher total alkalis content, coexist with high alkali olivine tholeiitic basalt (K_2O=1.4 wt%) (Tatsumi and Ishizaka, 1982), and low-Ca type 3 boninites, which have lower total alkalis content than type 2, coexist with low alkali tholeiitic basalt (K2O=0.2 wt%) (Reagan and Meijer, 1984). This fact indicates a close

genetical relationship between boninites and calcalkaline rocks and coexisting tholeiites which might have attained through common mechanism of generation of the parental magmas. Few mechanisms, however, about concurrent genesis of tholeiites and boninites are presented. Boninites and tholeiites have been treated separately, and coexisting tholeiites have been used only to determine tectonic settings of eruption. Crawford et al. (1981) thought that a MORB-source diapir intrudes hydrous sub-arc peridotite and initiates limited contact melting, generating boninites. Crawford et al. (1989) thought that subduction of an active spreading center subparallel to a trench fronting a intra-oceanic arc plays an important role in the genesis of boninites and tholeiites. In fact, these models are not enough to explain chemical affinities between boninites and coexisting tholeiites.

To know boninites is to know the contrastive geochemical characteristics between boninites and tholeiites which are closely related in time and space.

If the contrastive characteristics between boninites and tholeiites are equal to those between calcalkaline rocks and tholeiites, it is appropriate to conclude that calcalkaline-tholeiitic rock suits are originated through the similar processes as boninites-tholeiites suites are.

4.2 Geochemical characteristics of tholeiites versus calcalkaline rocks in the Shirahama Group.

As stated in the previous section, a stress is laid on the contrast between tholeiites and calcalkaline rocks in the Shirahama Group. Fig. 47 shows the conventional Harker variation diagrams. Filled circles are tholeiitic and open squares are calcalkaline rocks in the Shirahama Group. It is fairly apparent that tholeiites have higher TiO_2, P_2O_5 and lower MgO contents than calcalkaline rocks at a given SiO_2 content. CaO, FeO and K_2O show linear trend and have no systematic differences between tholeiites and calcalkaline rocks in this diagram.

The existence of mantle-derived bimodal magmatism makes this kind of diagram meaningless, that is, silica contents are no longer differentiation indices. As a measure of relative differentiation of boninites, calcalkaline rocks and tholeiites, FeO*/MgO ratio is utilized as an abscissa in the next step.

Fig. 48 shows the contrast between tholeiites and calcalkaline rocks in the Shirahama Group, utilizing five elements and seven elemental ratios as ordinates and FeO*/MgO ratio as an abscissa. It is illustrated with this diagram that calcalkaline rocks have higher SiO2, K2O, Rb, Zr and Rb/Sr and lower TiO2, CaO/Al2O3, K2O/Rb, TiO2/Zr, Y/Zr than tholeiites, and Ba/Zr is similar between them.

In the previous chapters, mixing between the tholeiitic and calcalkaline magmas is demonstrated. In order to eliminate this mixing phenomena, rocks which cannot be explained by crystal fractionation model from tholeiites and boninite or which have clear evidence of magma mixing are excluded

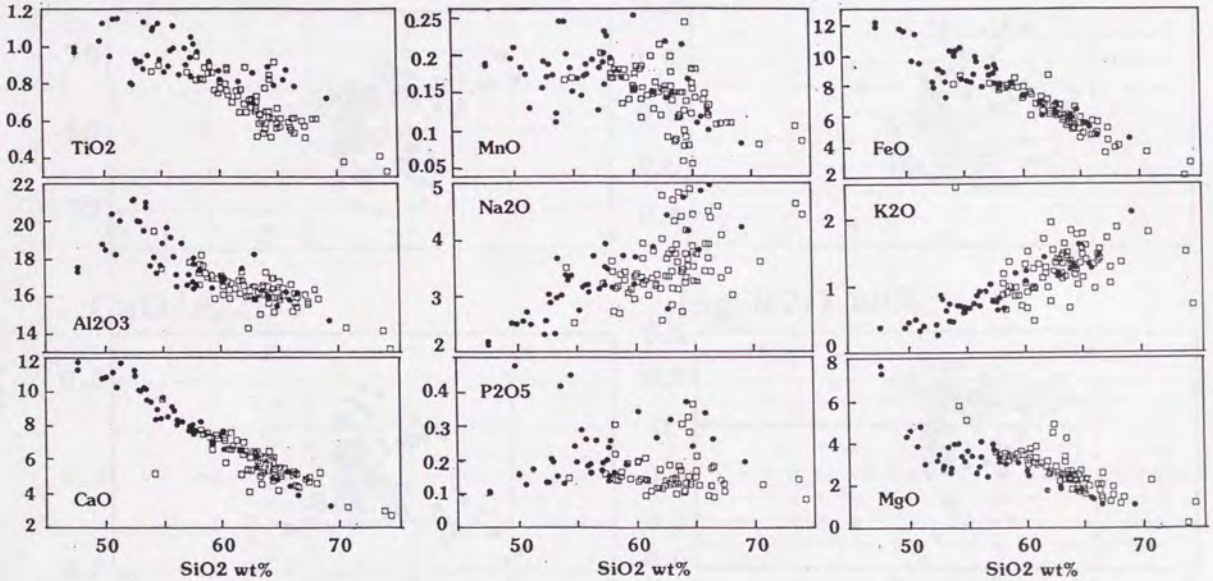

Figure 47. Harker diagram of volcanic rocks in the Shirahama Group on an anhydrous wt.% basis. Tholeiitic rocks are indicated by filled circles and calcalkaline rocks are by open squares.

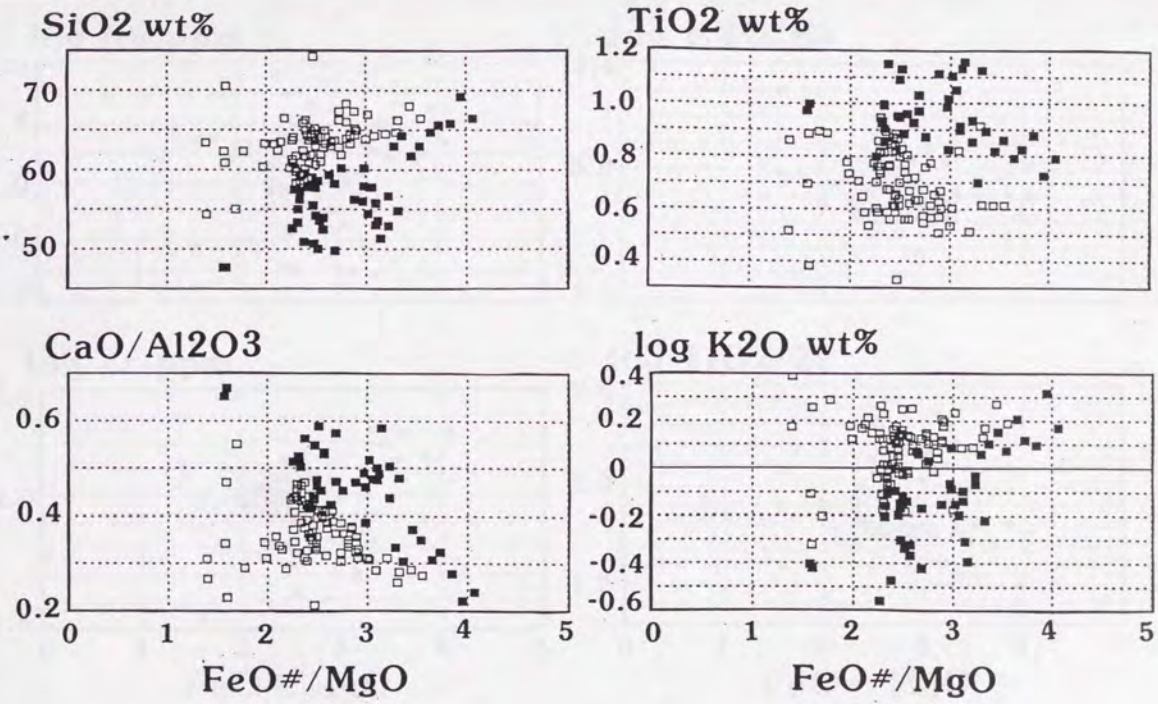

Figure 48 . SiO_2, TiO_2, CaO/Al_2O_3, K_2O, Rb, K_2O/Rb, Zr, TiO_2/Zr, Rb/Sr, Y/Zr, Ba/Zr and V/Zr versus FeO*/MgO ratios of calcalkaline and tholeiitic rocks in the Shirahama group. Filled squares are tholeiites and open squares are calcalkaline rocks.

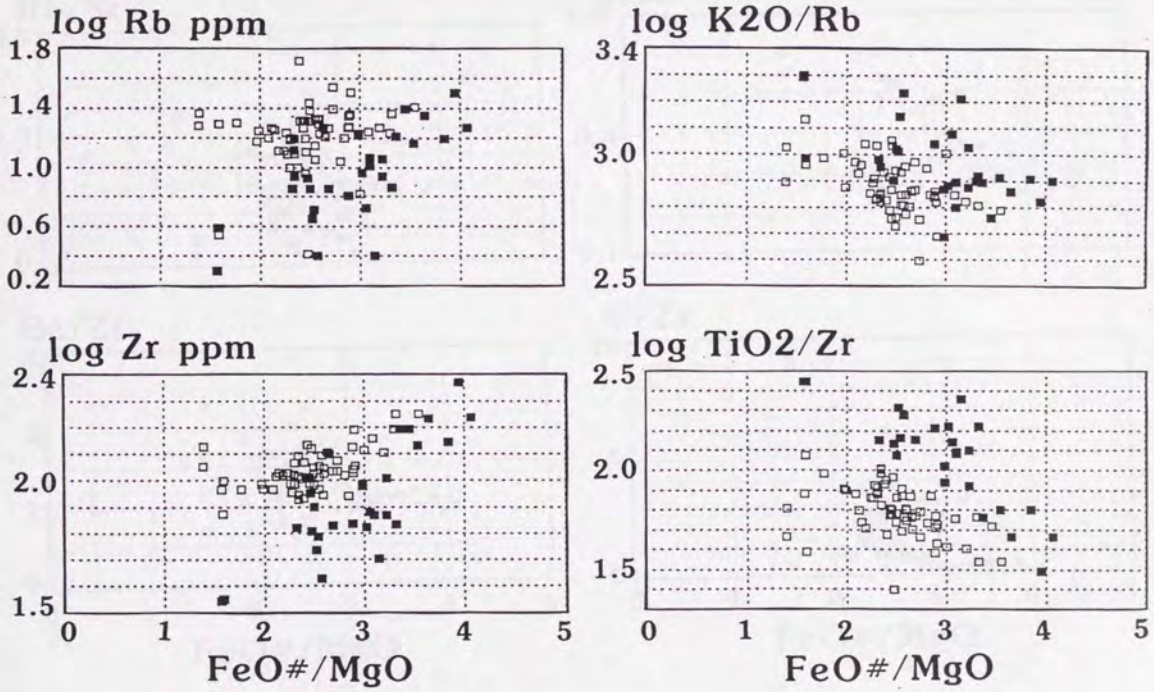
log Rb ppm
1.8
1.4
1.0
0.6
0.2
log K2O/Rb
3.4
3.0
2.5
log Zr ppm
2.4
2.0
1.5
log TiO2/Zr
2.5
2.0
1.5
0
1
2
3
4
5
FeO#/MgO
FeO#/MgO

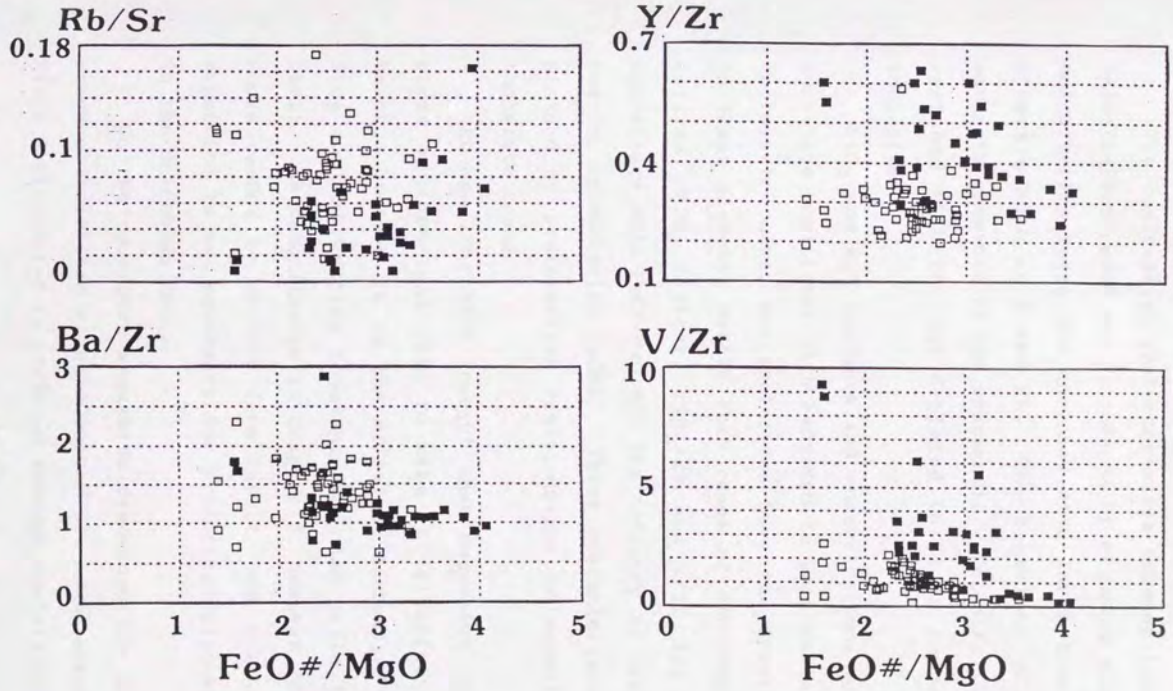
Rb/Sr
0.18
0.1
0
Y/Zr
0.7
0.4
0.1
Ba/Zr
3
2
1
0
V/Zr
10
5
0
0 1 2 3 4 5
FeO#/MgO
0 1 2 3 4 5
FeO#/MgO

from the diagrams (Fig. 49).

The contrastive characteristics between tholeiites and calcalkaline rocks are pronounced by clipping mixed hybrids. Calcalkaline rocks are enriched with large iron lithophile elements such as K and Rb. The behaviour of high field strength elements is not systematic. Calcalkaline rocks are enriched with Zr, but depleted in Ti in comparison with tholeiites.

SiO_2 and K_2O contents and concentrations of Rb and Zr correlate positively with FeO*/MgO in both calcalkaline and tholeiitic rocks, but tholeiites have the drastic increase in these elements within this range of FeO*/MgO. In tholeiites, TiO_2 content, TiO_2/Zr and V/Zr are negatively correlated with FeO*/MgO and the tendency is less conspicuous in calcalkaline rocks. These characteristics are explained by preferential fractionation of magnetite in the tholeiite trend.

It has long been thought that magnetite fractionation plays an important role to make calcalkaline rocks from basalt, because it is the efficient mechanism to increase SiO_2 content keeping constant FeO^*/MgO ratio (e.g. Gill, 1981). As demonstrated in Chapter 3, however, calcalkaline rocks cannot be derived from basalt, and fractionation of magnetite is not necessary for producing calcalkaline rocks in the Shirahama Group.

On the contrary, magnetite fractionation is needed to produce tholeiitic trend (Chapter 3). For example, tholeiitic dacite 311-3 is produced through tholeiitic basalt 305

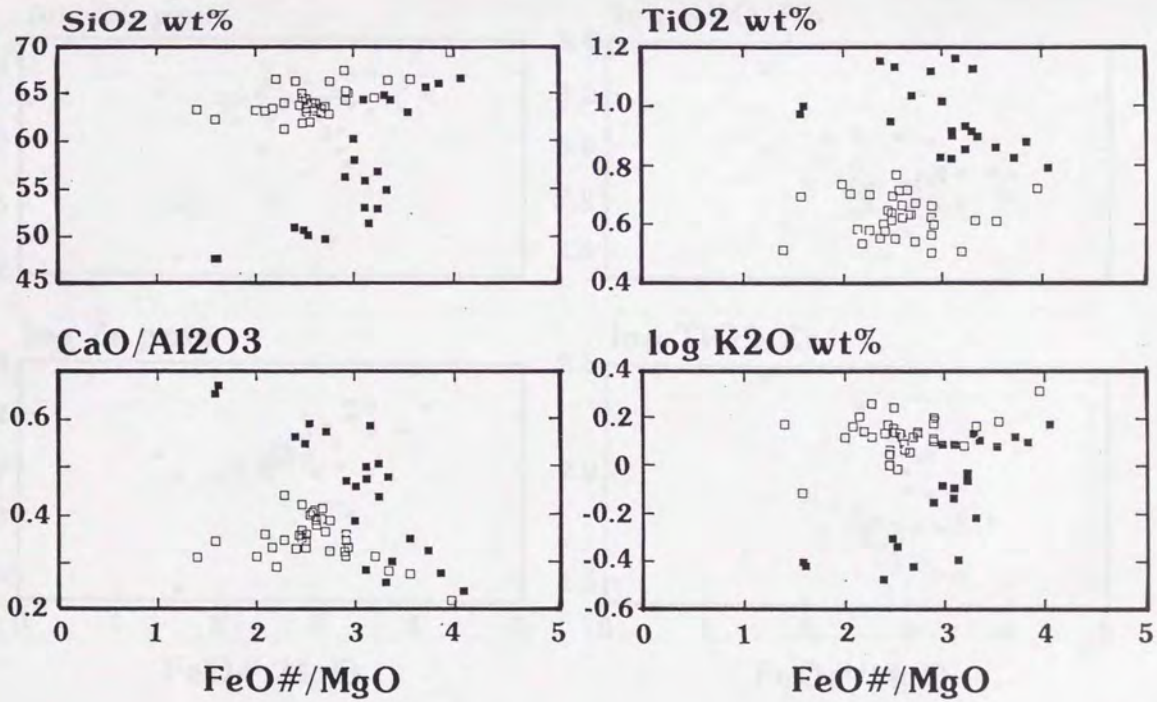

Figure 49 . SiO_2, TiO_2, CaO/Al_2O_3, K_2O, Rb, K_2O/Rb, Zr, TiO_2/Zr, Rb/Sr, Y/Zr, Ba/Zr, and V/Zr versus FeO^*/MgO ratios of selected calcalkaline and tholeiitic rocks which can be adopted to crystal fractionation model.

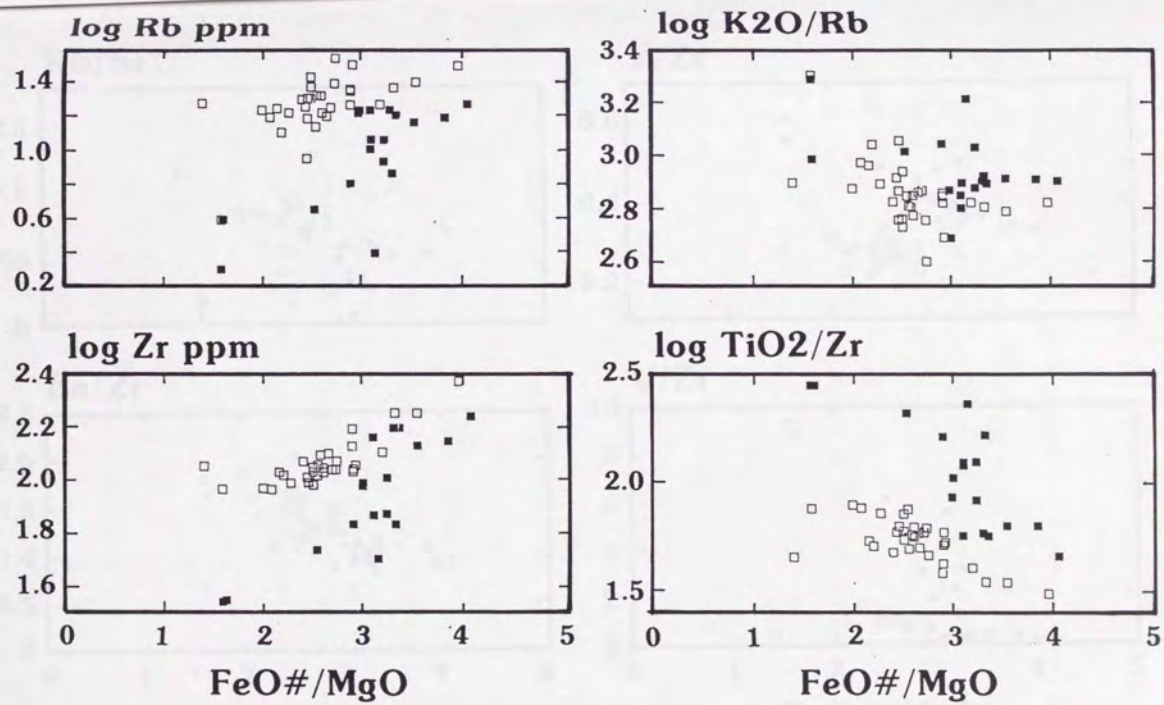
log Rb ppm
1.4
1.0
0.6
0.2
log K2O/Rb
3.4
3.2
3.0
2.8
2.6
log Zr ppm
2.4
2.2
2.0
1.8
1.6
log TiO2/Zr
2.5
2.0
1.5
0
1
2
3
4
5
FeO#/MgO
FeO#/MgO

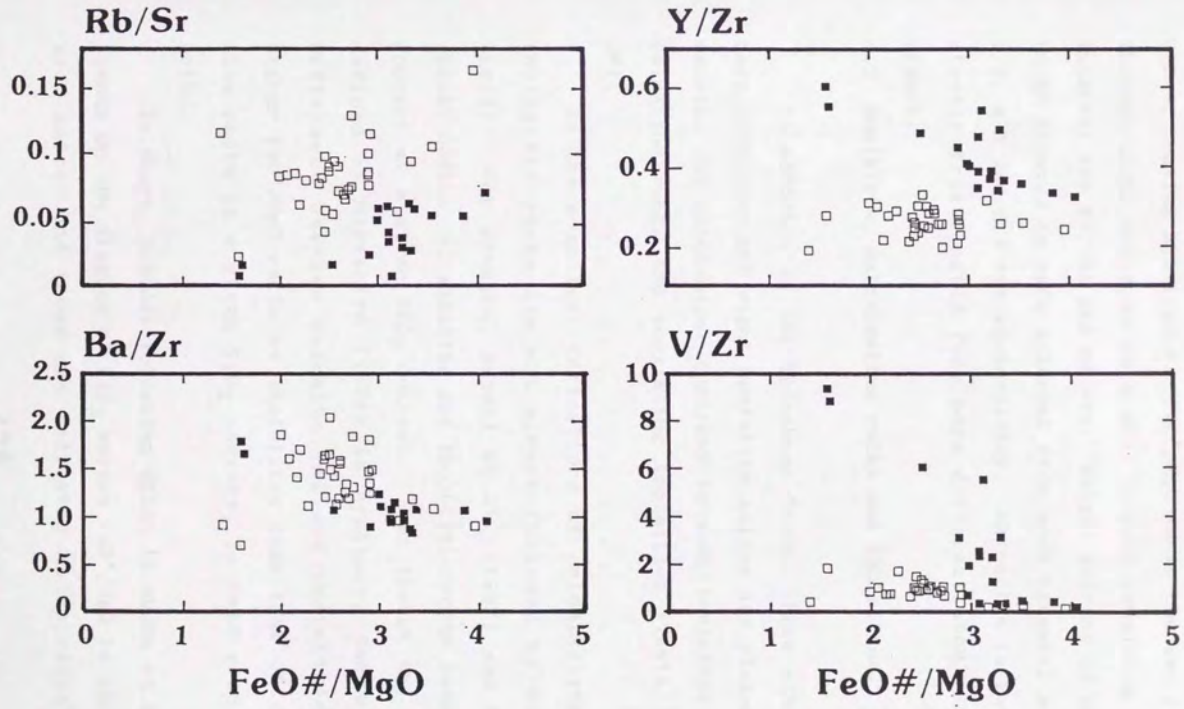
Rb/Sr
0.15
0.1
0.05
0
Y/Zr
0.6
0.4
0.2
Ba/Zr
2.5
2.0
1.5
1.0
0.5
0
V/Zr
10
8
6
4
2
0
0
1
2
3
4
5
FeO#/MgO
FeO#/MgO

and tholeiitic andesite 326 from tholeiitic primitive basalt 312-4, leaving 21% liquid. FeO^*/MgO ratio changes from 1.57 through 2.52 and 2.89 to 3.85. Liquid remaining in each interval are 67, 54 and 58 wt%. Weight percent of magnetite to be removed in each interval from each parental magma are 1.3, 4.6 and 5.4 wt% respectively. Magnetite is more efficiently fractionated from more differentiated tholeiitic magmas.

4.3 boninites, calcalkaline rocks and tholeiites.

In addition to the Shirahama Group, three other Japanese volcanoes and eight boninites suites are picked out to examine the geochemical contrast between boninites or calcalkaline rocks and coexisting tholeiites (Table 11, Fig. 50).

In these suites, definitions of calcalkaline versus tholeiitic rocks are not always followed by Miyashiro (1974). For example, Sasaki et al. (1987) and Fujinawa (1988) define calcalkaline and tholeiitic rocks based on K_2O content at a given SiO_2 content. Even though the boundary defined by Miyashiro (1974) is arbitary, the essential difference between calcalkaline and tholeiitic rocks; higher FeO^*/MgO ratio of tholeiites than that of calcalkaline rocks at a given SiO_2 content, is held good on each suit.

In short, bimodal volcanism which is shown as different trends on the diagram of SiO_2 versus FeO^*/MgO is apparent in each suite, and those are indicated as calcalkaline and

CA andesites & tholeiites	References	FeO*/MgO CA	TH
I Hakkoda volcano group	Sasaki *et al.* (1987)	1.6-2.7	1.7-3.9
II Adatara volcano	Fujinawa (1988)	1.8-2.8	2.0-4.2
III Abu volcano group	Koyaguchi (1986)	1.1-1.8	0.9-1.7
IV Shirahama Group	Tamura	1.4-3.5	1.6-4.1

Boninites, CA andesites & tholeiites		Boninite & CA	TH
1 New Caledonia	Cameron (1989)	0.4-0.7	1.3-1.7
2 Mariana forearc	Bloomer (1987)	0.5-1.4	0.9-8.0
3 Goshikidai	Sato (1981)	0.7-2.4	0.8-1.3
4 Shodo-Shima island	Tatsumi *et al.* (1982)	0.7-2.0	0.8-0.9 #
5 DSDP458	Wood *et al.* (1981)	0.9-1.8	1.5-2.3
6 Guam	Reagan *et al.* (1984)	0.7-1.7	0.7-2.8
7 Victoria	Crawford *et al.* (1985) (1987)	0.7-2.5	1.3-3.2
8 N Tonga trench	Falloon *et al.* (1989)	0.5-0.8	1.0-1.8

New data by Tamura are included.

Table 11. Four Japanese volcanoes which bear calcalkaline and tholeiitic rocks and eight boninites suites which bear boninites, calcalkaline rocks and tholeiites.

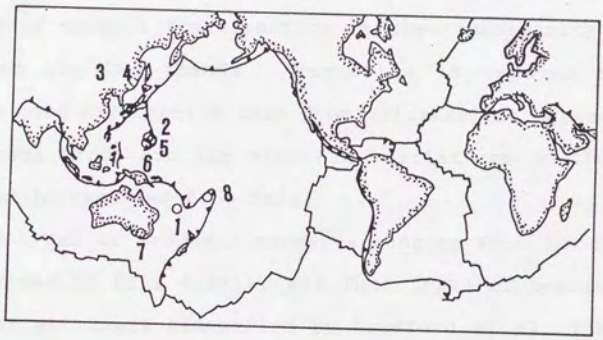

Figure 50. The location of eight boninites and tholeiites suites.

tholeiitic rocks. It is demonstrated in the Shirahama Group, as illustrated in Chapter 3, that the difference between calcalkaline and tholeiitic rocks is derived from the difference of compositions of primary magmas, one is high-Mg andesite and the other is high-alumina basalt. The difference of crystal fractionation is also incorporated in emphasizing the two trends. Magnetite is removed from tholeiites more efficiently than from calcalkaline magmas in the Shirahama Group and the wide SiO_2 variations in tholeiitic trend is resulted from this.

Three types of orogenic andesite ranging from low-K to high-K defined by Gill (1981), and four types of boninites which cover all types classified by Crawford et al. (1989) are examined.

In Japanese volcanoes, volcanic rocks from Hakkoda and Adatara volcanoes range from low-K to mediam-K, those from Abu volcano group from medium-K to high-K and those from the Shirahama Group are mediam-K on a basis of K_2O content at a given SiO_2 content.

In boninites suites, boninites from New Caledonia and Mariana forarc are classified as low-Ca type 1, those from Goshikidai and Shodo-shima island as low-Ca type 2, those from DSDP 458, Guam and Victoria as low-Ca type 3 and those from North Tonga trench as high-Ca boninites, following the classification of Crawford et al. (1989).

The same diagrams with Fig. 49 are made from data in references in Table 11 on an anhydrous wt.% basis. The range of FeO^*/MgO ratios are indicated in Table 11.

Fig. 51 illustrates contrastive characteristics of tholeiites versus boninites and calcalkaline rocks. Each square is a simplified diagram showing relative magnitude of element contents or elemental ratios in calcalkaline rocks and tholeiites or boninites and tholeiites. For example, in the Shirahama Group (IV), tholeiites have higher CaO/Al_2O_3, TiO_2, K_2O/Rb, TiO_2/Zr, Y/Zr and V/Zr and lower SiO_2, K_2O, Rb, Zr and Rb/Sr than calcalkaline rocks and Ba/Zr is similar between them at a given FeO^*/MgO.

It is amazing that in spite of pronounced variations in whole rock compositions within boninites, within calcalkaline rocks and within tholeiites, calcalkaline rocks and boninites have the same geochemical characteristics against coexisting tholeiites. In other words, the characteristics of calcalkaline rocks and boninites exist not in the absolute value such as MgO wt.%, but in the relative value against coexisting tholeiites as shown in Fig. 51. The answer to the question, "What are boninites?", is found in this relative relation between boninites and tholeiites or calcalkaline rocks and tholeiites which are closely related in time and space.

It is concluded that calcalkaline-tholeiitic rock suites are originated through the similar processes as boninites-tholeiites suites are. The origin of calcalkaline and tholeiitic magmas are attributed to the origin of the concurrent formation of boninites and tholeiites.

What governs the geochemical difference between boninites and coexisting tholeiites?

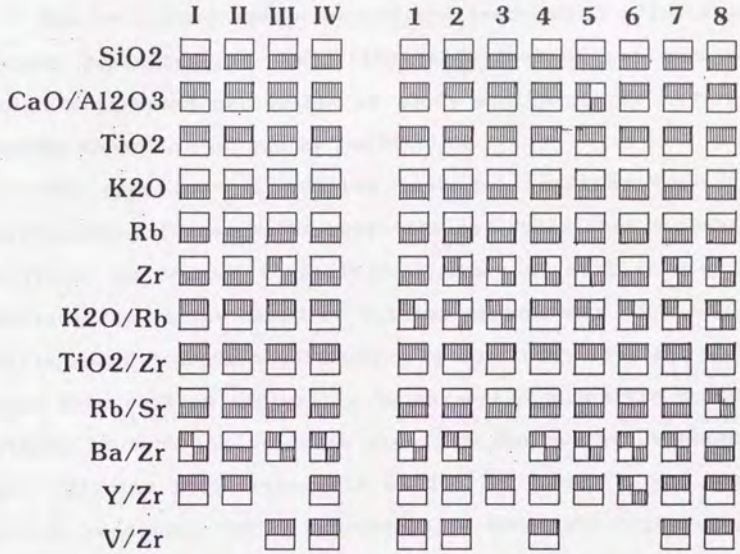

LEGEND

Tholeiites are higher in the left element or elemental ratio than calcalkalis or boninites compared at the similar FeO#/MgO ratio.

vice versa

There are no distinctly different trends in both series.

Figure 51. Simplified diagrams which illustrate the contrastive geochemical characteristics of tholeiites versus boninites and calcalkaline rocks.

Japanese volcanoes: I. Hakkoda volcano group, II. Adatara volcano, III. Abu volcano group, IV. Shirahama group

Boninites suites: 1. New Caledonia, 2. Mariana forarc, 3. Goshikidai, 4. Shodo-shima island, 5. DSDP 458, 6. Guam, 7. Victoria, 8. North Tonga trench

The concurrent formation and the geochemical affinities between boninites and coexisting tholeiites do not approve the heterogeneous peridotite of souce mantle or the heterogeneous depletion of source peridotite.

Two experimental studies have implications for the geochemical differences of boninites and tholeiites. Kushiro (1990) determined compositional range of melt formed in mantle wedge on the basis of melting experiments of a peridotite under hydrous conditions. He concluded that the melt range from olivine tholeiitic to magnesian andesitic compositions beneath the volcanic front in the northeast Honshu arc. Olivine tholeiitic melt at 1.2 Gp, 1200 ˚C and less hydrous condition (357a) and magnesian andesitic melt at 1.2 Gp, 1100 ˚C and hydrous condition (395a) have similar contrastive geochemical characteristics between tholeiites and boninites except K_2O content, which are that magnesian andesitic melt have higher SiO_2 and lower CaO/Al_2O_3 and TiO_2 than olivine tholeiitic melt.

Tatsumi et al. (1986) have carried out dehydration experiments on synthetic serpentine. They concluded that an element with a larger ionic radius is more readily transported by the aqueous fluid phase through the dehydration process. It is indicated that the enrichment of incompatible elements with large ion radii should be caused by the transfer of elements by the fluid phase from the down going lithosphere. In the experiments of Kushiro (1990), if H_2O is derived from the downgoing slab, large ion lithophile elements such as K or Rb will also be added to the souce

peridotite in proportion to the amount of H_2O, and it will cause the magnesian andesitic melt to have higher K_2O and Rb than tholeiites.

In the generation of island-arc magmas, partially melted mantle diapirs are considered (e.g. Sakuyama (1983), Tatsumi et al. (1983), Kushiro (1990)). If there exists a temperature gradient within a mantle diapir incorporated with the heterogeneous contents of slab-derived fluid phase, the one part at lower temperature (1100 °C) with higher content of the fluid phase will produce boninites and the other part at higher temperature (1200 °C) with lower content of the fluid phase will produce tholeiites. It is not enough, but within the limited data, the observed geochemical characteristics between boninites and coexisting tholeiites do not conflict with this simple model .

4.4 CONCLUSION

Boninites have exceptional chemical compositions but relative geochemical characteristics against coexisting tholeiites are not exceptional. The highly magnesian characteristics of boninites, some of which can be in equilibrium with mantle peridotite, has been exaggerated for many years, but such primary magmas also occur in tholeiites. In spite of pronounced variations within boninites suites, boninites have generality which is indicated in relative geochemical characteristics against coexisting tholeiites. This generality also exists in calcalkaline

calcalkaline rocks.

As be presented in the previous chapter, most calcalkaline rocks in the Shirahama Group can be produced by crystal fractionation from boninites.

It is concluded that calcalkaline rocks are "boninites", if high-Mg andesites and their derivatives are defined as "boninites" is the same way as Crawford et al. (1989).

Capter 5

Discussion; Genesis of andesites by bimodal magmatism derived from mantle diapir.

5.1 INTRODUCTION

In the previous chapters, a new hypothesis of the petrogenesis of island-arc magmas has been presented; calcalkaline rocks are the differentiation products of boninites, and accordingly boninites are ubiquitous in island-arcs and mantle-derived magmatism of boninites and tholeiites is the essential mechanism in island-arcs.

In this chapter, the hypothesis in this paper is examined whether it is consistent with the general constraints on calcalkaline rocks or the results of experimental data, and other hypothesis about the genesis of calcalkaline rocks are picked out to illustrate their mistakes.

First, it should be reviewed that the same conclusion of this paper have been presented in an imperfect way by several authors. Masuda and Aoki (1979) concluded from the study of volcanic rocks in the northeast Japan that magmas of the tholeiitic series and calcalkaline series appear to have been generated independently in the upper mantle so far as their trace element concentrations are concerned. In the Ichinomegata volcano, Aoki and Fujimaki (1982) concluded from the similarity of REE concentrations between tholeiites and calcalkaline rocks that both basalt and andesite magmas were formed independently by partial melting from mantle peridotite at similar melting degree but with different

water concentrations. Fujimaki (1988) clarified that the calcalkaline rocks are distinct from the tholeiitic rocks in Sr-isotopic ratios as well as in major- and trace-element chemistries in the Adatara volcano. From the geochemical data, he concluded that the tholeiitic magma and the calcalkaline magma are not derived from a common parental magma and that the calcalkaline magma is richer in SiO_2 and incompatible elements (in particular Rb and Zr), poorer in radiogenic Sr and possibly more oxidized than the tholeiitic magma.

On the other hand, the detailed petrological, geochemical and isotopic studies of various boninites suites have been done during the past decade by many authors, and a major-element-based classification for boninites is done by Crawford et al. (1989). Following the definition of boninites by Crawford et al., the conclusions described above are expressed in a phase, "Calcalkaline rocks are derived from boninites."

5.2 EXPERIMENTS ON BONINITES (HIGH-MG ANDESITES) AS A PRIMARY MAGMA

Boninites are produced by partial melting of mantle wedge. This is demonstrated by several experiments.

Yoder (1969) and Kushiro (1972, 1974) suggested by hydrous melting experiments on synthetic systems that primary andesitic magmas may be generated in peridotitic upper mantle.

Tatsumi (1981, 1982) and Umino and Kushiro (1989)

performed high-pressure melting experiments of boninites from Setouchi and Bonin Is.. Tatsumi (1981, 1982) demonstrated that Setouchi HMA (boninites), TGI (a bronzite olivine HMA) is in equilibrium with harzburgite assemblage above 10 kbar and lower than 1120 °C with water contents exceeding 8%, and that SD261 (an augite olivine HMA) is in equilibrium with lherzolite assemblage above 10 kbar and lower than 1070 °C with water contents exceeding 7%. Unmino and Kushiro (1989) demonstrated that the most magnesian boninite with olivine and bronzite microphenocrysts could coexists with harzburgite above 8 kbar and lower than 1256 °C with water contents exceeding 5%.

Kushiro (1990) performed melting experiments of hydrous peridotite and concluded that the melts range from olivine tholeiitic (1.2 Gp, 1200 °C) to magnesian andesitic (1.2 Gp, 1100 °C) beneath the volcanic front in the northeast Honshu arc.

Boninites (magnesian andesites) are formed in mantle wedge in the hydrous conditions.

On the other hand, few experimental data which demonstrate that some calcalkaline rocks are derived from the partial melts of the lower crust.

As Kushiro (1990) implied, boninites are ubiquitous in island-arcs and the best candidate for the calcalkaline primary magmas on the basis of experimental data.

5.3 GENERAL CONSTRAINTS ON CALCALKALINE ROCKS

Takahashi (1986) summarized some important constraints

on calcalkaline rocks. Those constraints are examined below.

(1) Calcalkaline rocks are represented by the lack of iron-enrichment trend?

As indicated by Takahashi (1986), it is often said that calcalkaline rocks lack iron-enrichment trend, but this is not correct. Mixing between calcalkaline and tholeiitic magmas and the vague assumption that calcalkaline rocks are produced from basalt by crystal fractionation lead to the misunderstanding. In fact, calcalkaline rocks have iron-enrichment trend upon fractional crystallization and it is demonstrated in the previous chapters.

(2) Calcalkaline magmas have relatively low liquidus temperature.

This general observation is reasonably explained by that calcalkaline primary magmas are boninites (magnesian andesites), which are produced at lower temperature and in more hydrous conditions than tholeiites in mantle wedge.

(3) Thick continental crust is necessary to form calcalkaline rocks?

Takahashi (1986) presentes this as one of important constraints, because he thought that thick continental crust is necessary to melt the lower crust. In fact, as Gill (1981) indicated that thick continental crust is not necessary to form calcalkaline rocks, and this is apparent from the fact that generally island-arc have crust <25 km thick (Gill, 1981).

(4) Calcalkaline rocks occur in association with tholeiites

or alkali basalt.

This general observation is well in accord with the fact that boninites occur in association with tholeiites which is presented in Chapter 4. Kushiro (1990) thought by the result of melting experiments of hydrous peridotite that the melt produced in mantle wedge range continuously from olivine tholeiitic to magnesian andesitic. From the observations of boninites-tholeiites suits and calcalkaline rocks-tholeiites suits, it is infered that some mechanisms which produce not continuous but bimodal melts may exist in mantle wedge.

(5) Calcalkaline rocks show evidence of magma mixing?

As presented in Chapter 2 and indicated by Morrice and Gill (1981), calcalkaline rocks do not always show evidence of magma mixing. This is not the constraint on calcalkaline rocks. The important thing is the exclusion of mixed hybrids from rocks in the calcalkalie field of Miyashiro (1974).

(6) Sr-isotopic ratios for calcalkaline rocks do not always high.

Many andesites are isotopically incompatible with crustal derivation (Gill, 1981) and compatible with mantle derivation.

Presented model in this paper is consistent with general constraints on calcalkaline rocks. In addition to these, the observed volume ratio of calcalkaline rocks to tholeiites is too large to be explained by other mechanisms

such as fractionation of basalt or lower crustal melting. On the other hand, it may be possible that larger volume of calcalkaline primary magmas (boninites) relative to those of tholeiites would be supplied by mantle diapirs in island-arcs to the crust.

Average sialic crust is similar in composition to orogenic andesites (Gill, 1981). Kushiro (1990) estimated chemical compositions of crust in Northeast and Southwest Honshu from deep-seated crustal inclusions in volcanic rocks and the velocity structure of the crust. Those in Central Northeast Honshu and Central Southwest Honshu are "magnesian" andesitic (MgO= about 5 wt%). It is accordingly appropriate to think addition of primary andesitic magmas to the crust for the evolution of island-arc crust.

5.4 CONCLUDING REMARKS

The idea in this paper, mantle-derived bimodal magmatism for the origin of island-arc magmas, seems to be extravagant, but in fact, it is not.

Ten years ago, very few petrologists were aware of the existence of boninites, and now it is known that boninites have been erupted throughout Earth history.

Thus the study in this paper is just in our time. The origin of calcalkaline andesites, which is almost synonymous with the petrogenesis of island-arc magmas, is attributed to the mechanisms in the mantle.

The next problem to be solved is how bimodal magmatism occurs in the upper mantle of the subduction zones. Mantle

diapirism in the island-arcs is the sincere demand of the volcanological and petrological studies (e.g. Sakuyama, 1983; Tatsumi et al., 1983). Regret to say, in spite of the geological demands, no satisfactory physical and petrological model of mantle diapir in the subduction zone has been presented.

The ascent of mantle diapir should be clarified by volcanologists and petrologists. The production of bimodal magmas will give a constraints on the internal structure, the genesis and the mode of transportation of mantle diapir in the subduction zone. A new physical and petrological model of mantle diapir is required to produce island-arc magmas.

REFERENCES

Allegre, C.J., Treuil, M., Minster, J.-F., Minster, B. and Albarede, F., 1977. Systematic Use of Trace Element in Igneous Process. Contrib. Mineral. Petrol., 60: 57-75.

Anderson, A.T., 1976. Magma mixing: Petrological process and volcanological tool. J. Volcanol. Geotherm. Res., 1: 3-33.

Aramaki, S. and Akimoto, S., 1957. Temperature estimation of pyroclastic deposits by natural remanent magnesism. Am. Jour. Sci.,255: 619-627.

Aramaki, S. and Ui, T., 1982. Japan. In: R.S. Thorpe (Editor), Andesite. John Wiley & Sons, 724 pp.: 259-292.

Aramaki, S. and Ui, T., 1983. Alkali mapping of the Japanese quaternary volcanic rocks. J. Volcanol. Geotherm. Res., 18: 549-560.

Bence, A.E. and Allbee, A.L., 1968. Empirical correction factors for the erectron microanalysis of silicates and oxides. J. Geol., 76: 382-403.

Bloomer, S.H., 1987. Geochemical characteristics of boninite- and tholeiite-series volcanic rocks from the Mariana forearc and the role of an incompatible element-enriched fluid in arc petrogenesis. Geol. Soc. of Am. Spec. Pap., 215: 151-164.

Bloomer, S.H. and Hawkins, J.W., 1987. Petrology and geochemistry of boninite series volcanic rocks from the Mariana trench. Contrib. Mineral. Petrol. 97: 361-377.

Brown, E. McC., 1981. Paleomagnetic estimates of temperatures reached in contact metamorphism. Geology 9: 112-116.

Bryan, W.B., Finger, L.W. and Chayes, F., 1969. Estimating Proportions in Petrographic Mixing Equations by Least-Squares Approximation. Science 163: 926-927.

Cameron, W.E., 1989. Contrasting boninite-tholeiite associations from New Caledonia. In: A.J. Crawford (Editor), Boninites and related rocks, Unwin Hyman, 465pp.: 314-339.

Carmichael, I.S.E. and Nicholls, J., 1967. Iron-Titanium Oxides and Oxygen Fugacities in Volcanic Rocks. J. Geophys. Res. 72: 4665-4687.

Cox, K.G., Bell, D. and Pankhurst, R.J., 1979. The Interpretation of Igneous Rocks. George Allen & Unwin,

London, 450pp.

Crawford, A.J. and Cameron, W.E., 1985. Petrology and geochemistry of Cambrian voninites and low-Ti andesites from Heathcote, Victoria. Contrib. Mineral. Petrol., 91: 93-104.

Crawford, A.J. and Keays, R.R., 1987. Petrogenesis of Victorian Cambrian Tholeiites and Implications for the Origin of Associated Boninites. J. Petrol., 28: 1075-1109.

Crawford, A.J., Fallon, T.J. and Green, D.H., 1989. Classification, petrogenesis and tectonic setting of boninites. In: A.J. Crawford (Editor), Boninites and related rocks, Unwin Hyman, 465 pp.: 1-49.

Dallwitz, W.B., 1968. Chemical Composition and Genesis of Clinoenstatite-Bearing Volcanic Rocks from Cape Vogel, Papua: A Discussion. XXIII Intern. Geol. Cong. 2: 229-242.

Ewart, A., Bryan, W.B. and Gill, J.B., 1973. Mineralogy and Geochemistry of the Younger Volcanic Islands of Tonga, S.W. Pacific. J. Petrol. 14: 429-65.

Fallon, T.J., Green, D.H. and Mcculloch, M.T., 1989. Petrogenesis of high-Mg and associated lavas form the north Tonga Trench. In: A.J. Crawford (Editor), Boninites and related rocks, Unwin Hyman, 465pp.: 357-395.

Fisher, R.V. and Schmincke, H.-U., 1984. Pyroclastic Rocks. Springer-verlag Berlin Heidelberg NewYork Tokyo. 472pp.

Fiske, R.S., 1963. Subaqueous pyroclastic flows in the Ohanapecosh Formation, Washington. Geoul. Soc. Am. Bull. 74: 391-406.

Fiske, R.S. and Matsuda, T., 1964. Submarine equivalents of ash flows in the Tokiwa Formation, Japan. Am. J. Sci. 262: 76-106.

Fiske, R.S., 1969. Recognition and significance of pumice in marine pyroclastic rocks. Geol. Soc. Amer. Bull. 80: 1-8.

Fiske, R.S. and Cashman, K.V., 1989. Submarine fallout deposit in the Shirahama Group (Mio-Pliocene), Japan (abs.). N. Mex. Bur. Min. Res. 131: 92.

Flower, M.F.J. and Levine, H.M., 1987. Petrogenesis of a tholeiite-boninite sequence from Ayios Mamas, Troodos ophiolite: evidence for splitting of a volcanic arc? Contrib. Mineral. Petrol. 97: 509-524.

Fujinawa, A., 1988. Tholeiitic and calc-alkaline magma series at Adatara volcano, northeast Japan: 1. Geochemical constraints on their origin. Lithos, 22: 135-158.

Fujinawa, A., 1990. Tholeiitic and calc-alkaline magma

series at Adatara volcano, Northeast Japan: 2. Mineralogy and phase relations. Lithos, 24: 217-236.

Gill, J.B., 1981. Orogenic Andesites and Plate Tectonics. Springer-Verlag Berlin Heidelberg New York.

Heiken, G. and Eichelberger, J.C., 1979. Eruptions at Chaos Crags, Lassen Volcanic National Park, California. J. Volcanol. Geotherm. Res., 7: 443-481.

Hernandez, J., 1982. Potassium Enrichment by Magma Mixing and Vapor Exsolution: an Example in the Miocene Volcanism of Eastern Morocco. Bull. Volcanol., 45-4: 385-399.

Hickery, R.L. and Frey, F.A., 1982. Geochemical characteristics of boninite series volcanics: implications for their source. Geochim. Cosmochim. Acta, 46: 2099-2115.

Hickey-Vargas, R. and Reagan, M.K., 1987. Temporal variation of isotope and rare earth element abundances in volcanic rocks from Guam: implications for the evolution of the Mariana Arc. Contrib. Mineral. Petrol. 97: 497-508.

Hickey-Vargas, R., 1989. Boninites and tholeiites from DSDP Site 458, Mariana forearc. In: A.J. Crawford (Editor), Boninites and related rocks, Unwin Hyman, 465pp.: 339-357.

Hoblitt, R.P. and Kellogg, K.S., 1979. Emplacement temperature of unsorted and unstratified deposits of volcanic rock debris as determined by paleomagnetic techniques. Geol. Soc. Am. Bull. 90: 633-642.

Ibaraki, M., 1981. Geologic ages of "Lepidocyclina", Miogypsina horizons in Izu Peninsula as determined by planktonic foraminifera. J. Geol. Soc. Jpn., 87: 417-420.

Ishizaka, K. and Carlson, R.W., 1983. Nd-Sr systematics of the Setouchi volcanic rocks, southwest Japan: a clue to the origin of orogenic andsite. Earth Plane. Sci. Lett., 64: 327-340.

Ito, T., Matsumoto, R., Kano, K. and Sakuyama, M., 1984. Welding of acidic tuff and altered rhyolite fragments caused by the intrusion of magma - Examples in the Neogene Shirahama Group in the southern part of Izu Peninsula, central Japan. J. Geol. Soc. Jpn.. 90: 191-205.

Jakes, P. and White, A.J.R., 1972. Major and trace element abundances in volcanic rocks of orogenic area. Bull. Geol. Soc. Am., 83: 29-40.

Jenner, G.A., 1981. Geochemistry of high-Mg andesites from cape vogel, Papua new guinea. Chem. Geol., 33: 307-332.

Kaneko, T., 1990. Genesis of the quaternary volcanic rocks of central Japan, based on trace element chemistry. Ph. D

thesis of the university of Tokyo, 126pp.

Kano, K., 1983. Structures of Submarine Andesitic Volcano-An example in the Neogene Shirahama group in the southern part of the Izu Peninsula, Japan. Geosci. Repts. Shizuoka Univ., 8: 9-37.

Kent, D.V., Ninkovich, D., Pescatore, T., and Sparks, S.R.J., 1981. Paleomagnetic determination of emplacement temperature of Vesuvius AD 79 pyroclastic deposits. Nature 290: 393-396.

Kikawa, E., Koyama, M. and Kinoshita, H., 1989. Paleomagnetism of Quaternary Volcanics in the Izu Peninsula and Adjacent Areas, Japan, and Its Tectonic Significance. J. Geomag. Geoelectr., 41: 175-201

Kobranova, V.N., 1989. Petrophysics. Mir Publishers Springer-Verlag. 357pp.

Kouchi, A. and Sunagawa, I., 1985. A model for mixing basaltic and dacitic magmas as deduced from experimental date. Contrib. Mineral. Petrol. 89: 17-23.

Koyaguchi, T.,1984. Mixing mechanisms of mafic and felsic magmas: Two stage magma mixing model. Ph.D thesis, Univ. of Tokyo, 253pp.

Koyaguchi, T., 1985. Magma mixing in a conduit. J. Volcanol. Geotherm. Res., 25: 365-369.

Koyaguchi, T., 1986. Textual and compositional evidence for magma mixing and its mechanism, Abu volcano group, Southwestern Japan. Contrib. Mineral Petrol. 93: 33-45.

Koyaguchi, T., 1986. Evidence for two-stage mixing in magmatic inclusions and rhyolitic lava domes on Niijima Island, Japan. J. Volcanol. Geotherm. Res., 29: 71-98.

Koyama, M., 1983. Paleomagnetic evidence for northward drift and local deformation of the Matsuzaki area, Izu Peninsula, Japan. Rock Magnetism and Paleogeophysics 10: 61-68.

Koyama, M., 1985. Tectonic history of the Izu Peninsula and adjacent areas based on paleomagnetism and stratigraphy. Ph.D thesis, Univ. of Tokyo, 133pp.

Koyama, M., 1988. The past and present of the Izu Peninsula: What can we find through scientific drilling? (in Japanese), in Site Proposals for Japanese Continental Drilling I, edited by S. Aramaki and N. Niitsuma, 1-32, Working Group on Japanese Continental Scientific Drilling, Shizuoka.

Kuno, H., 1950. Petrology of Hakone volcano and the adjacent

areas, Japan. Geol. Soc. Am. Bull. 61: 957-1020.

Kuno, H., 1960. High-alumina Basalt. J. Petrol. 1: 121-45.

Kuno, H., 1966. Lateral variation of basalt magma type across continental margins and island arcs. Bull. Volcanol., 29: 195-222.

Kuno, H., 1968. Differentiation of Basalt Magmas. In: H.H. Hess and A. Poldervaart (Editors), Basalts, Interscience Publishers. 862pp.: 623-688.

Kuno, H., 1968. Subaqueous Autobrecciated Lava. Bull. Volc. Soc. Jpn.. 13: 123-130.

Kuroda, N., Urano, H. and Shiraki, K., 1983. Least differentiated basalt from Mukoo-Jima in the Haha-Jima group, bonin islands. J. Geol. Soc. Jpn., 89: 303-306.

Kushiro, I., 1972. Effect of water on the composition of magmas formed at high pressure. J. Petrol. 13: 311-34.

Kushiro, I., 1974. Melting of hydrous upper mamtle and possible generation of andesitic magma: an approach from synthetic systems. Earth Planet. Sci. Lett. 22: 294-9.

Kushirdo, I., 1987. A petrological model of the Mantle wedge and lower crust in the Japanese island arcs. Geochem. Soc. Special Publication, 165-181.

Kushiro, I., 1990. Partial Melting of Mantle Wedge and Evolution of Island Arc Crust. J. Geophys. Res. 95: 15,929-15,939.

Lindsley, D.H. and Andersen, D.J., 1983. A two-pyroxene thermometer. Proceedings of the Thirteenth Lunar and Planetary Science Conference, Part 2, J. Geophys. Res., 88, supplement: A887-A906.

Longhi, J., Walker, D. and Hays, J.F., 1976. Fe and Mg in plagioclase. Proc. Lunar Sci. Conf. 7th: 1281-1300.

Masuda, Y., 1978. Two types of Island arc tholeiite in Japan. Earth Plane. Sci. Lett., 39: 298-302.

Masuda, Y. and Aoki, K., 1979. Trace element variation in the volcanic rocks from the Nasu Zone, Northeast Japan. Earth planet. Sci. Lett. 44: 139-49.

Matsumoto, R. and Urabe, T., 1980. An automatic analysis of major elements in silicate rocks with X-ray flurescence spectrometer using fused disc samples. J. Jpn. Assoc. Miner. Petrol. Econ. Geol. 75: 272-278.

Matsumoto, R., Katayama, T. and Iijima, A., 1985. Geology, igneous activity, and hydrothermal alteration in the Shimoda

district, southern part of Izu Peninsula, central Japan. J. Geol. Soc. Jpn. 91: 43-63.

Mattson, S.R., Vogel, T.A. and Wilband, J.T., 1986. Petrochemistry of the silicic-mafic complexes at vesturhorn and austurhorn, Iceland: Evidence for zone/stratified magma. J. Volcanol. Geotherm. Res., 28: 197-223.

McClelland, E.A. and Druitt, T.H., 1989. Paleomagnetic estimates of emplacement temperatures of pyroclastic deposits on Santorini, Greece. Bull. Volcanol. 51: 16-27.

Meijer, A., 1980. Primitive Arc Volcanism and a Boninite Series: Examples From Western Pacific Island Arcs. In: D.E. Hayes (Editor), The Tectonic and Geologic Evolution of Southeast Asian Seas and Islands Am. Geophys. Union. Monogr. 23: 269-282.

Miyashiro, A., 1974. Volcanic rock series in island arcs and active continental margin. Am. J. Sci. 274: 321-355.

Moritani, T. and Sawamura, K., 1965. Tertiary formation of the Matsuzaki district, Izu Peninsula, Japan. Bull. Geol. Surv. Jpn, 16: 535-545.

Pearce, J.A. and Norry, M.J., 1979. Petrogenetic Implications of Ti, Zr, Y, and Nb Variations in Volcanic Rocks. Contrib. Mineral. Petrol. 69: 33-47.

Pedersen, R.B. and Hertogen J., 1990. Magmatic evolution of the Karmoy Ophiolite Complex, SW Norway: relationships between MORB-IAT- boninitic-calc-alkaline and alkaline magmatism. Contrib. Mineral. Petrol. 104: 277-293.

Reagan, M.K. and Meijer, A., 1984. Geology and geochemistry of early arc-volcanic rocks from Guam. Geol. Soc. Am. Bull., 95: 701-713.

Rogers, G. and Saunders, A.D., 1989. Magnesian andesites from Mexico, Chile and the Aleutian Islands: implications for magmatism associated with ridge-trench collision. In: A.J. Crawford (Editor), Boninites and related rocks, Unwin Hyman, 465pp.: 416-445.

Sakuyama, M., 1979. Evidence of magma mixing; petrological study of Shirouma Oike calc-alkaline andesite volcano, Japan. J. Volcanol. Geotherm. Res. 5: 179-208.

Sakuyama, M., 1979. Lateral variation of H2O contents in quaternary magmas of northeastern Japan. Earth Planet. Sci. Lett., 43: 103-111.

Sakuyama, M., 1981. Petrological study of the Myoko and Kurohime volcanoes, Japan: Crystallization sequence and evidence for magma mixing. J. Petrol. 22: 553-583.

Sakuyama, M., 1983. Petrology of arc volcanic rocks and their origin by mantle diapirs. J. Volcanol. Geotherm. Res. 18: 297-320.

Sakuyama, M., 1984. Magma Mixing and Magma Plumbing Systems in Island Arcs. Bull. Volcanol., 47-4: 137-155.

Sakuyama, M. and Koyaguchi, T., 1984. Magma mixing in mantle xenolith- bearing calc- alkaline ejecta, Ichinomegata volcano, NE Japan. J. Volcanol. Geotherm. Res. 22: 199-224.

Sakuyama, M. and Nesbitt, R.W., 1986. Geochemistry of the Quaternary volcanic rocks of the Northeast Japan arc. J. Volcanol. Geotherm. Res., 29: 413-450.

Sato, H., 1981. Bulk Rock Chemistry of the Volcanic Rocks of Goshikidai and Adjacent Areas, northeast Shikoku, Japan. Sci. Rep. Kanazawa Univ., 26: 51-72.

Sato, H., 1989. Mg-Fe Partitioning between plagioclase and liquid in basalts of hole 504B, ODP leg 111: A study of melting at 1 atm. Proceedings of the Ocean Drilling Program, Scientific Results, 111: 17-26.

Saunders, A.D., Rogers, G., Marriner, G.F., Terrell, D.J. and Verma, S.P., 1987. Geochemistry of cenozoic volcanic rocks, Baja California, Mexico: Implications for the petrogenesis of post-subduction magmas. J. Volcanol. Geotherm. Res. 32: 223-245.

Takahashi, E., 1986. Genesis of calc-alkali andesite magma in a hydrous mantle - crust boundary: petrology of lherzolite xenoliths from the Ichinomegata crater, Oga peninsula, northeast Japan, Part II. J. Volcanol. Geotherm. Res., 29: 355-396.

Tamura, Y., 1986MS. The volcanic activities of the Shirahama group of the Matsuzaki district, Izu Peninsula, Japan. Grad. Thesis of Univ. of Tokyo.

Tamura, Y., 1989. The differentiation of magmas in the Shirahama Group, Izu Peninsula (abst.).Bull. Volcanol. Soc. Jpn.,34: 323.

Tatsumi, Y., 1981. Melting experiments on a high-magesian andesite. Earth Planet. Sci. Lett. 54: 357-65.

Tatsumi, Y., 1982. Origin of high-magnesian andesites in the Setouchi volcanic belt, southwest Japan, II. Melting phase relations at high pressures. Earth Planet. Sci. Lett. 60: 305-17.

Tatsumi, Y. and Ishizaka, K., 1982. Origin of high-magnesian andesites in the Setouchi volcanic belt, southwest Japan, I. Petrographical and chemical characteristics. Earth Planet. Sci. Lett., 60: 293-304.

Tatsumi, Y. and Ishizaka, K., 1982. Magnesian andesite and basalt from Shodo-Shima island, southwest Japan, and their bearing on the genesis of calc-alkaline andesites. Lithos, 15: 161-172.

Tatsumi, Y., Hamilton, D.L. and Nesbitt, R.W., 1986. Chemical characteristics of fluid phase released from a subducted lithosphere and origin of arc magmas: evidence from high-pressure experiments and natural rocks. J. Volcanol. Geotherm. Res., 29: 293-310.

Thompson, R.A. and Dungan, M.A., 1985. The petrology and geochemistry of the handkerchief mesa mixed magma complex, San Juan Mountains, Colorado. J. Volcanol. Geotherm. Res., 26: 251-274.

Tsuchi, R., Kuroda, N., Kano, K. and Ibaraki M., 1986. Geological map of Shizuoka Prefecture. Shizuoka Prefecture.

Tsukui, M. and Aramaki, S., 1990. The Magma Reservoir of the Air Pyroclastic Eruption - A Remarkably Homogenous High-Silica Rhyolite Magma Reservoir. Bull. Volcanol. Soc. Jpn., 35: 231-248.

Umino, S., 1985. Volcanic geology of chichijima, the bonin islands (Ogasawara Islands). J. Geol. Soc. Jpn., 91: 505-523.

Umino, S., 1986. Magma mixing in boninite sequence of Chichijima, Bonin Islands. J. Volcanol. Geotherm. Res., 29: 125-158.

Umino, S. and Kushiro, I., 1989. Experimental studies on boninite petrogenesis. In: A.J. Crawford (Editor) Boninites and related rocks, Unwin Hyman, 465pp.: 89-111.

Uto, K., 1986. Variation of Al2O3 content in late cenozoic Japanese basalts: A Re-examination of Kuno's high-alumina basalt. J. Volcanol. and Geothermal Res., 29: 397-411.

Walker, D.A. and Cameron, W.E., 1983. Boninite Primary Magmas: Evidence from the Cape Vogel Peninsula, PNG. Contrib. Mineral. Petrol., 83: 150-158.

Wood, D.A., Marsh, N.G. Tarney, J., Joron, J.-L., Fryer, P. and Treuil, M., 1981. Geochemistry of igneous rocks recovered from a transect across the Mariana Trough, arc, fore-arc, and trench sites 453 through 461,DSDP Leg 60. Intit. Rep. DSDP Leg 60, 611-45.

Wright, J.V., 1978. Remanent magnetism of poorly sorted deposits from the Minoan eruption of Santorini. Bull. Volcanol. 41: 131-135.

Wright, T.L. and Doherty, P.C., 1970. A Linear Programming

and Least Squares Computer Method for Solving Petrologic Mixing Problems. Geol. Soc. Am. Bull., 81: 1995-2008.

Yamazaki,T., Kato, I., Muroi, I, and Abe, M., 1973. Textual analysis and flow mechanism of the Donzurubo subaqueous pyroclastic flow deposits. Bull. Volcanol. 37: 231-244.

Yoder, H.S., 1969. Calcalkalic andesites: experimental data bearing on the origin of their assumed characteristics. In: A.R. McBirney (Editor), Proc. Andesite Conf., Dept. Geol. Mineral Indus., Oregon, Bull. 65: 77-89.

Appendix 1

Whole-rock chemical compositions of volcanic rocks in the Shirahama Group

Sample No.	277	278	279	260	261	262	263	264	265-1	265-2
SiO2	70.63	64.98	66.47	60.32	62.23	74.34	63.24	63.21	61.70	54.26
TiO2	0.38	0.56	0.54	0.78	0.70	0.33	0.74	0.71	0.73	0.86
Al2O3	14.29	15.83	15.39	16.93	15.91	13.17	16.18	16.21	16.14	19.52
FeO	3.61	5.94	5.56	7.32	7.08	2.90	6.70	6.40	7.29	8.07
MnO	0.08	0.16	0.13	0.19	0.15	0.09	0.15	0.20	0.15	0.17
MgO	2.26	2.30	2.54	3.71	4.48	1.17	3.36	3.07	3.17	5.78
CaO	3.24	5.01	4.44	5.84	5.43	2.77	5.02	5.77	5.20	5.20
Na2O	3.60	3.28	3.43	3.26	3.13	4.44	3.14	2.83	3.79	3.51
K2O	1.80	1.78	1.41	1.51	0.78	0.71	1.33	1.47	1.70	2.47
P2O5	0.13	0.15	0.09	0.15	0.12	0.09	0.15	0.14	0.12	0.15
Total	100.00	100.00	100.00	100.00	100.00	100.00	100.00	100.00	100.00	100.00
FeO*/MgO	1.60	2.59	2.19	1.97	1.58	2.47	1.99	2.09	2.30	1.40
Rb	19.6	19.7	12.8	15.0	3.9	2.6	17.6	15.7	15.7	23.1
Sr	175.3	183.2	208.3	207.8	176.1	151.6	212.5	186.9	190.7	204.3
Ba	230.5	200.4	176.4	103.1	64.0	83.2	172.4	147.9	115.5	205.0
Y	24.4	26.9	28.9	32.2	25.7	35.9	29.0	27.7	33.7	41.2
Zr	99.5	88.0	104.6	96.6	92.2	131.9	93.2	92.5	96.3	134.4
V	38.8	64.5	80.9	132.1	166.0	19.1	77.7	94.2	128.2	167.2
Cr	1.3		2.9	0.9	11.0		3.7		8.6	4.5
Ni		2.2	1.6	1.9	5.5		3.1	1.8	3.0	3.9
Cu	2.0			8.1	18.9	16.1	10.3	4.3	16.0	10.8
Zn	76.1			63.3	67.7	37.2	60.4	49.8	59.5	71.9
Ga				16.4	16.7	13.2	15.5	15.4		
Nb	2.7			2.5	2.1	2.9	2.2	1.5	2.4	3.6
La	8.0			0.4	0.5	14.7	8.6	0.1	13.6	10.9
Ce	24.7			12.0	14.4	16.3	16.5	26.4	19.2	18.7
Sc				22.3	24.6	15.2	25.9	22.7		
Th	1.2			2.2	0.6	2.0	2.7	3.0	1.9	1.7

Sample No.	265-3	275-1	275-3	270	266	267	268	274-1	274-2	274-3
SiO2	62.32	60.18	59.49	63.49	63.69	64.51	64.56	66.06	63.23	60.82
TiO2	0.89	0.81	0.86	0.63	0.61	0.61	0.61	0.57	0.65	0.89
Al2O3	14.26	16.08	15.89	16.09	16.12	15.86	15.16	15.19	16.12	16.16
FeO	8.68	7.91	8.48	6.06	6.03	5.68	6.60	5.71	6.41	6.03
MnO	0.21	0.16	0.17	0.15	0.09	0.09	0.14	0.15	0.18	0.19
MgO	4.88	3.45	3.58	2.28	2.48	2.28	2.69	2.03	2.25	3.81
CaO	4.14	7.35	7.45	6.26	5.73	5.41	5.56	5.31	6.09	7.60
Na2O	2.56	3.25	3.07	3.75	3.61	3.66	3.54	3.91	3.83	3.94
K2O	1.94	0.67	0.86	1.15	1.51	1.77	1.02	0.97	1.11	0.48
P2O5	0.13	0.14	0.15	0.13	0.13	0.14	0.13	0.10	0.13	0.10
Total	100.00	100.00	100.00	100.00	100.00	100.00	100.00	100.00	100.00	100.00
FeO*/MgO	1.78	2.30	2.37	2.66	2.43	2.49	2.45	2.81	2.85	1.59
Rb	19.9	9.9	10.0	15.9	18.3	20.4	9.0	10.9	15.7	3.5
Sr	142.0	227.2	232.7	245.5	224.1	225.1	222.3	204.5	221.9	206.9
Ba	120.5	120.2	110.0	167.7	163.4	182.9	166.9	144.3	108.4	89.9
Y	29.7	26.9	32.4	36.7	28.1	33.7	23.1	33.2	33.3	59.1
Zr	92.2	104.9	100.9	125.6	102.8	111.9	102.1	104.4	87.5	74.6
V	150.3	173.2	202.5	92.6	105.0	90.5	93.0	81.5	75.9	196.6
Cr	7.0	6.9	8.9	2.3	3.5	2.1	3.5		3.3	3.5
Ni	3.8	3.6	5.1	2.3	3.1	2.8	4.0	0.7	0.7	2.9
Cu	9.7	17.8	35.4	17.6	13.8	11.7	8.4	5.2	5.5	9.9
Zn	64.8	63.8	64.7	53.8	47.6	44.0	44.8	57.4	75.2	126.9
Ga										
Nb	2.6	2.8	1.7	2.5	2.9	2.3	1.5	1.9	1.6	2.9
La	15.3	8.1	11.1	14.5	0.3	9.4	10.5	7.8	14.5	5.4
Ce	16.3	9.8	23.8	23.5	22.3	23.3	26.5	23.9	21.9	27.7
Sc										
Th	2.1	2.1	2.1	2.6	2.6	1.8	0.7	1.9	1.8	2.0

Sample No.	271	273	211	242	241	282	283	281-1	281-2	239
SiO2	62.92	62.69	62.43	64.32	64.32	63.22	64.13	60.89	60.80	59.75
TiO2	0.72	0.72	0.68	0.84	0.66	0.67	0.62	0.74	0.76	0.76
Al2O3	15.84	15.92	16.34	15.88	16.43	16.09	16.06	16.72	16.38	16.96
FeO	6.70	6.61	6.29	6.05	5.80	6.43	5.92	7.36	7.57	7.83
MnO	0.15	0.16	0.12	0.08	0.10	0.16	0.15	0.16	0.14	0.14
MgO	2.53	2.56	2.65	2.51	2.04	2.48	2.28	2.89	3.33	3.40
CaO	6.51	6.50	6.12	5.77	6.14	6.19	5.99	6.88	6.67	7.32
Na2O	3.34	3.36	4.02	3.24	3.34	3.44	3.46	3.27	3.21	3.12
K2O	1.17	1.35	1.22	1.32	1.17	1.18	1.26	0.95	0.99	0.71
P2O5	0.13	0.13	0.14			0.15	0.13	0.14	0.15	
Total	100.00	100.00	100.00	100.00	100.00	100.00	100.00	100.00	100.00	100.00
FeO*/MgO	2.65	2.58	2.38	2.41	2.85	2.60	2.60	2.55	2.28	2.31
Rb	16.1	21.1				16.8	21.2	11.2	12.2	
Sr	235.5	234.6				233.2	236.4	243.4	227.5	
Ba	155.9	146.4				164.2	175.0	161.1	149.1	
Y	35.8	37.3				30.0	27.5	26.8	28.2	
Zr	124.8	123.9				106.1	111.2	92.2	90.4	
V	133.0	120.5				119.1	98.0	123.9	132.7	
Cr	3.4	3.9				3.7	0.4	5.9	3.7	
Ni	2.2	3.4				3.6	1.9	5.6	4.2	
Cu	19.9	20.9				14.1	15.4	31.5	27.6	
Zn	54.7	56.2				53.7	46.1	47.8	64.9	
Ga										
Nb	3.3	3.0				1.6	2.5	2.0	2.2	
La	5.6	10.9				11.8	1.9	9.7	7.9	
Ce	22.8	34.1				11.2	28.1	21.1	21.7	
Sc										
Th	2.2	2.2				1.9	3.1	1.6	2.3	

Sample No.	240	12	190	280-1	280-2	294	76	74	51	285-3
SiO2	58.91	64.03	61.95	62.42	63.48	65.27	60.61	58.67	58.72	60.20
TiO2	0.89	0.58	0.77	0.65	0.58	0.57	0.80	0.82	0.82	0.78
Al2O3	16.97	15.59	16.59	16.02	16.04	16.04	16.78	17.28	17.21	16.53
FeO	8.05	5.47	6.76	6.05	5.73	5.55	7.55	7.85	8.00	7.36
MnO	0.18	0.15	0.17	0.16	0.15	0.14	0.18	0.18	0.18	0.18
MgO	3.27	2.40	2.66	2.86	2.66	1.92	3.03	3.24	3.25	3.29
CaO	7.39	5.40	6.57	5.39	5.28	5.52	6.65	7.62	7.60	7.16
Na2O	3.38	4.42	3.39	4.79	4.32	3.25	3.33	3.19	2.69	3.40
K2O	0.96	1.83	0.98	1.54	1.62	1.61	0.94	1.00	1.37	0.91
P2O5		0.11	0.17	0.13	0.13	0.13	0.14	0.15	0.16	0.20
Total	100.00	100.00	100.00	100.00	100.00	100.00	100.00	100.00	100.00	100.00
FeO*/MgO	2.46	2.28	2.54	2.11	2.15	2.89	2.50	2.42	2.46	2.24
Rb			14.0	18.2	17.7	22.2			12.6	12.8
Sr			259.3	209.9	208.7	222.6			240.5	278.8
Ba			147.4	153.4	150.4	198.3			115.1	169.2
Y			34.0	23.6	23.0	28.2			32.8	36.5
Zr			103.0	103.4	106.8	110.3			89.2	106.5
V			126.8	67.5	77.7	76.1			150.9	227.1
Cr			6.1	2.5	1.4	4.1			8.8	28.2
Ni			2.5	1.3	3.5	2.0			4.2	5.6
Cu			13.7	17.7	18.1	17.2			17.4	71.2
Zn			57.6	43.4	45.0	49.5			80.7	58.1
Ga										
Nb			2.9	1.8	1.9	2.3			2.6	2.8
La			7.5	1.6	6.3	3.2			6.5	13.2
Ce			31.7	13.8	26.3	17.6			21.5	24.1
Sc										
Th			2.0	0.9	1.5	2.3			0.1	3.6

Sample No.	46	7	218	36	Mz1W	205	224	295-1	295-2	286
SiO2	58.46	57.39	58.52	58.25	67.32	58.17	54.92	62.79	63.55	59.21
TiO2	0.83	0.86	0.81	0.82	0.57	0.82	0.90	0.67	0.64	0.86
Al2O3	18.22	17.80	17.63	17.74	15.66	17.28	17.49	16.55	16.60	17.12
FeO	7.79	8.18	7.87	7.85	5.20	7.72	8.66	6.00	5.80	8.22
MnO	0.17	0.20	0.18	0.19	0.11	0.17	0.17	0.16	0.09	0.14
MgO	3.10	3.57	3.36	3.41	1.90	3.30	5.09	2.20	2.33	3.51
CaO	7.51	7.83	7.59	7.68	4.74	7.75	9.63	6.38	5.45	6.62
Na2O	3.14	3.23	3.14	2.72	3.31	3.62	2.52	3.66	3.91	3.29
K2O	0.66	0.78	0.90	1.19	1.05	0.87	0.62	1.41	1.44	0.85
P2O5	0.14	0.16		0.14	0.13	0.31		0.19	0.18	0.19
Total	100.00	100.00	100.00	100.00	100.00	100.00	100.00	100.00	100.00	100.00
FeO*/MgO	2.51	2.29	2.34	2.30	2.74	2.34	1.70	2.73	2.49	2.34
Rb						12.3		24.8	27.1	12.4
Sr						244.6		330.0	309.0	319.4
Ba						104.8		198.8	214.4	144.5
Y						72.2		27.8	24.7	24.5
Zr						123.1		108.5	105.6	84.6
V						157.0		112.9	115.2	189.6
Cr						1.9		4.8	1.8	9.9
Ni						4.6		2.7	2.7	2.3
Cu						19.4		13.2	10.0	11.8
Zn						82.2		53.1	51.6	62.4
Ga										
Nb						3.2		4.2	3.6	3.2
La						5.0		9.2	6.6	9.8
Ce						22.3		31.2	15.3	24.7
Sc										
Th						1.0		3.5	2.3	2.3

Sample No.	249-2	228	229	230	237	238	56	236-3	236-2	233
SiO2	59.27	64.98	65.28	63.95	60.05	61.57	67.08	67.98	68.31	64.05
TiO2	0.90	0.67	0.61	0.77	0.75	0.76	0.60	0.61	0.61	0.66
Al2O3	16.92	16.48	16.43	16.53	17.01	16.81	16.04	16.32	15.82	16.36
FeO	7.93	5.43	4.90	6.11	7.18	6.82	3.58	3.87	4.05	6.08
MnO	0.18	0.18	0.18	0.12	0.16	0.20	0.11	0.11	0.11	0.15
MgO	3.37	2.26	1.97	2.18	3.14	2.84	1.19	1.13	1.45	2.47
CaO	7.03	5.03	5.50	5.65	7.44	6.57	4.94	4.67	5.29	6.23
Na2O	3.42	3.51	3.74	3.42	2.94	3.31	4.60	3.45	3.01	2.73
K2O	0.99	1.46	1.39	1.27	1.33	1.12	1.72	1.87	1.36	1.29
P2O5							0.14			
Total	100.00	100.00	100.00	100.00	100.00	100.00	100.00	100.00	100.00	100.00
FeO*/MgO	2.35	2.41	2.49	2.80	2.29	2.40	3.02	3.44	2.80	2.46
Rb										
Sr										
Ba										
Y										
Zr										
V										
Cr										
Ni										
Cu										
Zn										
Ga										
Nb										
La										
Ce										
Sc										
Th										

Sample No.	236-1	235	234	329	330	303-1	303-2	302	309-2	300
SiO2	63.66	61.78	65.98	64.00	67.40	61.88	61.27	63.32	66.27	64.72
TiO2	0.60	0.76	0.58	0.56	0.51	0.65	0.70	0.52	0.62	0.92
Al2O3	16.34	17.30	16.60	16.21	15.54	16.88	16.43	15.01	16.09	16.33
FeO	6.00	6.82	4.75	5.50	4.41	6.29	6.81	5.86	4.77	5.45
MnO	0.15	0.15	0.14	0.12	0.11	0.13	0.15	0.14	0.12	0.08
MgO	2.65	2.48	2.00	2.16	1.53	2.57	3.00	4.20	1.44	1.65
CaO	6.08	6.28	5.17	6.49	5.04	7.10	7.20	4.63	4.53	4.22
Na2O	3.12	3.16	3.44	3.47	4.07	3.20	3.01	4.71	4.50	4.90
K2O	1.40	1.27	1.33	1.38	1.28	1.19	1.33	1.50	1.49	1.35
P2O5				0.11	0.11	0.12	0.11	0.10	0.18	0.37
Total	100.00	100.00	100.00	100.00	100.00	100.00	100.00	100.00	100.00	100.00
FeO*/MgO	2.26	2.75	2.37	2.55	2.89	2.45	2.27	1.40	3.32	3.30
Rb				21.4	18.5	20.8	17.0	19.1	23.2	17.1
Sr				226.6	215.4	212.6	212.2	165.6	247.9	269.9
Ba				127.7	194.1	123.2	107.7	102.2	206.4	136.5
Y				28.7	28.0	26.9	28.0	21.5	45.1	53.6
Zr				113.2	133.4	102.9	97.5	112.5	177.5	156.9
V				102.2	63.2	155.5	166.1	47.6	55.0	43.6
Cr				10.1		20.9	14.9	4.7		
Ni				5.7	3.3	3.3	5.3	6.5	1.9	1.3
Cu				19.5	12.2	38.7	29.7	31.1	4.8	3.4
Zn				44.8	38.1	55.6	57.2	49.2	75.9	93.8
Ga								14.5		18.3
Nb				3.3	3.4	2.6	2.2	2.7	4.6	5.7
La						12.7	12.4	1.1	17.0	11.6
Ce						22.1	19.7	18.0	32.2	22.5
Sc								12.5		26.7
Th							1.0	0.2	1.0	2.0

Sample No.	309-1	307	346	345-2	334-2	332	311-1	315-1	317-2	319-2
SiO2	66.48	64.30	63.82	73.75	58.18	64.97	64.48	60.80	66.28	64.91
TiO2	0.61	0.82	0.54	0.41	0.95	0.67	0.51	0.87	0.56	0.60
Al2O3	15.96	16.91	17.25	14.13	16.63	16.77	16.99	15.94	15.67	16.45
FeO	4.93	5.09	5.31	2.06	8.11	4.57	5.18	7.45	4.82	5.13
MnO	0.12	0.06	0.12	0.11	0.18	0.06	0.24	0.12	0.13	0.12
MgO	1.39	1.65	1.77	0.21	3.52	1.57	1.62	3.06	2.01	1.76
CaO	4.37	4.81	5.36	3.06	7.74	5.22	5.29	6.61	5.12	5.41
Na2O	4.39	4.81	4.85	4.63	3.43	4.45	4.17	3.68	3.91	3.89
K2O	1.55	1.22	0.67	1.50	1.04	1.51	1.23	1.27	1.37	1.57
P2O5	0.18	0.33	0.31	0.14	0.22	0.21	0.28	0.21	0.12	0.15
Total	100.00	100.00	100.00	100.00	100.00	100.00	100.00	100.00	100.00	100.00
FeO*/MgO	3.54	3.09	3.00	9.66	2.30	2.90	3.20	2.43	2.40	2.91
Rb	25.3	17.3	6.6	12.2	15.3	22.9	18.5	20.6	20.5	32.1
Sr	240.7	287.7	335.6	224.5	264.4	271.7	329.1	252.4	265.0	279.2
Ba	190.0	141.9	81.2	213.1	115.9	192.4	121.5	165.1	170.2	168.1
Y	46.1	50.0	42.3	44.9	38.4	41.5	40.3	37.3	24.8	25.9
Zr	177.7	143.8	130.6	170.0	116.3	155.2	127.3	136.0	117.2	113.5
V	51.9	49.9	21.3	6.8	189.0	59.9	19.7	144.8	71.8	87.4
Cr		0.2			17.5		2.9	6.7	1.5	0.8
Ni	2.6	1.7			8.4	2.0	1.3	6.2	2.5	3.4
Cu	5.5	7.2	2.7	2.1	33.2	10.1	4.6		7.0	12.4
Zn	78.3	85.9	102.1	91.7	71.6	56.5	110.7			
Ga									16.1	17.0
Nb	6.0	5.5	4.4	4.4	3.7	4.3	5.0		3.2	3.2
La	15.1	10.2	10.0	10.9	11.1		11.8			
Ce	34.4	29.6	42.7	36.7	32.6		38.9			
Sc									10.3	13.5
Th	2.3	0.8	1.5	1.3	1.4		0.2		2.1	2.2

Sample No.	319-1	320	320-1	322-2	327	325	324
SiO2	60.07	62.98	45.02	66.22	64.32	64.98	63.69
TiO2	0.77	0.70	0.41	0.55	0.63	0.58	0.63
Al2O3	17.13	16.49	25.24	16.16	16.31	15.92	16.45
FeO	7.10	6.12	8.03	4.81	5.64	5.48	5.84
MnO	0.15	0.09	0.08	0.13	0.13	0.16	0.15
MgO	2.96	2.45	4.52	1.76	1.95	2.23	2.18
CaO	7.22	5.88	15.79	5.21	5.80	5.56	5.95
Na2O	3.35	3.75	0.71	3.66	3.75	3.78	3.60
K2O	1.04	1.39	0.16	1.38	1.32	1.13	1.33
P2O5	0.19	0.15	0.04	0.13	0.15	0.17	0.17
Total	100.00	100.00	100.00	100.00	100.00	100.00	100.00
FeO*/MgO	2.39	2.50	1.78	2.74	2.89	2.45	2.68
Rb	52.2	23.9	0.4	34.8	18.9	15.5	18.2
Sr	302.2	277.9	341.1	271.1	249.7	273.8	254.4
Ba	126.5	143.6	0.8	154.7	142.7	157.9	128.0
Y	28.5	24.0	11.6	23.5	30.1	23.7	27.7
Zr	85.5	96.1	8.4	118.7	106.9	97.2	108.0
V	157.6	130.7	219.3	78.3	111.6	81.8	96.6
Cr	6.5	4.7	29.2		3.9	9.4	5.2
Ni	3.2	2.4	17.2	2.0	2.4	4.6	3.8
Cu	20.4	12.9	12.7	10.2	14.5	10.8	11.3
Zn		56.5	60.4	51.6	58.4	53.0	62.0
Ga	17.1	17.3	16.7	16.4	16.1	15.3	17.8
Nb	2.8	2.6	0.6	3.0	2.8	3.0	3.0
La		10.1	12.2	15.2	21.1	14.2	16.8
Ce		17.8	1.5	20.5	27.7	32.8	22.6
Sc	18.7	21.3	32.9	11.1	21.1	16.1	20.2
Th	1.8	2.4		2.4	0.8	1.5	1.4

Sample No.	257-1	284-1	49	255-5	285-1	285-2	44	861208-1	23	216
SiO2	62.89	55.41	49.75	50.91	53.55	52.38	57.72	57.69	52.55	60.13
TiO2	0.70	0.87	1.03	1.15	0.89	0.81	0.85	0.84	0.80	0.88
Al2O3	18.26	19.69	18.83	18.29	21.07	21.18	18.03	17.72	21.29	16.90
FeO	6.16	8.28	11.68	11.35	7.20	8.20	8.12	8.09	7.83	7.36
MnO	0.14	0.17	0.19	0.17	0.11	0.16	0.20	0.16	0.19	0.15
MgO	1.87	3.36	4.35	4.77	2.84	3.19	3.36	3.30	3.45	2.67
CaO	6.07	8.54	10.80	10.32	9.53	11.21	7.54	7.49	10.95	7.64
Na2O	2.76	2.73	2.51	2.71	3.66	2.31	3.24	3.93	2.54	3.21
K2O	1.15	0.67	0.38	0.34	0.72	0.43	0.80	0.64	0.27	1.07
P2O5	-	0.29	0.48	-	0.42	0.14	0.14	0.15	0.13	-
Total	100.00	100.00	100.00	100.00	100.00	100.00	100.00	100.00	100.00	100.00
FeO*/MgO	3.28	2.47	2.69	2.38	2.54	2.57	2.42	2.45	2.27	2.76
Rb		8.4			5.2	2.5				
Sr		214.4			342.5	308.1				
Ba		183.9			68.3	30.6				
Y		38.5			38.7	22.7				
Zr		63.9			61.0	42.4				
V		163.8			189.7	158.2				
Cr		106.9			5.8	11.5				
Ni		28.3			5.1	5.8				
Cu		21.3			11.9	41.6				
Zn		102.3			71.4	55.3				
Ga										
Nb		1.9			1.7	1.7				
La		17.3			6.1	10.4				
Ce		11.4			18.9	9.9				
Sc										
Th					0.7	1.0				

Sample No.	219	200-1	200-2	200-3	206	222	IW-1	249-1	J-28	328
SiO2	65.59	54.94	55.95	53.31	58.20	53.53	53.90	54.23	50.64	57.71
TiO2	0.82	0.94	0.99	0.93	0.97	1.14	0.96	1.09	0.95	1.05
Al2O3	16.26	18.89	18.16	19.55	17.41	20.77	17.65	18.08	20.43	16.41
FeO	5.38	8.37	8.69	8.85	8.03	8.20	10.23	9.93	9.58	9.34
MnO	0.11	0.15	0.17	0.17	0.20	0.12	0.24	0.24	0.18	0.23
MgO	1.45	3.61	2.93	3.83	2.99	2.63	3.98	3.98	3.86	3.06
CaO	5.25	9.71	8.88	10.26	8.19	10.15	9.43	8.37	11.20	7.83
Na2O	3.82	2.51	3.18	2.32	3.17	2.97	3.01	3.38	2.54	3.50
K2O	1.32	0.69	0.86	0.63	0.67	0.49	0.48	0.70	0.50	0.63
P2O5	-	0.19	0.18	0.15	0.16	-	0.13	-	0.13	0.24
Total	100.00	100.00	100.00	100.00	100.00	100.00	100.00	100.00	100.00	100.00
FeO*/MgO	3.72	2.32	2.97	2.31	2.68	3.11	2.57	2.50	2.48	3.05
Rb		7.2			7.2					5.3
Sr		276.9			275.9					281.4
Ba		79.5			93.9					82.0
Y		26.9			35.2					35.9
Zr		65.9			67.6					75.7
V		233.6			168.7					129.0
Cr		33.1			4.3					4.4
Ni		11.8			2.8					1.9
Cu		56.2			29.7					34.1
Zn		69.3			81.8					78.8
Ga										
Nb		2.6			2.4					2.4
La		14.0			4.4					
Ce		21.9			16.8					
Sc										
Th		1.0			1.7					

Sample No.	304	301	306	305	308	345	345-2	334-1	333	312-5
SiO2	56.19	66.52	57.15	50.04	60.20	64.72	73.75	57.89	69.23	47.69
TiO2	1.00	0.79	0.99	1.13	0.83	0.79	0.41	1.02	0.72	1.00
Al2O3	16.54	16.23	16.62	18.51	17.03	15.51	14.13	16.57	14.65	17.61
FeO	9.56	4.62	9.19	11.53	7.38	6.32	2.06	9.07	4.44	11.76
MnO	0.17	0.10	0.13	0.21	0.25	0.17	0.11	0.22	0.08	0.19
MgO	4.09	1.14	3.92	4.58	2.48	1.73	0.21	3.04	1.12	7.36
CaO	8.32	3.87	7.68	10.90	6.57	4.75	3.06	7.64	3.24	11.78
Na2O	3.06	4.98	3.12	2.49	3.70	4.16	4.63	3.47	4.22	2.13
K2O	0.91	1.49	1.03	0.46	1.22	1.61	1.50	0.82	2.09	0.38
P2O5	0.17	0.26	0.17	0.16	0.34	0.24	0.14	0.26	0.20	0.10
Total	100.00	100.00	100.00	100.00	100.00	100.00	100.00	100.00	100.00	100.00
FeO*/MgO	2.33	4.07	2.34	2.52	2.98	3.64	9.66	2.99	3.95	1.60
Rb	13.0	18.6	15.6	4.5	16.5	22.4	12.2	16.9	31.6	3.9
Sr	261.1	260.8	255.8	264.6	332.9	240.3	224.5	284.7	193.9	227.0
Ba	135.6	164.3	117.5	58.2	117.3	198.3	213.1	107.5	206.9	58.8
Y	30.4	56.4	30.7	26.5	38.6	47.0	44.9	38.6	57.1	19.6
Zr	103.1	173.1	103.8	54.6	95.0	171.9	170.0	96.3	234.4	35.5
V	260.8	30.4	243.9	332.3	65.0	67.2	6.8	188.0	31.6	313.4
Cr	12.0		11.1	16.3				7.5		48.3
Ni	5.8	1.6	5.8	4.5	1.8	1.3		3.0	3.3	21.7
Cu	47.6	2.5	52.8	44.8	6.7	15.3	2.1	22.1	7.5	46.1
Zn	76.2	101.8	83.8	100.7	107.3	84.2	91.7	112.7	67.9	81.6
Ga		17.6								18.4
Nb	2.8	5.6	3.7	2.6	4.0	4.5	4.4	2.8	6.3	1.7
La	14.9	17.3	11.5	1.3	14.6	11.7	10.9	8.9	18.6	2.4
Ce	17.7	33.0	31.8	21.5	21.2	34.6	36.7	20.1	32.2	8.6
Sc		23.2								32.6
Th	2.0	3.0	1.8	0.5	1.0	2.8	1.3	1.2	2.8	1.7

Sample No.	312-4	312-42	312-2	312-1	312-3	313	314	311-2	311-3	315-2
SiO2	47.63	59.26	52.82	64.27	61.76	52.96	51.31	56.67	65.80	62.91
TiO2	0.97	0.93	0.93	0.90	0.82	0.92	1.16	0.85	0.88	0.86
Al2O3	17.39	16.45	20.07	15.89	17.50	20.04	20.08	18.84	15.81	15.78
FeO	12.11	8.10	9.01	5.77	5.97	9.07	9.47	7.87	5.17	6.84
MnO	0.19	0.17	0.17	0.21	0.15	0.19	0.13	0.19	0.12	0.22
MgO	7.72	3.07	2.79	1.72	1.73	2.93	3.01	2.44	1.35	1.93
CaO	11.32	6.94	10.12	4.84	6.52	10.03	11.76	8.23	4.40	5.51
Na2O	2.17	3.72	3.02	4.75	3.87	2.89	2.50	3.71	4.88	4.44
K2O	0.39	1.18	0.86	1.28	1.42	0.80	0.41	0.93	1.25	1.19
P2O5	0.10	0.19	0.20	0.38	0.27	0.19	0.17	0.26	0.34	0.32
Total	100.00	100.00	100.00	100.00	100.00	100.00	100.00	100.00	100.00	100.00
FeO*/MgO	1.57	2.63	3.23	3.36	3.46	3.10	3.14	3.23	3.85	3.54
Rb	2.0	18.6	11.4	16.2	24.8	10.2	2.5	8.7	15.5	14.6
Sr	229.4	271.1	299.9	276.2	272.1	297.9	315.0	291.5	290.0	270.1
Ba	62.6	151.6	71.5	168.0	167.2	80.1	58.3	105.3	148.4	146.1
Y	21.0	37.5	28.9	57.0	42.8	28.8	27.4	37.7	46.7	48.7
Zr	34.9	126.7	74.1	156.2	156.9	73.7	50.5	102.1	139.2	135.5
V	325.2	162.5	169.1	53.8	86.3	177.4	279.6	128.2	60.0	61.2
Cr	44.8	9.0	16.9	2.6	3.8	4.3	5.8	3.1		0.2
Ni	23.4	4.6	0.9	2.4		2.1	2.8	2.8	1.7	2.0
Cu	56.7	33.6	40.5	6.2	14.6	47.6		21.7	6.0	5.8
Zn	83.6	69.1	106.6	93.7	74.1	105.1		99.3	82.1	116.0
Ga		18.8				20.0				
Nb	0.9	4.2	2.4	5.4	4.9	3.1		3.7	4.3	4.3
La		9.5	4.5	17.7	14.0	10.2		13.6	9.4	
Ce	7.5	27.7	18.5	37.1	36.4	29.2		23.7	17.9	
Sc		26.8				28.6				
Th		2.0		2.7	1.9	0.8		0.9	2.1	

Sample No.	316	317-1	318	322-1	326	323
SiO2	57.62	54.77	54.41	55.71	56.15	57.29
TiO2	0.95	1.12	1.10	0.90	1.11	0.90
Al2O3	16.79	17.67	17.27	19.19	17.20	17.18
FeO	8.81	10.44	10.26	8.17	9.79	8.68
MnO	0.19	0.18	0.20	0.15	0.19	0.18
MgO	3.52	3.14	3.40	2.63	3.39	3.70
CaO	7.98	8.47	8.93	9.11	8.06	7.96
Na2O	3.18	3.36	3.27	3.16	3.21	3.13
K2O	0.76	0.60	0.70	0.73	0.70	0.78
P2O5	0.20	0.24	0.45	0.26	0.19	0.19
Total	100.00	100.00	100.00	100.00	100.00	100.00
FeO*/MgO	2.50	3.32	3.02	3.10	2.89	2.35
Rb	7.2	7.3	9.2	11.6	6.4	8.7
Sr	276.7	263.6	264.2	280.7	257.1	285.2
Ba	96.3	56.8	62.4	70.6	61.4	68.9
Y	30.8	33.4	40.1	35.2	30.8	33.7
Zr	79.3	67.7	66.6	74	68.5	88.4
V	165.4	210.5	201.0	186.5	214.2	200.1
Cr	5.2	8.7	6.4	8.4	7.8	12.2
Ni	3.4	2.8	3.3	3.3	2.8	4.4
Cu	16.3	48.4	51.6	33.9	54.0	25.5
Zn	75.6			77.5	97.2	81.0
Ga		18.3	18.0	18.8	19.0	18.8
Nb	3.2	2.4	2.6	1.9	2.5	2.7
La				24.3		1.7
Ce				25.2	23.1	23.9
Sc		35.3	32.0	29.3	37.5	31.2
Th		2.4	1.7	2.5	1.0	2.5

Appendix 2

Modal compositions (volume per cent) of representative samples in the Shirahama Group

Modal compositions (volume per cent) of representative samples in the Shirahama Group

	TH								CA								
	1	2	3	4	5	6	7	8	1	2	3	4	5	6	7	8	9
SAMPLE NO.	312-4	305	255	313	318	311-2	312-1	219	261	263	303-2	266	317-2	332	330	311-1	309-2
(vol %)																	
Ol	4.0	4.1	2.2		0.1												
Opx					±	1.0	1.0	±	2.2	5.9	1.5	0.9	0.9		1.5	1.4	1.1
Augite	5.9	0.9	1.3	1.4	0.7	2.8	0.7	0.4	4.1	1.3	2.7	1.9	0.8	1.8	2.2	±	1.1
Hb													±		0.3	0.1	
Pl	39.4	33.2	9.9	26.0	10.7	18.4	7.7	7.4	30.7	19.8	15.6	24.7	15.6	23.8	20.1	10.3	14.1
Opaque	1.7	0.6	0.1	0.3	0.1	0.7	0.7	0.2	0.6	0.9	0.6	1.4	0.2	0.6	1.0	0.4	0.7
Qtz												0.3					
GM	48.9	60.9	86.3	72.1	88.3	76.8	89.5	91.9	62.2	71.9	79.4	70.6	82.3	73.7	74.8	87.7	82.9

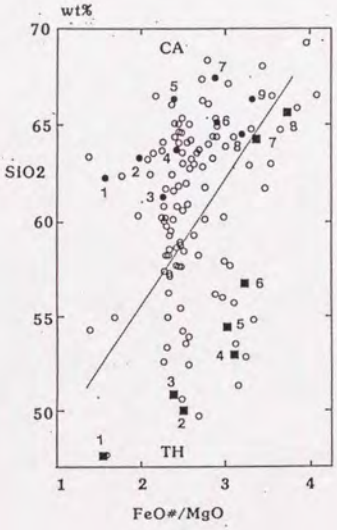

Abbreviations; Ol; olivine. Opx; orthopyroxene. Hb; hornblende. Pl; plagioclase. Qtz; quartz. GM; groundmass. ±; present but rare.

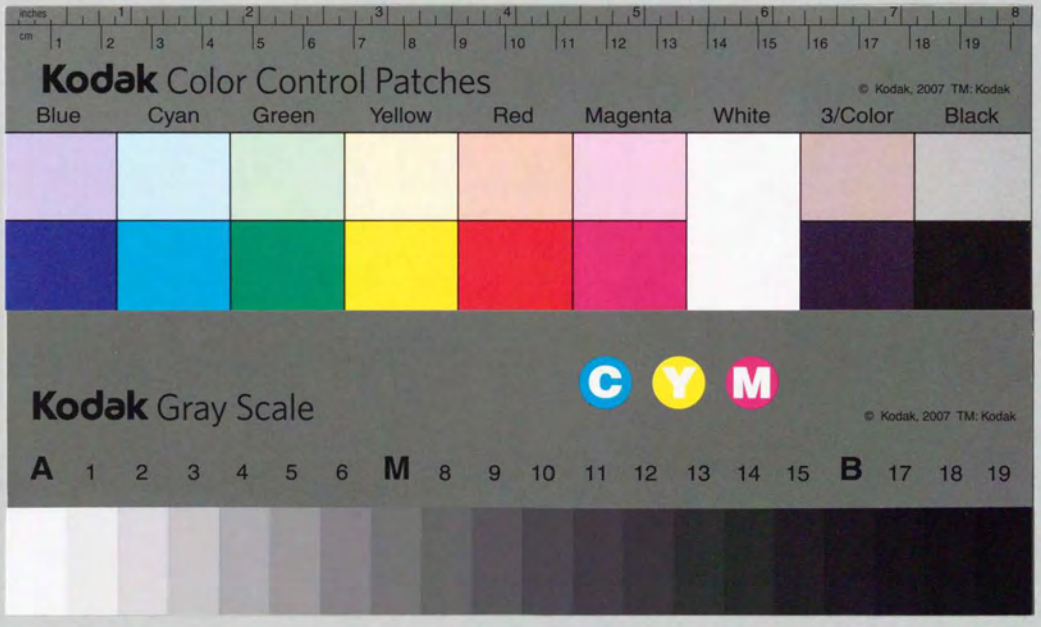
inches
cm
Kodak Color Control Patches
© Kodak, 2007 TM: Kodak
Blue
Cyan
Green
Yellow
Red
Magenta
White
3/Color
Black
C
Y
M
Kodak Gray Scale
© Kodak, 2007 TM: Kodak
A 1 2 3 4 5 6 M 8 9 10 11 12 13 14 15 B 17 18 19